Seppo Hänninen

Single phase earth faults in high impedance grounded networks

Characteristics, indication and location

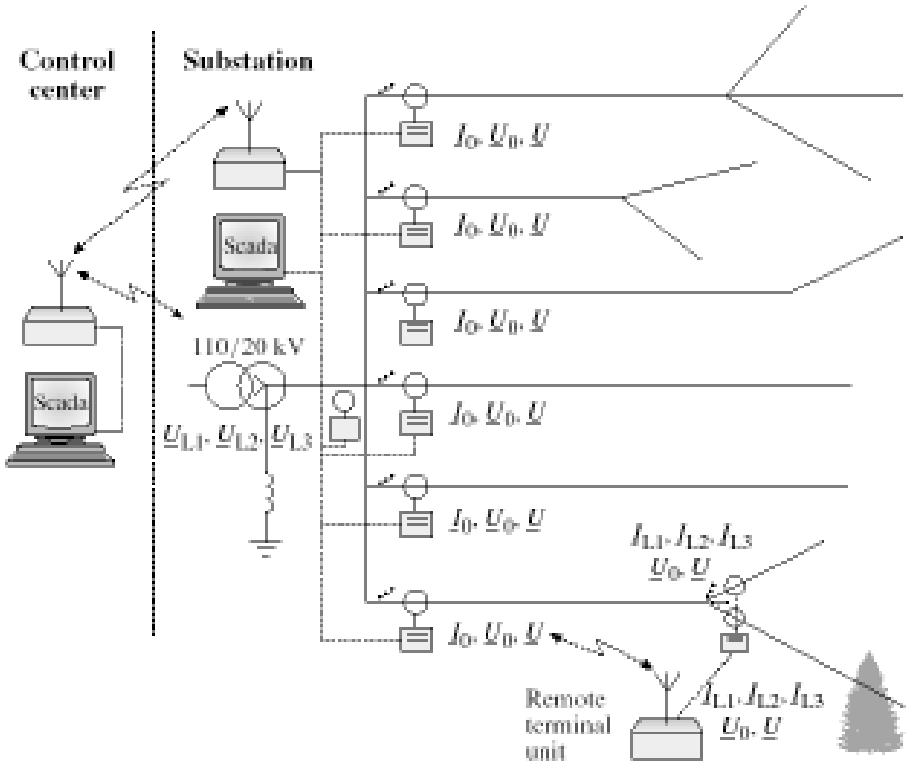

TECHNICAL RESEARCH CENTRE OF FINLAND ESPOO 2001

VTT PUBLICATIONS 453

Single phase earth faults in high impedance grounded networks

Characteristics, indication and location

Seppo Hänninen

VTT Energy

Dissertation for the degree of Doctor of Technology to be presented with due permission for public examination and debate in Auditorium S5 at Helsinki University of Technology (Espoo, Finland) on the 17th of December, 2001, at 12 o'clock noon.

TECHNICAL RESEARCH CENTRE OF FINLAND
ESPOO 2001

ISBN 951–38–5960–6 (soft back ed.)
ISSN 1235–0621 (soft back ed.)

ISBN 951–38–5961–4 (URL: http://www.inf.vtt.fi/pdf/)
ISSN 1455–0849 (URL: http://www.inf.vtt.fi/pdf/)

JULKAISIJA – UTGIVARE – PUBLISHER

Valtion teknillinen tutkimuskeskus (VTT), Vuorimiehentie 5, PL 2000, 02044 VTT
puh. vaihde (09) 4561, faksi (09) 456 4374

Statens tekniska forskningscentral (VTT), Bergsmansvägen 5, PB 2000, 02044 VTT
tel. växel (09) 4561, fax (09) 456 4374

Technical Research Centre of Finland (VTT), Vuorimiehentie 5, P.O.Box 2000, FIN–02044 VTT, Finland
phone internat. + 358 9 4561, fax + 358 9 456 4374

VTT Energia, Energiajärjestelmät, Tekniikantie 4 C, PL 1606, 02044 VTT
puh. vaihde (09) 4561, faksi (09) 456 6538

VTT Energi, Energisystem, Teknikvägen 4 C, PB 1606, 02044 VTT
tel. växel (09) 4561, fax (09) 456 6538

VTT Energy, Energy Systems, Tekniikantie 4 C, P.O.Box 1606, FIN–02044 VTT, Finland
phone internat. + 358 9 4561, fax + 358 9 456 6538

Technical editing Maini Manninen

Otamedia Oy, Espoo 2001

Hänninen, Seppo. Single phase earth faults in high impedance grounded netwotrks. Characteristics, indication and location. Espoo 2001. Technical Research Centre of Finland, VTT Publications 453. 78 p. + app. 61 p.

Keywords power distribution, distribution networks, earth faults, detection, positioning, fault resistance, arching, neutral voltage, residual current, transients

Abstract

The subject of this thesis is the single phase earth fault in medium voltage distribution networks that are high impedance grounded. Networks are normally radially operated but partially meshed. First, the basic properties of high impedance grounded networks are discussed. Following this, the characteristics of earth faults in distribution networks are determined based on real case recordings. Exploiting these characteristics, new applications for earth fault indication and location are then developed.

The characteristics discussed are the clearing of earth faults, arc extinction, arcing faults, fault resistances and transients. Arcing faults made up at least half of all the disturbances, and they were especially predominant in the unearthed network. In the case of arcing faults, typical fault durations are outlined, and the overvoltages measured in different systems are analysed. In the unearthed systems, the maximum currents that allowed for autoextinction were small. Transients appeared in nearly all fault occurrences that caused the action of the circuit breaker. Fault resistances fell into two major categories, one where the fault resistances were below a few hundred ohms and the other where they were of the order of thousands of ohms.

Some faults can evolve gradually, for example faults caused by broken pin insulators, snow burden, downed conductor or tree contact. Using a novel application based on the neutral voltage and residual current analysis with the probabilistic method, it is possible to detect and locate resistive earth faults up to a resistance of 220 kΩ.

The main results were also to develop new applications of the transient based differential equation, wavelet and neural network methods for fault distance estimation. The performance of the artificial neural network methods was

comparable to that of the conventional algorithms. It was also shown that the neural network, trained by the harmonic components of the neutral voltage transients, is applicable for earth fault distance computation. The benefit of this method is that only one measurement per primary transformer is needed. Regarding only the earth faults with very low fault resistance, the mean error in absolute terms was about 1.0 km for neural network methods and about 2.0 km for the conventional algorithms in staged field tests. The restriction of neural network methods is the huge training process needed because so many different parameters affect the amplitude and frequency of the transient signal. For practical use the conventional methods based on the faulty line impedance calculation proved to be more promising.

Preface

This work is motivated by the practical and theoretical problems studied in several research projects carried out at VTT Energy, and in two technology programmes EDISON and TESLA, during the period 1994–2000.

The work has been supervised by Professor Matti Lehtonen from the Power Systems Laboratory in the Helsinki University of Technology. He has also been the manager of our research group, Electric Energy and IT at VTT Energy, and the leader of the technology programmes EDISON and TESLA. I am deeply grateful to him for the research management, advice, co-operation and support during the academic process.

For practical arrangements and help in organising the field tests and measurements I wish to thank Mr. Veikko Lehesvuo, Mr. Tapio Hakola and Mr. Erkki Antila of ABB Substation Automation Oy. I am also grateful to the distribution companies, who offered the possibility for field tests and measurements in their networks. I am especially indebted to Mr. Jarmo Ström and Mr. Matti Lehtinen of Espoo Electricity, Mr. Stefan Ingman and Mr. Seppo Pajukoski of Vaasa Electricity, Mr. Seppo Riikonen and Mr. Matti Seppänen of North-Karelian Electricity, and both Mr. Arto Järvinen and Mr. Markku Vänskä of Häme Electricity for their assistance in the measurements. I owe special thanks to Miss Gerit Eberl and Professor Peter Schegner from the Dresden University of Technology in Germany, Professor Urho Pulkkinen of VTT Automation and Mr. Reijo Rantanen of Kolster Oy Ab for their co-operation during the work. The financial support of VTT Energy, Tekes National Technology Agency and ABB Substation Automation Oy is also gratefully appreciated. Regarding the English language, I want to thank Mr. John Millar for his good service in checking the manuscript. Many thanks go also to all my superiors and colleagues at VTT Energy for an inspiring work environment.

The warmest thanks I want to address to my wife Eila, my daughters Ulrika and Johanna and my son Heikki. Their support and encouragement made this work possible.

Helsinki, October 2001

Seppo Hänninen

List of publications

This thesis consists of the present summary and the following publications, referred to as Papers A–G:

A Hänninen, S. & Lehtonen, M. 1998. Characteristics of earth faults in electrical distribution networks with high impedance earthing. EPSR (Electric Power Systems Research), Vol. 44, No. 3, pp. 155–161.

B Hänninen, S., Lehtonen, M. & Hakola, T. 2001. Earth faults and related disturbances in distribution networks. Proceedings of IEEE PES SM2001, Vancouver, Canada, July 15–19, 2001. CD-ROM 01CH37262C. 6 p.

C Hänninen, S. & Lehtonen, M. 1999. Method for detection and location of very high resistive earth faults. ETEP (European Transactions on Electrical Power) Vol. 9, No. 5, pp. 285–291. http://www.ETEP.de

D Hänninen, S., Lehtonen, M. & Pulkkinen, U. 2000. A probabilistic method for detection and location of very high resistive earth faults. EPSR (Electric Power Systems Research), Vol. 54, No. 3, pp. 199–206.

E Hänninen, S., Lehtonen, M., Hakola, T. & Rantanen, R. 1999. Comparison of wavelet and differential equation algorithms in earth fault distance computation. PSCC'99. 13th Power Systems Computations Conference, Trondheim, Norway, June 28–July 2, Proceedings Vol. 2. Pp. 801–807.

F Eberl, G., Hänninen, S., Lehtonen, M. & Schegner, P. 2000. Comparison of artificial neural networks and conventional algorithms in ground fault distance computation. Proceedings of IEEE PES WM2000, Singapore, January 23–27, 2000. CD-ROM 00CH37077C. 6 p.

G Hänninen, S. & Lehtonen, M. 2001. Earth fault distance computation with artificial neural network trained by neutral voltage transients. Proceedings of IEEE PES SM2001, Vancouver, Canada, July 15–19, 2001. CD-ROM 01CH37262C. 6 p.

Author's contribution

The author's contribution to the preparation of the publications, which are enclosed as the Appendices A–G, is briefly reviewed in this chapter. The papers summarise the work based on the successive research projects, of which the author as the project manager was in charge. Papers A–B deal with the characteristics of earth faults. The author was responsible for the data acquisition, analyses and the development of the analysis methods.

Papers C–D introduce high impedance earth fault indication and location methods. The author developed the PC based prototype version for the high impedance earth fault indication and location method, based on inventions of professor Lehtonen. The author participated in the development process by verifying the whole system functions on substation level and by testing the method presented in Paper C. The author has developed the probabilistic method for high impedance earth fault location based on Bayesian theorem presented in Paper D.

Papers E–G discuss transient based fault distance computation methods. The author has had the main role in developing the wavelet method and the artificial neural network method based on neutral voltage transient presented in Papers E and G. The neural network application of Paper F was mainly done by Miss Eberl under supervision of Professors Lehtonen and Schegner. In the last mentioned project, the author has participated in guidance of the development work and input data scaling, and the author has done the signal pre-processing.

The author has mainly written Papers A–E and G and he actively participated in the writing of Paper F. Professor Lehtonen has been the supervisor of this work and the co-author of the papers. He also participated in the development of the earth fault indication and location methods. Professor Pulkkinen participated in guidance of the probabilistic approach for fault location in Paper D. Mr. Hakola and Mr. Rantanen arranged and helped in organising the field tests and measurements, which were of vital importance for verification of the fault indication and location methods in Papers B and E.

Contents

List of symbols and notations

ANN	artificial neural network
ATP-EMTP	alternative transients program - electromagnetic transients program
DAR	delayed auto-reclosure
HSAR	high speed auto-reclosure
HV/MV	high voltage/medium voltage
LV	low voltage
L1, L2, L3	phases of the symmetrical three phase system
MEK	mean absolute error
P	permanent fault
RC	remote controlled
SCADA	supervision control and data acquisition
SE	self-extinguished fault
VHF	very high frequency
VLF	very low frequency
1, 2, 0	positive, negative and zero sequence
$\underline{a}$, $\underline{a}^2$	complex rotation operators
C	capacitance
C_e	phase-to-ground capacitance of the unearthed network
C_E	phase-to-ground capacitance of the system
C_{eq}	equivalent capacitance
C_0	zero-sequence capacitance
E	voltage (source), phase voltage
f	frequency
$f(t)$	discrete signal
f_c	charge frequency
f_0	charge frequency for ANN training, fault at the busbar
f'_0	charge frequency of real network, fault at the busbar
f_{30}	charge frequency for ANN training, fault at a distance of 30 km
f'_{30}	charge frequency of real network, fault at a distance of 30 km
$f_0(x)$	current density function of a healthy feeder
$f_1(x)$	current density function of a faulty feeder
$g(t)$	output of the filter

i	integer
$\hat{i}_C$	current transient amplitude
i_k	current sample
I	current
I_{ave}	average value of the compensated feeder currents
$\underline{I}_C$	capacitive current
$\underline{I}_{CE1,CE2,CE3}$	phase to ground capacitive currents
$\underline{I}_e$	earth fault current
$\underline{I}_{ef}$	earth fault current reduced by fault resistance
$\underline{I}_f$	fault current
$\underline{I}_L$	current of the suppression coil
I_{Lmax}	maximum phase current
I_{Lmin}	minimum phase current
$Im[f(t)]$	imaginary part of function
I_{max}	maximum value of the compensated feeder currents
I_{min}	minimum value of the compensated feeder currents
$\underline{I}_P$	current of the parallel resistor
I_w	wavelet coefficient for current
$\underline{I}_{1,2,0}$	positive, negative and zero sequence current
$\Delta\underline{I}_{0i}$	compensated zero sequence current of the feeder i
$\Delta\underline{I}_{0im}$	measured change of zero-sequence current of the feeder i
j	integer
k	integer
l	length
L	inductance
L_{eq}	equvalent inductance
L_T	phase inductance of the substation transformer
$L'_{1,2,0}$	positive, negative and zero sequence inductance
n	integer
$Pr(i\|x)_I$	fault probability by using the point probability method
$Pr(i\|x)_I$	fault probability by using the overall probability method
R	resistance
R_e	earthing resistor
R_f	fault resistance
R_{LE}	phase-to-ground resistance of the system
R_P	parallel resistor

SF	scaling factor
t	time (point)
Δt	sampling period
T	period of the fundamental frequency
U	voltage
U_0	neutral voltage
u_k	voltage sample
$\underline{U}_{L1,L2,L3}$	phase-to-ground voltages
U_w	wavelet coefficient for voltage
$\Delta\underline{U}_{0m}$	measured change of neutral voltage (zero sequence voltage)
$\underline{U}_{1,2,0}$	positive, negative and zero sequence voltages
W_s	wavelet coefficient
$\underline{X}_{1C,2C,0C}$	positive, negative and zero sequence capacitive reactances
$\underline{X}_{1l,2l,0l}$	positive, negative and zero sequence line reactances
$\underline{Z}$	impedance
$\underline{Z}_{1,2,0}$	positive, negative and zero sequence impedances
$\underline{Z}_{0i}$	zero-sequence impedance of the feeder i
$\underline{Z}_e$	earthing impedance
$\underline{Z}_f$	fault impedance
$\underline{Z}_l$	impedance of the line
$\underline{Z}_T$	impedance of the transformer
μ	mean of Normal distribution
μ_0	mean of current distribution in healthy feeders
μ_1	mean of current distribution in faulty feeders
μ_{1C}	mean of current distribution in overall probability method
μ_{1U}	expected fault current in overall probability method
σ	parameter of wavelet function
σ^2	variance of Normal distribution
σ_0^2	healthy feeder current variance in point probability method
σ_{1C}^2	faulty feeder current variance
σ_{1U}^2	expected fault current variance in overall probability method
ω	angular frequency
ω_f	fundamental angular frequency
ω_c	angular frequency of the charge transient
Ψ	wavelet function

1. Introduction

In this thesis, the term high impedance grounding is used to make difference to resistance and solid grounding. In practice this means either ungrounded system where the insulation between neutral and ground is of same order as phase insulation, or compensated neutral system where the neutral point is earthed by suppression coil in order to reduce the fault current. The medium voltage, 20 kV, distribution networks in Finland are mainly of overhead construction with high impedance grounding and are generally radially configured. The networks are operated with an isolated neutral point, but compensation of the earth fault current with the Petersen coil is also used in the substations where a reduction of fault current is needed. While ungrounded systems prevail in the Nordic countries, they are not widely used elsewhere because of the high potential of restriking arcs, which can result in high, destructive transient overvoltages that can be a hazard to equipment and personnel.

The most common fault type in electrical distribution networks is the single phase to earth fault. According to earlier studies, for instance in Nordic countries, about 50–80% of the faults are of this type (Paulasaari et al. 1995, Winter 1988). Earth faults are normally located by splitting the feeder into sections and closing the substation circuit breaker against the fault until the faulty line section is found. The operation of manually controlled switches requires a patrol moving in the terrain. Therefore, to decrease the customer's outage time, the development of indication and location methods for earth faults is essential.

In the past years the indication and location of earth faults have been the object of active study worldwide, and several methodologies have been investigated. On the other hand, numerical relays as part of advanced distribution automation, and modern current and voltage sensors facilitate greater accuracy and selectivity of the protection functions. However, practical implementations of the advanced methods are rare. In comparison to the short circuit fault (Pettissalo et al. 2000), reliable earth fault indicators are lacking, and the fault distance computation is still an open issue for utilities. Therefore, the indication and location methods of earth faults are still in development phase.

With regard to earth fault indication and location, perhaps the most influential factor is the fault resistance. According to our investigations, fault resistances fell into two major categories: one where the fault resistances were below a hundred ohms and the other where they were in the order of thousands of ohms. The last mentioned high impedance disturbances are beyond the reach of protective relays, zero sequence overvoltage relays or overcurrent relays. They are difficult to detect and even if detected, it can be most difficult to discriminate this situation from normal electrical events in the distribution feeders. A fallen or broken distribution conductor can result in a high impedance fault, and it may be a potential hazard if not detected and de-energized.

The difficulty with the accurate location of ground faults in high impedance grounded networks is that the fundamental frequency fault currents are often small compared to the load currents, even in the case of very low fault resistances. The use of fundamental frequency components works only in meshed operation, or when the faulty feeder is possible to connect into a closed ring with one healthy feeder (Winter 1993, Roman & Druml 1999). The utilisation of ground fault initial transients has proved to be the most promising method for the purpose of fault location in radial operation (Schegner 1989, Igel 1990, Lehtonen 1992). However, the practical implementations in relays are restricted, due to the requirement of a sampling rate of 10–20 kHz.

The aim of this study is to determine the characteristics of real earth faults in Finnish network circumstances. Based on these characteristics new methods for high impedance fault indication and location are developed. The contribution of this work is also to study new applications of the transient based differential equation, wavelet and neural network methods for fault distance estimation. The scope is restricted to radially operated systems. In this thesis, the following definitions are used. Low resistance fault means, that the value of fault resistance is 50 Ω or smaller. In the case of a high resistance fault the corresponding value is clearly higher than 50 Ω, typically several thousands of ohms. Fault indication means, that fault is detected somewhere in the distribution network without knowledge of the fault location. Fault location means the determination of the faulty feeder or line section. Fault location is also used as a general term when we are talking about fault distance computation. In fault distance computation, the question is the shortest feeder length from substation to fault point. This does not mean the exact knowledge of fault point,

since if the feeder has many laterals, several possible fault points may be obtained. The actual fault location can be found among these candidate locations by some other means such as by fault indicators or by trial and error.

The work behind this thesis is part of the research work carried out at VTT Energy during the period 1994–2000. The projects belonged to two technology programmes: EDISON on Distribution automation in Finnish utilities (1993–1997) and TESLA on Information technology and electric power systems (1998–2002). This work has been carried out in co-operation with VTT Energy, Helsinki University of Technology, Dresden University of Technology, ABB Substation Automation Oy and various distribution companies. The aim of these projects in the technology programmes was to develop new applications for distribution automation and to decrease outages times.

The thesis is organised as follows. First we discuss the basic properties of the high impedance grounded networks and the calculation of currents and voltages during an earth fault. In chapter 3 the characteristics of the earth faults are analysed based on comprehensive and long-term recordings in real distribution networks. The characteristics discussed can be exploited for high resistance fault indication and location and, in the case of low resistance faults, for fault distance estimation. In chapter 4 the existing methods for the indication and location of high impedance earth faults are reviewed and a novel method, which is based on the analysis of neutral voltage and residual current, is presented. Finally in chapter 5, four different methods are proposed for fault distance estimation in the case of low resistance faults, two of which are based on the line terminal impedance and two on artificial neural networks. The two first mentioned conventional methods have been in pilot use in real network circumstances. The methods are evaluated and compared using real field test data.

The thesis consists of this summary and the original Papers A–G, which are here enclosed as the Appendices A–G.

2. An earth fault in a high impedance grounded network

The way the neutral is connected to the earth determines the behaviour of a power system during a single phase to ground fault. From the safety point of view the earth fault current causes a hazard voltage between the frames of the faulted equipment and earth. In this chapter, the basic properties of unearthed, compensated and high resistance earthed networks are discussed, with special attention given to the calculation of currents and voltages during a fault. Some focus is also given to the fault impedance, which affects the neutral voltage and earth fault current. In Sections 2.6 and 2.7 two important phenomena, the extinction of power arc and earth fault initial transients, are described. The extinction of earth fault arc has a considerable influence to the number of short interruptions to the customers and the initial transients can be utilised for earth fault distance estimation. At the end of this chapter, the measurements are described which were carried out in the distribution utilities in the course of this work.

2.1 Networks with an unearthed neutral

Ungrounded systems have no intentional direct grounding but are grounded by the natural capacitance of the system, see Fig. 1 (Blackburn 1993). The currents of single phase to ground faults are low and depend mostly on the phase to ground capacitances of the lines. The voltage between faulted equipment and earth is small, which improves safety. On the other hand, transient and power-frequency overvoltages can be higher than those obtained, for example, with resistance earthed systems (Lakervi & Holmes 1995). When the fault happens, the capacitance of the faulty phase is bypassed, and the system becomes unsymmetrical. A model for the fault circuit can most easily be developed using Thevenin's theorem. Before the fault, the voltage at the fault location equals the phase voltage E. The other impedances of the network components are small compared to those of the earth capacitances C_e, and can hence be neglected. This leads to the model in Fig. 2.

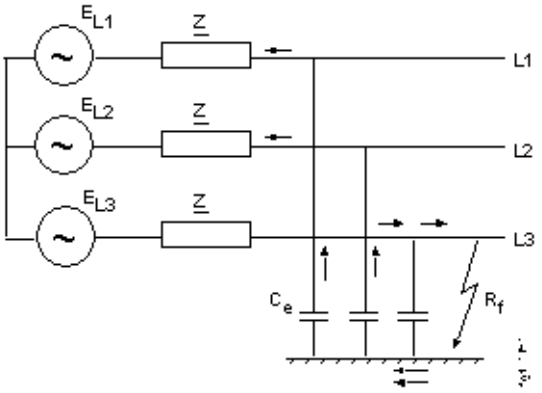

Figure 1. Earth fault in a network with an unearthed neutral (Lehtonen & Hakola 1996).

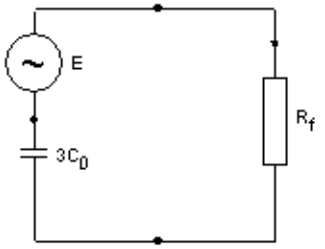

Figure 2. Equivalent circuit for the earth fault in a network with an unearthed neutral (Lehtonen & Hakola 1996).

In the case where the fault resistance is zero, the fault current can be calculated as follows:

$$I_e = 3\omega C_e E \tag{1}$$

where $\omega = 2\pi f$ is the angular frequency of the network. The composite earth capacitance of the network C_e depends on the types and lengths of the lines connected in the same part of the galvanically connected network. In radially operated medium voltage distribution systems this is, in practice, the area supplied by one HV/MV substation transformer.

In earth faults there is usually some fault resistance R_f involved, the effect of which is to reduce the fault current:

$$I_{ef} = \frac{I_e}{\sqrt{1+\left(\frac{I_e}{E}R_f\right)^2}} \tag{2}$$

where I_e is the current obtained from eq. (1). In unearthed systems this does not, in practice, depend on the location of the fault. However, the zero sequence current of the faulty feeder, measured at the substation, includes only that part of the current that flows through the capacitances of the parallel sound lines. This causes problems in the selective location of faults by the protective relaying. The zero sequence voltage U_0 is the same that the fault current causes when flowing through the zero sequence capacitances:

$$U_0 = \frac{1}{3\omega C_0} I_{ef} \tag{3}$$

Using eqs. (1) and (2) this can also be written in the following form:

$$\frac{U_0}{E} = \frac{1}{\sqrt{1+\left(3\omega C_0 R_f\right)^2}} \tag{4}$$

which states, that the highest value of neutral voltage is equal to the phase voltage. This value is reached when the fault resistance is zero. For higher fault resistances, the zero sequence voltage becomes smaller. In the case of a phase to ground fault with zero fault impedance, the unfaulted phase to ground voltages are increased essentially by $\sqrt{3}$ as shown in Fig. 3. Its maximum value is about 1.05U (U = line-to-line voltage) when the fault resistance is about 37% of the impedance consisting of the network earth capacitances. These systems require line voltage insulation between phase and earth (Klockhaus et al. 1981). In a normal balanced system the phase to neutral voltages and phase to ground voltages are essentially the same, but in the case of an earth fault, they are quite different. The neutral shift is equal to the zero sequence voltage. In networks with an unearthed neutral, the behaviour of the neutral voltage during the earth

fault is of extreme importance, since it determines the overall sensitivity of the fault detection.

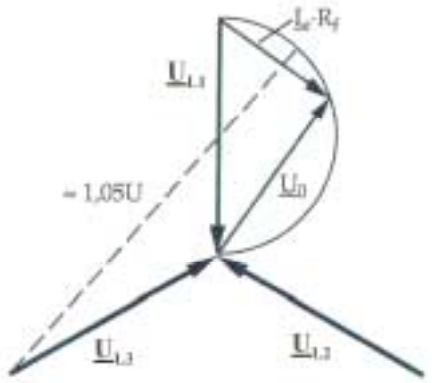

Figure 3. Voltages during an earth fault in an unearthed network (Mörsky 1992).

2.2 Networks with a compensated neutral

The idea of earth fault compensation is to cancel the system earth capacitance by an equal inductance, a so called Petersen coil connected to the neutral, which results in a corresponding decrease in earth fault currents, see Figs 4 and 5. The equivalent circuit for this arrangement is shown in Fig. 6. Instead of one large controlled coil at the HV/MV substation, in rural networks it is possible to place inexpensive small compensation equipment, each comprising a star-point transformer and arc-suppression coil with no automatic control, around the system. With this system the uncompensated residual current remains somewhat higher than in automatically tuned compensation systems (Lakervi & Holmes 1995).

In Fig. 4, the circuit is a parallel resonance circuit and if exactly tuned, the fault current has only a resistive component. This is due to the resistances of the coil and distribution lines together with the system leakage resistances (R_{LE}). Often the earthing equipment is complemented with a parallel resistor R_p, the task of which is to increase the ground fault current in order to make selective relay protection possible.

The resistive current is, in medium voltage networks, typically from 5 to 8% of the system's capacitive current. In totally cabled networks the figure is smaller, about 2 to 3% (Hubensteiner 1989), whereas in networks with overhead lines solely, it can be as high as 15% (Claudelin 1991).

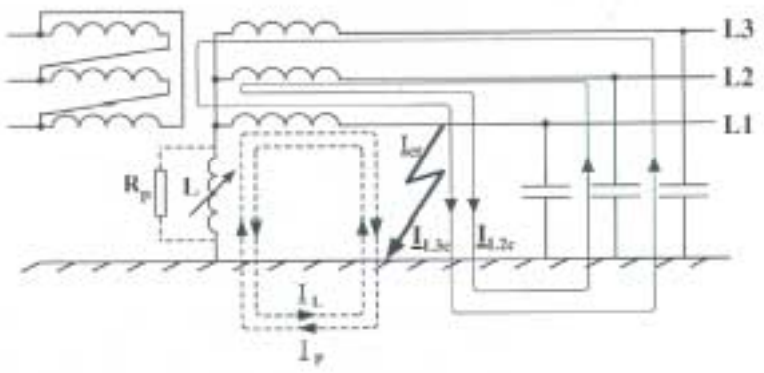

Figure 4. Earth fault in a network with a compensated neutral. $\underline{I}_t=\underline{I}_L-\underline{I}_P$ is the current of the suppression coil and a parallel resistor, $\underline{I}_{L2c}$ and $\underline{I}_{L3c}$ are the capacitive currents of the sound phases, and $\underline{I}_{ef}=\underline{I}_{L2c}+\underline{I}_{L3c}-\underline{I}_t$ is the earth fault current at the fault point (Mörsky 1992).

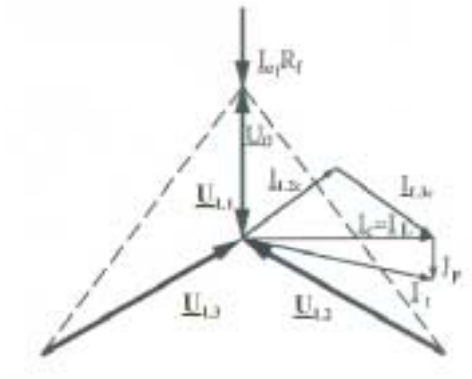

Figure 5. The phasor diagram of currents and voltages in the case of eart fault in fully compensated system. $\underline{I}_C=\underline{I}_{L2c}+\underline{I}_{L3c}$ is the current of earth capacitances, $\underline{I}_t=\underline{I}_L-\underline{I}_P$ is the current of the suppression coil and a parallel resistor, $\underline{I}_{ef}=\underline{I}_c-\underline{I}_t=\underline{I}_P$ is the earth fault current (Mörsky 1992).

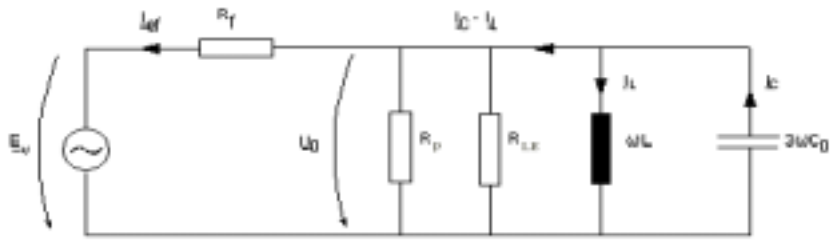

Figure 6. Equivalent circuit for the earth fault in a network with a compensated neutral (Lehtonen & Hakola 1996).

Using the equivalent circuit of Fig. 6, we can write for the fault current:

$$I_{ef} = \frac{E\sqrt{1 + R_{LE}^2\left(3\omega C_0 - \frac{1}{\omega L}\right)^2}}{\sqrt{\left(R_f + R_{LE}\right)^2 + R_f^2 R_{LE}^2\left(3\omega C_0 - \frac{1}{\omega L}\right)^2}}. \tag{5}$$

In the case of complete compensation, the above can be simplified as follows:

$$I_{ef} = \frac{E}{R_{LE} + R_f} \tag{6}$$

The neutral voltage U_0 can be calculated correspondingly:

$$U_0 = \frac{I_{ef}}{\sqrt{\left(\frac{1}{R_{LE}}\right)^2 + \left(3\omega C_0 - \frac{1}{\omega L}\right)^2}} \tag{7}$$

which in the case of complete compensation, is reduced to the following form:

$$\frac{U_0}{E} = \frac{R_{LE}}{R_{LE} + R_f} \tag{8}$$

For the above equations it was assumed that no additional neutral resistor R_p is used. If needed, the effect of R_p can be taken into account by replacing R_{LE} in eqs. (5) to (8) by the parallel coupling of R_{LE} and R_p.

As in the case with an unearthed neutral, the highest zero sequence voltage equals the phase voltage of the system. During earth faults, the neutral voltages are substantially higher in the systems with a compensated neutral than in the case with an unearthed one. Hence a more sensitive indication for high resistance faults can be gained in the former case.

2.3 Networks with high resistance grounding

The grounding resistor may be connected in the neutral of a power transformer or across the broken delta secondary of three phase-to-ground connected distribution transformers. These systems are mainly used in such MV and LV industrial networks, where the continuity of service is important because a single fault does not cause a system outage. If the grounding resistor is selected so that its current is higher than the system capacitive earth fault, then the potential transient overvoltages are limited to 2.5 times the normal crest phase voltage. The limiting factor for the resistance is also the thermal rating of the winding of the transformer.

Earth fault current can be calculated using the equivalent circuit of Fig. 7 as follows:

$$I_{ef} = \frac{E\sqrt{1 + \left(R_e\, 3\omega C_0\right)^2}}{\sqrt{\left(R_f + R_e\right)^2 + \left(R_f R_e\, 3\omega C_0\right)^2}}. \tag{9}$$

When the reactance of the earth capacitance is large compared to the earthing resistance, the above can be simplified as follows:

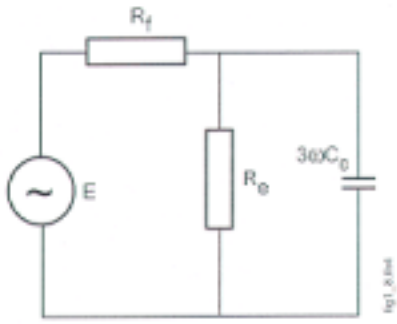

Figure 7. Equivalent circuit for the earth fault in a high-resistance earthed system (Lehtonen & Hakola 1995).

$$I_{ef} = \frac{E}{R_e + R_f} \tag{10}$$

The neutral voltage is

$$U_0 = \frac{I_{ef}}{\sqrt{\left(\frac{1}{R_e}\right)^2 + (3\omega C_0)^2}} \tag{11}$$

The highest neutral voltage in high resistance earthed networks is equal to the phase to ground voltage when the fault resistance is zero. The corresponding phase to ground voltage in two sound phases is equal to the line voltage. Due to the fact that Finnish medium voltage distribution networks are unearthed (80%) or compensated (20%), the high resistance earthed systems are not discussed later in this work (Nikander & Lakervi 1997).

2.4 Sequence network representation

Symmetrical components are often used when analysing unsymmetrical faults in power systems. All cases of neutral earthing, presented in Sections 2.1–2.3, can be analysed using the sequence network model and the appropriate connection of component networks, which depend on the fault type considered. The simplified equations of previous sections can be derived from the general model.

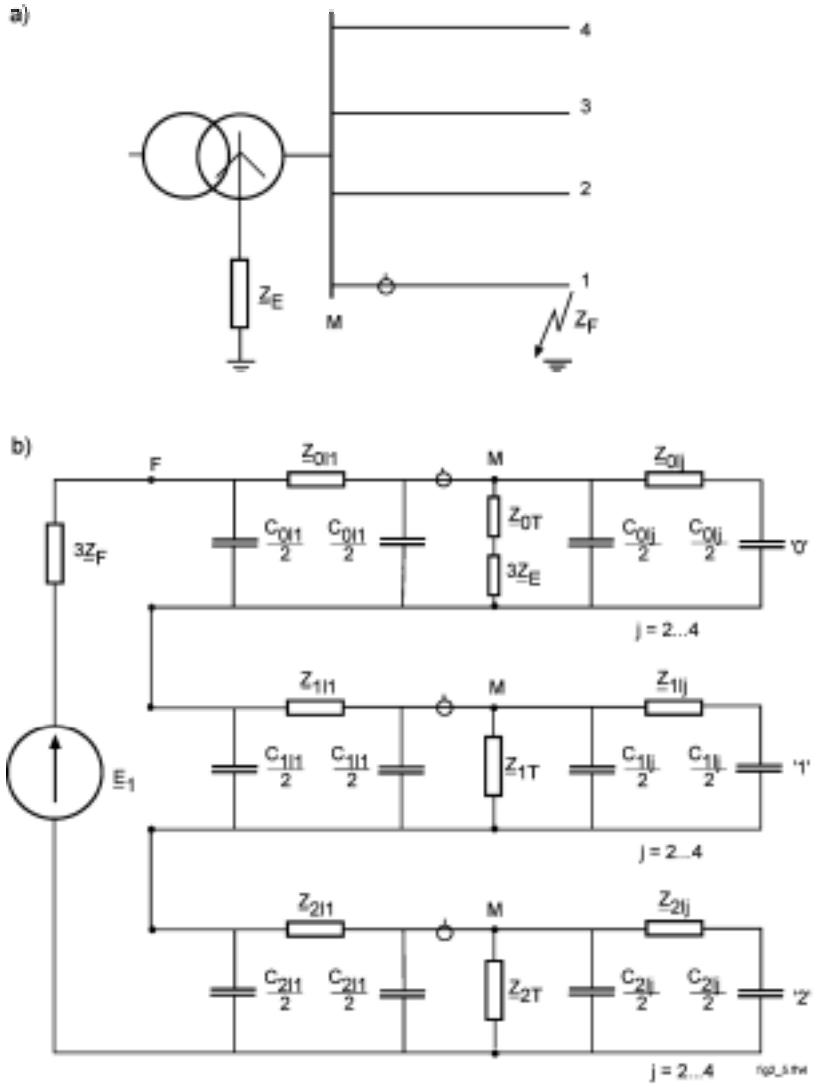

Figure 8. Single phase to earth fault in a distribution network. M is the measurement point, F refers to the fault location. $\underline{Z}_E$ is the earthing impedance and $\underline{Z}_F$ is the fault impedance. a) The network and b) the corresponding symmetrical component equivalent circuit. Z_{0T}, Z_{1T} and Z_{2T} are zero sequence, positive sequence and negative sequence impedances of the substation transformer. j = 2...4 refers to the impedances of the parallel sound lines (Lehtonen & Hakola 1995).

For a phase to ground fault in radial operating system, the sequence networks and their interconnections are shown in Fig. 8. For example in unearthed network $\underline{Z}_E = \propto$ and the distributed capacitive reactances $\underline{X}_{1C}$, $\underline{X}_{2C}$ and $\underline{X}_{0C}$ are very large, while the series reactance (or impedance) values $\underline{Z}_{0l1}$, $\underline{Z}_{1l1}$, $\underline{Z}_{2l1}$, $\underline{Z}_{1T}$, $\underline{Z}_{2T}$, are relatively small. Thus, practically, $\underline{X}_{1C}$ is shorted out by $\underline{Z}_{1T}$ in the positive sequence network, and $\underline{X}_{2C}$ is shorted out by $\underline{Z}_{2T}$ in the negative sequence network. Since these impedances are very low, $\underline{Z}_{1T}$ and $\underline{Z}_{2T}$ approach zero relative to the large value of $\underline{X}_{0C}$. Therefore, the sequence currents can be approximated by the following equation in the case of zero fault resistance (Blackburn 1993).

$$\underline{I}_1 = \underline{I}_2 = \underline{I}_0 = \frac{\underline{E}_1}{\underline{Z}_{1T} + \underline{Z}_{1l1} + \underline{Z}_{2T} + \underline{Z}_{2l1} + \underline{X}_{0C}} \cong \frac{\underline{E}_1}{\underline{X}_{0C}} \tag{12}$$

and

$$\underline{I}_f = 3\underline{I}_0 = \frac{3\underline{E}_1}{\underline{X}_{0C}} \tag{13}$$

The unfaulted phase L2 and L3 currents will be zero when determined from the sequence currents of Eq. 12. This is correct for the fault itself. However, throughout the system the distribution capacitive reactances $\underline{X}_{1C}$ and $\underline{X}_{2C}$ are actually in parallel with the series impedances $\underline{Z}_{1l}$, $\underline{Z}_{1T}$ and $\underline{Z}_{2l}$, $\underline{Z}_{2T}$ so that in the system $\underline{I}_1$ and $\underline{I}_2$ are not quite equal to $\underline{I}_0$. Thus the phase to ground capacitive currents $\underline{I}_{CE2}$ and $\underline{I}_{CE3}$ exist and are necessary as the return paths for the fault current $\underline{I}_f$. When faults occur in different parts of the ungrounded system, $\underline{X}_{0C}$ does not change significantly. Since the series impedances are quite small in comparison, the earth fault current is practically the same and is independent of the fault location. The zero sequence current measured at the substation includes that current flowing in the fault point, less the portion that flows trough the earth capacitances of the faulty line itself, see Fig. 8.

2.5 Fault impedance

Earth faults are seldom solid but involve varying amounts of impedance. However, it is generally assumed in protective relaying and most fault studies that the connection of the phase conductor with the ground involves very low and generally negligible impedance. For the higher voltages of transmission and subtransmission this is true. In distributions systems, however, very large to basically infinite impedances can exist. Many faults are tree contacts, which can be of high impedance, especially in wintertime when the ground is frozen, see Papers A–C. Covered and also bare conductors lying on the ground may or may not result in a significant fault current and can be highly variable. Many tests have been conducted over the years on wet soil, dry soil, rocks, asphalt, concrete and so on, with quite variable and sometimes unpredictable results (see, for example, Sultan et al. 1994, Russell & Benner 1995). Thus in most fault studies, the practice is to assume zero ground impedance for maximum fault current values. In addition, it is usual to assume that the fault impedance is purely resistive.

Fault impedance includes also the resistance of the power arc, which can be approximated by the following formula (Warrington 1962)

$$R = 8750l / \left(0.305 I^{1.4}\right) \tag{14}$$

R is expressed in Ω, l is the length of the arc in meters in still air, and I is the fault current in amperes. Another highly variable factor is the resistance between the line pole or the tower and ground. The general practice is to neglect this in most fault studies, relay applications and relay settings.

2.6 Extinction of earth fault arc

Most earth faults cause an arc in their location. The capacitive fault current is interrupted, either by switchgear or self-extinction of the power arc, at the instantaneous current zero. The factors affecting the power arc extinction in free air are the current magnitude, recovery voltage, time the arc existed, length of the spark gap and wind velocity. The current magnitude and the recovery voltage

are the most important (Poll 1984, Lehtonen & Hakola 1996). As a consequence of the arc extinction the zero sequence system is de-energized and the voltage of the faulted phase is re-established. This causes a voltage transient often called the recovery voltage. The power arc extinction depends on the rising speed of the recovery voltage over the spark gap. The lower steepness of the recovery voltage is the main reason why the possibility of arc extinction with higher current is much greater in a compensated than in an isolated system, see Fig. 9. In compensated network, the arc suppression is very sensitive to the suppression coil tuning. By examining field tests (Poll 1983, Nikander & Lakervi 1997), the compensation degree must be relatively high (about 75%–125%) before the self-extinction of the earth fault arc can be considerably improved. In partially compensated networks with low compensation degree the use of correctly dimensioned additional star point resistor parallel with the coil reduces the steepness and the amplitude of the recovery voltage transient.

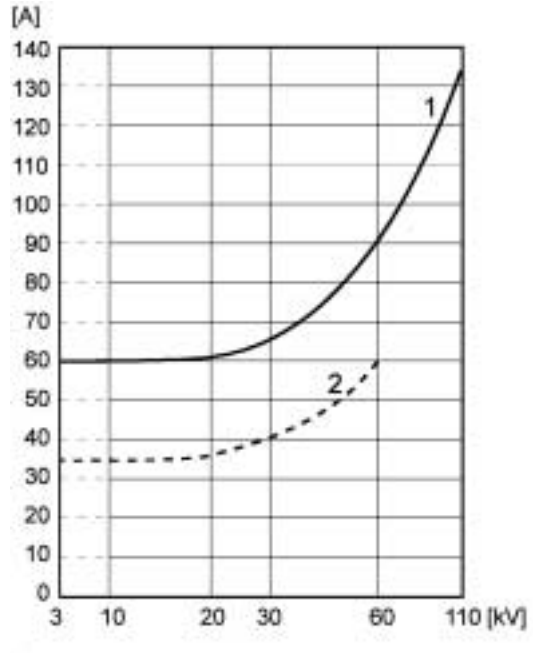

Figure 9. Current limits of earth fault extinction in compensated (1) and unearthed systems (2). Horizontal axis: Nominal voltage. Vertical axis: The residual fault current in a compensated network or the capacitive fault current in an unearthed system (VDE 0228 1987).

According to Fig. 9 the current limits of earth fault extinction are 60 A and 35 A in 20 kV compensated and unearthed systems, respectively. In rural overhead line networks, horn gaps are widely used for the overvoltage protection of small distribution transformers. The power arc is not as free to move as in the case of a flashover of an insulator string for instance. Due to this the above mentioned current limits have been reported to be considerable lower, 20 A and 5A respectively (Taimisto 1993, Haase & Taimisto 1983).

2.7 Transient phenomena in earth fault

Earth fault initial transients have been used for fault distance computation due to the fact, that the transient component can easily be distinguished from the fundamental frequency load currents. It has in many cases higher amplitude than the steady state fault current, see Fig. 10. When an earth fault happens, three different components can be distinguished. The discharge transient is initiated when the voltage of the faulty phase falls and the charge stored in its earth capacitances is removed. Because of the voltage rise of the two sound phases, another component, called charge transient, is created. The interline compensating components equalize the voltages of parallel lines at their substation terminals. In compensated networks there is, in addition, a decaying DC-transient of the suppression coil circuit (Lehtonen 1992). This component is usually at its highest, when the fault takes place close to voltage zero. If the coil is saturated, the current may also include harmonics.

The charge transient component is best suitable for fault location purposes. The charge component has a lower frequency and it dominates the amplitudes of the composite transient. If we suppose, that fault is located at the 110/20 kV substation, the angular frequency of the charge component in the undamped conditions can be calculated as follows (Pundt 1963, Willheim & Waters 1956), see Fig. 11:

$$\omega_c = \frac{1}{\sqrt{L_{eq} C_{eq}}} = \frac{1}{\sqrt{3L_T \left(C + C_E\right)}} \tag{15}$$

where

$$L_{eq} = 1.5 L_T ; \qquad C_{eq} = 2\left(C + C_E\right) \tag{16}$$

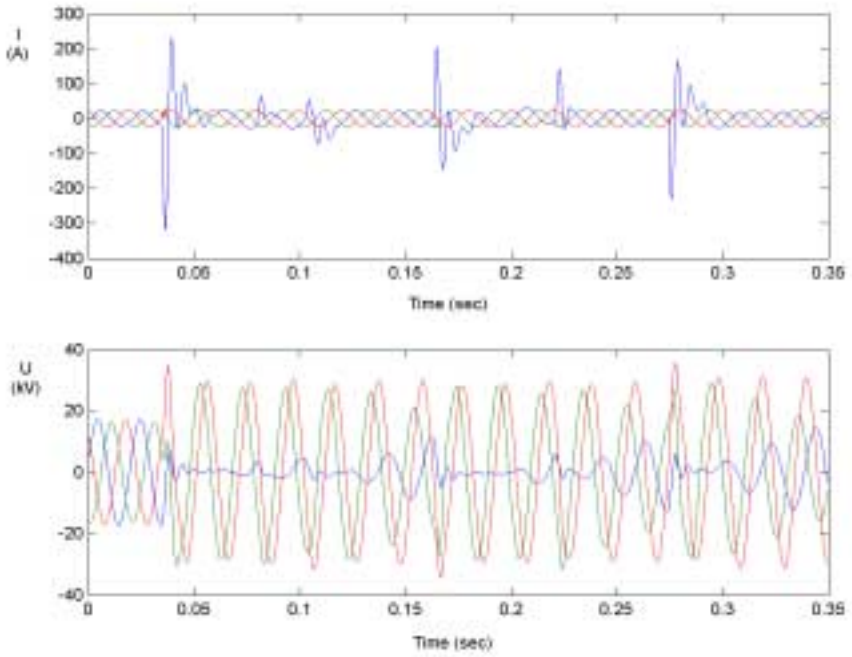

Figure 10. Transient phenomenon in the phase currents (I) and phase voltages (U) recorded in a compensated network.

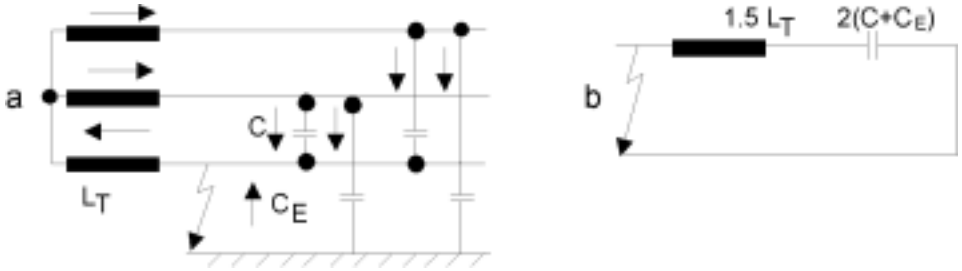

Figure 11. The network model for the charge transient (a) and the corresponding circuit (b).

and where L_T is the substation transformer phase inductance, C is the phase to phase capacitance and C_E is the phase to earth capacitance of the network. If the fault happens at the instantaneous voltage maximum, the transient amplitude is

$$\hat{i}_c = \frac{C_{eq}\omega_c}{3C_E\omega_f} I_e \qquad (17)$$

where ω_f is the fundamental frequency and I_e is the uncompensated steady state earth fault current. The amplitude depends linearly on the frequency ω_c. Since it is not unusual for this to be 5000 rad/s, the maximum amplitudes can be even 10–15 times that of the uncompensated fundamental frequency fault current.

In real systems there is always some damping, which is mostly due to the fault resistance and resistive loads. Damping affects both frequencies and amplitudes of the transients. The critical fault resistance, at which the circuit becomes overdamped, is in overhead line networks typically 50–200 Ω, depending on the size of the network and also on the fault distance. If the resistive part of the load is large, damping is increased, and the critical resistances are shifted into a lower range. Basically the distribution network is a multi-frequency circuit, since every parallel line adds a new pair of characteristic frequencies into the system. These additional components are, however, small in amplitude compared to the main components. According to the real field tests, the amplitudes of charge transients agreed with equation 17 (Lehtonen 1992). In the case of the discharge component the amplitude was typically 5 to 10% of the amplitude of the charge component. The fault initial moment, i.e. the instantaneous value of the phase voltage, affects the amplitude of the transients. However, the faults are more likely to take place close to the instantaneous voltage maximum, when the amplitudes are relatively high. The frequencies varied through a range of 500–2500 Hz and 100–800 Hz for discharge and charge components respectively.

2.8 Measurements in distribution utilities

The characteristics of earth faults were determined based on long-term surveys in real distribution networks. The developed indication and location methods were tested using field test with artificial faults. The methods were also in pilot use in real networks. The measurements were carried out together with VTT, ABB Substation Automation Oy and distribution utilities. ABB Substation Automation Oy supplied the recorder equipment and measuring instruments. The phase currents and voltages were measured from the secondary of the

matching transformers of the protection relays. The zero sequence voltage was measured from the open delta secondary of the three single-phase voltage transformers. In the following, a short summary of the measurements is presented.

Real earth faults were recorded at the Gesterby substation of Espoo Electricity, where the distribution network is isolated, and at the Gerby substation of Vaasa Electricity, where the distribution network is compensated during the years 1994–1996 and 1998–1999. The recorders were triggered if the predetermined threshold value of neutral voltage was exceeded. In the case of fault, phase voltages and currents, neutral voltage and residual currents were measured from the feeders surveyed. In the last mentioned recording project, recorders were additionally triggered regularly at 10-minute intervals, so that the network parameters could be determined also in normal network conditions, see papers A and B. Altogether 732 real disturbances were recorded.

During the years 1995–1996, the developed prototype system for the neutral voltage survey was in test use at the Renko and Lammi substations of Häme Electricity and at the Honkavaara and Kitee substations of North Karelia Electricity. In the former case the neutrals were isolated and in the latter case compensated. The measuring system consisted of the disturbance recorders and PC in the substation with modem connection via telephone network to VTT. Phase voltages of 0.14 sec periods were recorded with 1.5 kHz sampling rate at the one minute interval. The data were analysed at the substation. Together 227 neutral voltage variations were detected. These data were used for development of high resistive earth fault indication methods, see Paper C.

High resistive earth fault field experiments were carried out during the normal network conditions at the Lammi substation of Häme Electricity 14.11.1995 and at the Maalahti substation of Vaasa Electricity 9.5.1996, where the distribution networks are unearthed. Field tests were also carried out at the Kitee substation of North Karelia Electricity 11.9.1996, where the distribution network is compensated. During the tests, fault resistances from 20 to 220 kΩ with 20 kΩ steps were connected to each phase of the three phase systems in turn at a distant line location. At the Lammi substation, so-called tree experiments were also made, where each phase of the line was connected to a growing tree. Simultaneously, the phase voltages, neutral voltage and residual current of faulty

feeder were recorded. At the Kitee substation additionally, the residual currents of five parallel feeders were measured. In the case of Maalahti and Kitee, one phase voltage and phase currents of the faulty line were also measured at one pole-mounted disconnector substation. The test data were recorded using both 1.5 kHz and 10 kHz sampling rate at the Lammi substation. In the other substations, the sampling rate was 500 Hz. The measurements were made with one 8-channel Yokogava measuring instrument and with three 4-channel digital storage oscilloscopes, see Papers C and D.

For testing the fault distance computation algorithms, the same earth fault test data were used as reported in Lehtonen (1992). These field experiments were carried out in South-West Finland Electricity 19.–20.6.1990 where the distribution network is partially compensated, in Vaasa Electricity 11.–12.12.1990 where the distribution network is compensated and in Espoo Electricity 18.–19.12.1990 where the distribution network is unearthed. The same experiments were repeated many times with different fault resistances and line locations. The voltage and current of the faulty phase were measured with 20 kHz sampling rate, see Papers E–G.

3. Characteristics of the earth faults based on the measurements

To develop protection and fault location systems, it is important to obtain real case data from disturbances and faults that have occurred in active distribution networks. In this chapter the characteristics of earth faults are analysed based on comprehensive and long-term recordings. In addition, the characteristics of the faults are discussed which can be exploited for high resistance fault indication and location and, in the case of low resistance faults, for fault distance estimation.

3.1 Fault recording

The characteristics of earth faults and related disturbances were studied by recording disturbances during the years 1994–1996 and 1998–1999 in networks with an unearthed or a compensated neutral. The networks were mainly of overhead construction, with a smaller share of underground cables. The recorders were triggered when the neutral voltage exceeded a threshold value. In the first recording project, see Paper A, due to the size of the sample files and to the slowness of the telecommunication system, the detection sensitivity had to be set relatively low. Therefore, a large part of the high resistance faults was lost. In the second project, see paper B, the current and voltage samples were analysed at the substation immediately after their recording. The sensitivity of the triggering could be increased, resulting in a more comprehensive recording of the high resistance faults.

In the occurrence of disturbances, the traces of phase currents and voltages, and neutral currents and voltages were recorded at the faulted feeder. In what follows, the clearing of earth faults, the relation between short circuits and earth faults, arc extinction, arcing fault characteristics, the appearance of transients, and the magnitudes and evolving of fault resistances are discussed.

3.2 Fault clearing

During the recording projects, altogether 732 real case events were recorded from the feeders under surveillance. The majority of the disturbances disappeared of their own accord without any action from the circuit breaker. If these temporary disturbances were to be excluded, the division of faults into earth faults and short circuits would be about 70% and 30% in the unearthed network, and about 60% and 40% in the compensated network, respectively, see Figs. 12 and 13. This division is dependent on the network circumstances, which were equally divided into fields and forests in the case of the surveyed lines. Paper A shows contrary results acquired from a third power company, where 74% of the faults were short circuits and 26% earth faults. Here the number of faults was acquired with the aid of numerical relays in the substations. The lines were in the majority located in forests, and the period surveyed was about three years. About 82% of the earth faults that demanded the action of a circuit breaker were cleared by auto-reclosing and 17% of the earth faults were permanent. The share among permanent faults was fifty-fifty between earth faults and multiphase faults.

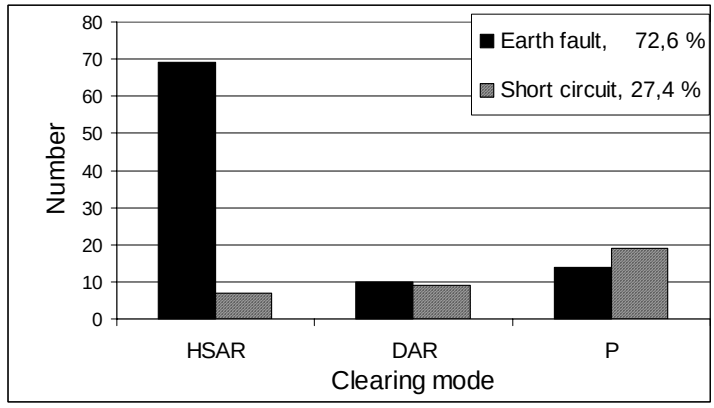

Figure 12. Number of the disturbances classified by means of clearing in the unearthed network (HSAR = high-speed auto-reclosure, DAR = delayed auto-reclosure, P = permanent fault).

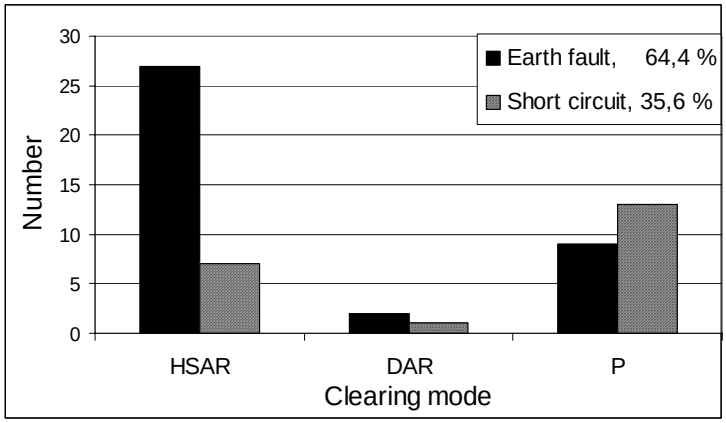

Figure 13. Number of the disturbances classified by means of clearing in the compensated network.

The aforementioned figures are possible to compare to the statistics of the Finnish Electricity Association Sener (2000) concerning only the permanent faults. The outage statistics of Sener cover 83.6% of the feeder length in the medium voltage distribution networks of the whole country. According to these statistics, the share between permanent earth fault and multiphase fault was 46% and 54%, respectively, and taking into account only the regional unearthed networks, 48% and 52%.

3.3 Fault resistances

There are clearly two major categories of earth faults, see Figs 14 and 15. In the first category, the fault resistances are mostly below a few hundred ohms and circuit breaker tripping is required. These faults are most often flash-overs to the grounded parts of the network. Distance computation is possible for these faults. In the other category, the fault resistances are in the order of thousands of ohms. In this case, the neutral potentials are usually so low that continued network operation with a sustained fault is possible. The average time from a fault initiation to the point when the fault resistance reached its minimum value was below one second. The starting point for a disturbance was when the neutral voltage exceeded the triggering level. The disturbances developed very quickly and, as a whole, the fault resistances reached their minimum values in the very

beginning of the disturbances. However, some faults evolve gradually. Paper C shows the computed fault resistances for the real case disturbances which were caused by a broken pin insulator, snow burden, downed conductor, faulty transformer or tree contact. These faults could be detected from the change in neutral voltage many hours before the electric breakdown. The last mentioned results were acquired from a neutral voltage survey at four substations belonging to North-Karelian Electricity and Häme Electricity during the years 1995 and 1996.

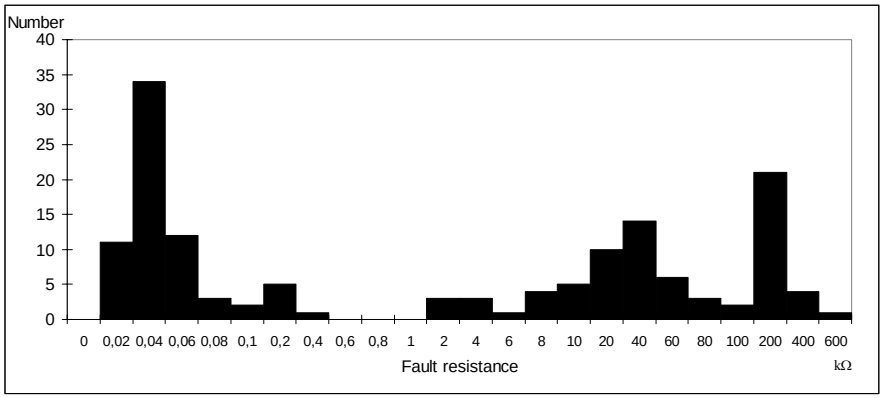

Figure 14. The division of the fault resistances in the unearthed network recorded during the years 1994–1996.

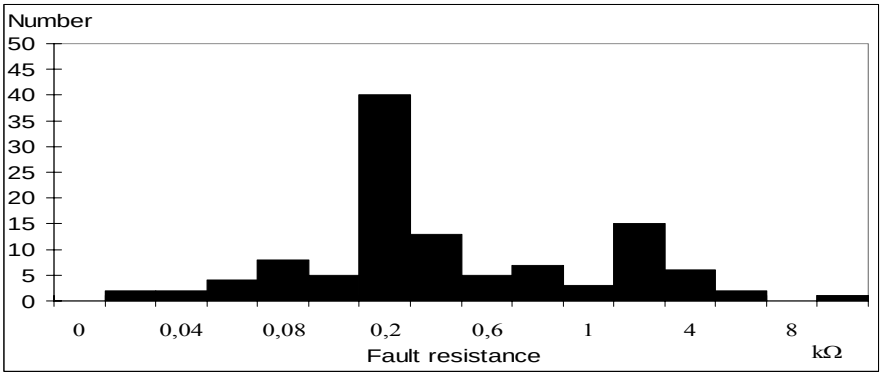

Figure 15. The division of the fault resistances in the compensated network recorded during the years 1994–1996.

3.4 Arcing faults

In an arcing earth fault, the arc disappears at the current zero crossing, but is immediately re-established when the voltage rises. In the isolated neutral network, about 67% of the disturbances were arcing faults. The average duration of the arcing current was approximately 60 ms. In the compensated network, the corresponding figures were 28% and approximately 30 ms. The overvoltages in the unearthed network were higher than in the compensated neutral network, and more than double the normal phase voltage. An arcing fault creates an increase in the harmonic levels of the feeder. In particular, high resistance arcing faults are highly random as viewed from their current waveforms. This is due to the dynamic nature of the unstable interface between the phase conductor and the fault path. Mechanical movement, non-linear impedance of the fault path and arc resistance affect the fault current and make the time domain characteristics of the fault appear to be random, see Fig 16.

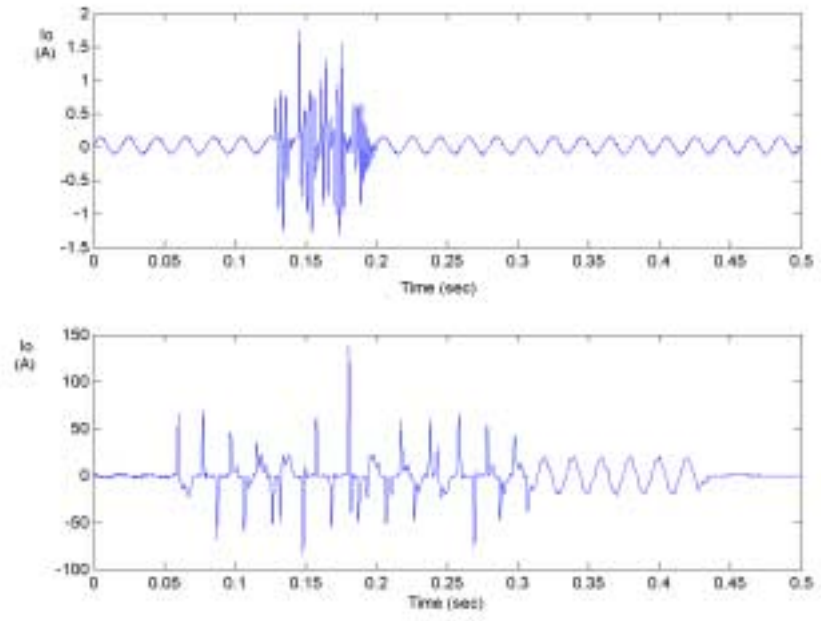

Figure 16. Zero sequence current I_0 during a high resistance arcing fault (upper curve) and during a low resistance arcing fault (lower curve), recorded in the unearthed network.

3.5 Autoextinction

An earth fault arc can extinguish itself without any auto-reclosing function. One indication of autoextinction is subharmonic oscillation in the neutral voltage, showed in Paper B (Poll 1983). This oscillation is due to discharge of the extra voltage in the two sound phase-to-earth capacitances via the inductances of the voltage transformers. In the case of autoextinction, the average and maximum measured residual currents were 0.9 A and 9.5 A in the unearthed network, and 5.7 A and 23.8 A in the compensated network, respectively, see Fig. 17. In unearthed network, 95% of disturbances extinguished in shorter time than 0.3 sec. High resistance faults disappeared noticeably more slowly in the compensated network. About 50% of faults lasted less than 0.5 sec and 80% of the faults less than 1 sec. Especially in the unearthed systems, the maximum currents that allowed for autoextinction were clearly smaller than had previously been believed, see Fig. 9 (Poll 1984). It must be taken into account that, in the unearthed network, surge arresters were used for overvoltage protection, whereas in the compensated neutral system spark gaps were used. The difference to the earlier reported results is that they were determined from artificial earth fault test whereas the results of Fig. 17 were measured from real earth faults.

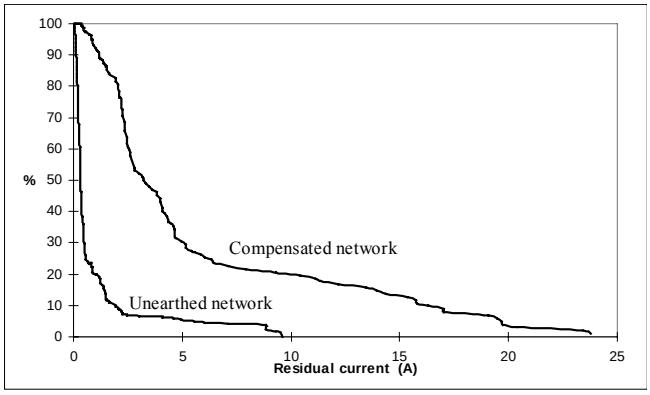

Figure 17. Cumulative characteristic of faults which extinguished themselves versus maximum residual current.

The maximum capacitive earth fault current in the unearthed network under surveillance was either about 70 A or 35 A. This was due to the fact that during the heavy electrical load, the distribution network of the substation was divided

into two calvanically isolated parts. In the compensated network, the maximum earth fault current was about 23 A (with zero fault resistance). The downward slopes of the curves in Fig. 17 may primarily be due to faults to uncontrolled parts of the network, where fault resistance is high and the air gap is smaller than in the case of the faults to grounded parts of the network equipment. The low current values in the case of autoextinction may also be due to the relay settings, which allowed short time only for arc in the case of low resistive faults. The delay of the high-speed autoreclosure was 0.4 s in the unearthed network and 0.6 s in the compensated network. However according to earlier studies, the maximum current for autoextinction, which was measured in real unearthed network, was 5 A (Poll 1984, Haase & Taimisto 1983). According to this study, 95% of earth faults extinguished itself, when the earth fault current was 5 A or lower in the unearthed network.

3.6 Transients

The transient components of the voltages and currents are based on the charging of the capacitances of the two healthy phases and the discharging of the faulted phase's capacitance. Transients could be detected in nearly all fault occurrences that demanded the function of the circuit breaker, see Fig 18. In addition, about 70% of the transients were oscillatory, see Paper A. These characteristics of the transient phenomenon can be made use of in the relay protection systems and in fault location. The fault distance computation using transients was possible in all permanent fault cases. For these, the charge transient frequency varied in the range of 246 Hz to 616 Hz.

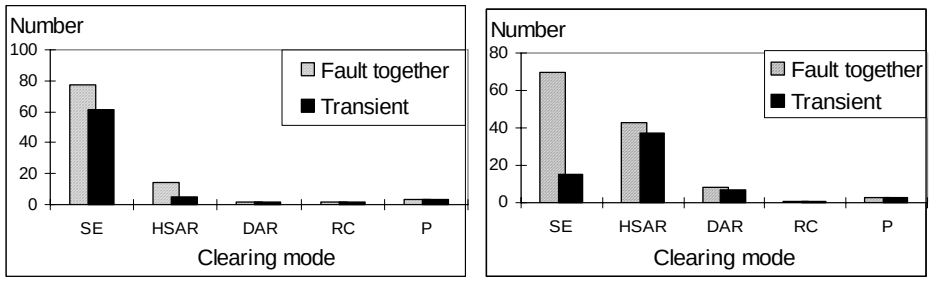

Figure 18. Appreance of transients classified by means of fault clearing in the compensated network (left) and in the unearthed network (right) recorded during the years 1994–1996.

3.7 Discussion of the characteristics

The characteristics were mainly determined for 20 kV networks of overhead construction, with a smaller share of underground cables. In the unearthed network, more than a half of the disturbances were arcing faults. These can lead to overvoltages higher than double the normal phase to ground voltage. Only a few arcing faults occurred in the compensated network. An arcing fault creates an increase in the harmonic levels in the feeder. The performance of the protection relay algorithms is dependent on obtaining accurate estimates of the fundamental frequency components of a signal from a few samples. In the case of an arcing fault, the signal in question is not a pure sinusoid and thus can cause errors in the estimated parameters (Phadke & Thorp 1990). Harmonic content can be exploited for fault indication purposes in high resistance faults.

An earth fault arc can extinguish itself without any auto-reclosing function and interruptions can thus be avoided. Especially in the unearthed systems, the maximum currents that allowed for autoextinction were, in spite of the use of surge arresters, clearly smaller than had previously been believed. Fault resistances fell into two major categories, one where the fault resistances were below a few hundred ohms and the other where they were in the order of thousands of ohms. In the first category, faults are most often flash-overs to the grounded parts of the network. Distance computation is possible for these faults. The hazard potentials usually are so low for disturbances in the other category that continued network operation with a sustained fault is possible. The fault resistances reached their minimum values in the very beginning of the disturbances. However, some faults evolve gradually, for example faults caused by a broken pin insulator, snow burden, downed conductor, or tree contact. These faults are possible to detect from the change of neutral voltage before the electric breakdown. Transients could be detected in nearly all fault occurrences that demanded the function of the circuit breaker. In addition, about 70% of the transients were oscillatory. Characteristics of these phenomena can be made use of in the relay protection systems and in fault distance estimation.

4. Methods for high impedance earth fault indication and location

High impedance faults are difficult to detect with conventional overcurrent or neutral voltage protection devices because the zero sequence voltage or the fault current may not be large enough to activate them. In the past two decades many techniques have been proposed to improve the detection and location of these faults in distribution systems (Aucoin & Jones 1996). A short review of the existing methods is presented in Section 4.1. In Section 4.2, a new method is presented for the detection and location of high resistance permanent single-phase earth faults. We have developed the method further in Sections 4.3 and 4.4, and two alternative probabilistic approaches are proposed for the faulty feeder and line section location.

4.1 Review of the indication and location methods

The conventional method for permanent, high impedance fault detection is to use zero sequence overvoltage relays or to monitor the slight and fast variations in the neutral voltage. The faulted feeder can be found by transferring the supply of one feeder at a time to another substation and by observing the biggest change in the neutral voltage (Lamberty & Schallus 1981). However, this is time consuming. The other indication and location methods proposed in the literature, are based on the direct measurement of the basic components of the currents and voltages, on analysing their variations or their harmonic components with different methods, or on mixed versions of these methods.

4.1.1 Direct measurements of the electric quantities

The ratio ground relay concept, as implemented in the prototype relay, relies on tripping when the ratio of $3I_0$, the zero sequence current, to I_1, the positive sequence current, exceeds a certain pre-set level. This concept is implemented using an induction disc type relay with two windings. The operating winding produces torque proportional to $(3I_0)^2$ and the restraint winding produces torque proportional to $(I_1)^2 - (I_2)^2$. The two opposing torques produce the ratio trip

characteristic desired (Lee & Bishop 1983). The sensitivity of the method in an earth fault test was only 700 Ω. ABB (1997, 1995) has equipped some relays and fault indicators with a definite time current imbalance unit. Monitoring the highest and the lowest phase current values detects the imbalance of the power system i.e. the imbalance = $100\%(I_{L\max} - I_{L\min})/I_{L\max}$. Primarily, the algorithm is intended to indicate a conductor break, which can lead to a high impedance fault in the overhead network.

Roman & Druml (1999) have developed a so-called admittance method for the compensated networks, which measures the zero sequence currents of all feeders of the bus centrally. In addition, the phase and zero sequence voltages are required as a reference. Out of these values, the zero sequence admittances for each feeder are calculated and continuously monitored. The feeder with the highest alteration of the zero sequence admittance is identified as the faulty feeder. It is also possible to locate the fault point by connecting the faulted line and one sound line to a loop. The measured zero sequence current differences in the beginning of the looped lines are proportional to the ratio of the zero sequence admittance up to the fault location. The system detected faults of 30 kΩ in real field tests. Nikander & Järventausta (1998) and Nikander et al. (2000) have used the same principles for compensated and unearthed networks. Every feeder terminal operates independently, with no need to transfer information between the feeder terminals or between feeder terminals and upper level automation systems before indication of an event. Faults of 186 kΩ were reported to be detected and located in the preliminary field tests.

High resistance permanent earth faults in compensated systems can be detected by observing the neutral to ground voltage (Winter 1988). Three parameters, the mismatch, the damping (Brandes & Haubrich 1983) and the imbalance (Poll 1981, 1983) illustrate the symmetrical conditions of the network. The characteristic of the relative neutral voltage as a function of the mismatch is a tangent circle of the neutral point. It can be determined by measuring the change of the neutral voltage, when a small serial reactance is switched on to the suppression coil for a short time. The other parameters, the imbalance and the damping can be determined from the characteristic. The damping is the ratio of the resistive leakage current to the capacitive zero sequence current. The resistive earth fault changes the damping parameter. This can be detected by

continuously monitoring the neutral voltage characteristic. The sensitivity of the method was reported to be about 130 kΩ (Winter 1988).

Leitloff et al. (1997) developed three different algorithms to detect resistive faults and to select the faulty feeder in a compensated network. The static algorithm is based on a vector comparison of the residual currents in all the feeders. This comparison is carried out by taking a reference phase constructed from the sum of the residual currents of all the feeders, which is equal to the neutral current. The sensitivity was about 33 kΩ. The variant of the static algorithm is identical to the basic version but it is applied to the variations of the measured electrical quantities. The third algorithm enables fault detection by using the phase to ground admittance. As with the dynamic version, it makes use of the variations of the residual current. In addition to that, the variation of the neutral to ground voltage, the phase to ground voltages and the values of the global phase to ground admittances of the feeders before the fault occurrence are needed. It requires a periodic injection of a residual current by an automatic tuning system for the arc suppression coil (Chilard et al. 1999). The sensitivity of the last two mentioned algorithms was reported to be about 100 kΩ (Leitloff et al. 1994). The compensated systems pulse method, where the compensation degree is altered in a pulse-wise manner, can also be used for the identification of the faulty line (Christgau & Wolfenstetter 1982, Crucius & Kries 2001).

4.1.2 Harmonic analysis

High impedance ground faults generate harmonics because of a nonlinear resistance at the conductor-ground interface. Jeerings & Linders (1990) proposed that the change in the phasor value of the third harmonic current component is a sufficient criterion for fault indication in many cases. The harmonic change is measured by comparing a signal, which is averaged over a short period of time (1–2 seconds) with one averaged over a longer period (20–30 minutes) in one relay application (Atwell et al. 1990). A relay sensitivity of 1% of the current transformer rating has been achieved (Reason 1994). Yu & Khan (1994) used the magnitudes of the 3^{rd} and 5^{th} harmonic currents and the angle of the 3^{rd} harmonic current.

In frequency domain analysis, using Fourier transforms, many methods compare the odd harmonics or non-harmonics of the phase current. Russell et al. (1988) have used the 180 Hz and 210 Hz harmonic components. The fundamental frequency of the electric power system in this latter case was 60 Hz. Shiping & Russell (1991) proposed the energy algorithms, which monitor the energy variations of the phase current at a particular frequency or frequency band in the range, 2–10 kHz. The time is used as an element to discriminate high impedance faults from normal system events. A detector is also designed for monitoring the energy variance for the second, fourth and sixth harmonics of the residual current $3I_0$, and by requiring the increment of randomness of all these harmonics to indicate the fault (Lien et al. 1999). Randomness algorithms exploit the accompanying arc phenomena of intermittent arc re-ignition and extinction in the frequency band from 2 kHz to 3.6 kHz (Benner et al. 1989). Sultan et al. (1994) designed an arcing fault detector, which exploits the random behaviour of the fault current by comparing the positive and negative current peaks in one cycle to those in the next cycle, in order to measure the flicker and the asymmetry. Girgis et al. (1990) applied Kalman filtering theory to obtain the best estimation of the time variations of the fundamental and harmonic components, so as to avoid errors caused by conventional Fourier or classical filtering.

The algorithms mentioned above are not fully successful. This is either because of being unable to detect high impedance faults with very low current or is due to false tripping during normal system switching events, which produce similar transients to those of high impedance faults (Russell & Chinchali 1989). To mitigate these problems, Russell & Benner (1995) recommended a comprehensive expert system, which combines the above algorithms. A commercial device is also available (Benner & Russell 1997).

Recently, some new methods have been proposed for the purpose of better fault detection. Kim & Russell (1995) developed an algorithm to analyse the transient behaviour of various events on distribution feeders by quantifying wave distortion with the crest factor. Mamishev et al. (1996) and Huang & Hsieh (2001) have described some applications of the concepts of fractal geometry to analyse the chaotic properties of high impedance fault currents. The existence of chaotic behaviours are proved by evaluating fractal dimensions and the phase plane (Ko et al. 1998). Jota & Jota (1998) developed a fuzzy reasoning system

for the analysis of the feeder responses to impulse waves, which are periodically injected at the feeder inlet. These responses are compared to standard responses, which were previously stored in a database in the frequency range from 6 kHz to 12.5 MHz.

Because of fast response and efficient learning, Artificial Neural Networks have been applied in several electric power applications. Sultan et al. (1992) trained a neural network based detector using the Backpropagation algorithm, and Butler et al. (1997) used supervised clustering based neural networks. Wai & Yibin (1998) have used wavelet transform, which features variable time-frequency location rather than the windowed Fourier Transform. The transient signal can be decomposed in both the time and frequency domains via the wavelet transform, enabling more efficient monitoring of fault signals as time varies. The proposed methods have been applied to discriminate high impedance faults from normal switching events (Huang & Hsieh 1999). Vaughan & Moore (2000) have proposed a detection system based on very low frequency radio waves (VLF) from 3 kHz to 30 kHz. Shihab & Wong (2000) and Tungkanawanich et al. (2000) have proposed systems utilising the very high frequency radio waves (VHF), from 30 MHz to 300 MHz, released during arcing faults.

4.2 Neutral voltage and residual current analysis

A new method for high resistance fault detection and location, based on the change of neutral voltage and zero sequence currents, is presented in Paper C. The method consists of two independent algorithms, called neutral voltage analysis and residual current analysis.

The fault impedance $\underline{Z}_f$, of the neutral voltage analysis algorithm, can be determined in terms of the measured positive-sequence and zero-sequence voltages, and the zero-sequence impedance of the network as follows (Lehtonen 1998):

$$\underline{Z}_f = \left(\frac{\underline{U}_1}{\underline{U}_0} - 1 \right) \underline{Z}_0 \tag{18}$$

where $\underline{Z}_0$ is the zero-sequence impedance of the network**.** In an unearthed network, $\underline{Z}_0$ is the parallel connection of the phase-to-ground capacitances and phase-to-ground resistances, the so called ”leakage resistances”. For systems earthed via a Petersen coil, the circuit must be complemented with parallel connection of the coil impedance. For the detection of a high resistance earth fault, it is essential to determine the resistive part of the fault impedance. In eq. (18), $\underline{U}_0$ represents the phasor sum of the phase voltages and $\underline{U}_1$ is the positive sequence component of the phase voltage, measured at the moment considered. Applying eq. (18) for three times and using for $\underline{U}_1$ the following values: $\underline{U}_1$, $\underline{a}\underline{U}_1$ and $\underline{a}^2\underline{U}_1$, the faulted phase can also be determined. Here $\underline{a}$ is the phase shift operator, $\underline{a} = 1 \angle 120^o$.

From the three calculated values of $\underline{Z}_f$, the resistive part shows the highest value in the faulted phase. Because the fault impedance must be resistive, the calculated resistive parts of $\underline{Z}_f$ for the other two ”healthy” phases are negative. The triggering level of the algorithm is set so that a high resistance earth fault is indicated, if the calculated maximum real part of $\underline{Z}_f$ is smaller than the fixed threshold value and is at least four times the magnitude of the imaginary part of the corresponding $\underline{Z}_f$.

The detection of very high fault resistances is difficult due to the neutral voltage present in the normal network conditions. This is mainly caused by the natural imbalances of the feeders. The sensitivity of the method can be improved by using the change in the neutral voltage, which is determined as a difference between the real neutral voltage in the network at the moment being considered and the corresponding mean value of the last ten minutes. After calculation of the fault impedance $\underline{Z}_f$, and supposing that the fault resistance is very much higher than the network zero sequence impedance ($\underline{Z}_f >> \underline{Z}_0$), the earth fault current can be solved as follows

$$\underline{I}_f = \frac{\underline{U}_1}{\underline{Z}_f} \tag{19}$$

The faulted feeder is most often located by comparison of the residual current magnitudes. The residual current algorithm presented in Paper C utilises the simultaneous changes of neutral voltages and residual currents. The idea of the

algorithm is to compensate the effect of the earth capacitances by using the measured change of the neutral voltage and the known zero sequence impedance of the feeder under consideration (Lehtonen 1999).

$$\Delta \underline{I}_{0i} = \Delta \underline{I}_{0im} - \frac{\Delta \underline{U}_{0m}}{\underline{Z}_{0i}} \tag{20}$$

where $\Delta \underline{I}_{0i}$ is the compensated zero sequence current of the feeder i, $\Delta \underline{I}_{0im}$ is the measured change of zero-sequence current of the feeder i, $\Delta \underline{U}_{0m}$ is the measured change in the neutral voltage (zero sequence voltage) and $\underline{Z}_{0i}$ represents the zero-sequence impedance of the feeder i (including both the earth capacitance and leakage resistance).

Depending on the measurement accuracy, the resulting compensated current of a healthy feeder is nearly zero and in the case of the faulty feeder, it corresponds to one third of the earth fault current at the fault point. This method can also be used to discriminate the faulty line section, if the disconnector stations are provided with modern remote terminal units. This method requires accurate knowledge about the zero sequence impedances of each feeder. An advantage of the method is that, in the case of auto-reclosure, modern relays restore the values of the neutral voltage and zero sequence currents in the healthy feeders. These values can be used to update the zero sequence impedance data. When combining this information with the knowledge of the compensated zero sequence currents and the faulty phase, a very powerful means for detecting the faulty feeder, and further the faulty branch of the line, can be implemented.

4.3 Probabilistic approach

In the case of very high fault resistances, the magnitudes of the compensated feeder currents are small. Therefore, instead of direct comparison, it is more reasonable to quantify a probability estimate of whether the feeder concerned has failed. The compensated current values of the feeders and the estimated fault current are later regarded as random variables. These are assumed to be independent and identically distributed random variables obeying Normal distributions, with parameters μ = mean and σ^2 = variance (Taylor & Karlin

1984). In Paper D, two different probabilistic methods, the point probability method and the overall probability method, are presented.

In the point probability method, the expected fault current is modelled by a fixed value I_f. For the method, two different probability density functions are defined. Let $i = 1, \ldots, n$ denote feeders at the substation and variables $x_1, \ldots, x_n$ the possible compensated current values. Now, the current density function of a "healthy" feeder is denoted by $f_0(x)$. Since the compensated current values of the sound feeders should be zeros, the mean of $f_0(x)$ is also taken to be zero, i.e., $\mu_0 = 0$. The second probability density function is that of the faulty feeder, denoted by $f_1(x)$. In this case, the mean value should be equal to the expected fault current, $\mu_1 = I_f$.

Assuming that there is one fault in the network, the probability that feeder i has failed is, according to the Bayesian theorem (Box & Tiao 1973):

$$\Pr\left(\textit{feeder i has failed} \middle| I_{01},\ldots,I_{0n}\right) = \frac{\dfrac{f_1(I_{0i})}{f_0(I_{0i})}}{\displaystyle\sum_{i=1}^{n}\frac{f_1(I_{0i})}{f_0(I_{0i})}} \tag{21}$$

The point probabilities, in the cases of healthy and faulty feeders, are obtained by substituting the compensated current values I_{0i} to the normal distribution density functions $f_0(x)$ or $f_1(x)$, respectively.

In the second method, the expected fault current value I_f is no longer fixed but is assumed to be a random variable having a normal density function. Instead of the point probability value $f_1(x_i)$, the expected value $\overline{f_1(x_i)}$ is used.

$$\overline{f_1(x_i)} = \frac{1}{\sqrt{2\pi\left(\sigma_{1C}^2 + \sigma_{1U}^2\right)}} e^{-0.5\left(\frac{\mu_{1C}-\mu_{1U}}{\sigma_{1C}^2+\sigma_{iU}^2}\right)^2} \tag{22}$$

where μ_{1C}, σ_{1C}^2 and μ_{1U}, σ_{1U}^2 are the corresponding parameters of the normal distribution functions of the feeder current and expected fault current. In this

case, the mean values of the fault currents are supposed to be $\mu_{1U} = I_f$ and $\mu_{1C} = I_{0i}$.

When the maximum and minimum observed values of the compensated feeder currents, $I_{\max}$ and $I_{\min}$, are not taken into account, the sound feeder current variance is calculated as follows:

$$\sigma_0^2 = \frac{1}{n-2}\sum_{i=1}^{n}(x_i - \mu_0)^2 \tag{23}$$

The failed feeder current variance is derived in Paper D as:

$$\sigma_{1C}^2 \cong \left(\frac{I_{\max}}{3I_{ave}} + \frac{2}{3}\right)\sigma_0^2 \tag{24}$$

In the case of an unearthed network, the variance σ_{1U}^2 of the current density function $f_{1U}(x)$ can be defined as:

$$\sigma_{1U}^2 \cong (1+n)\sigma_0^2/3 \tag{25}$$

Depending on the compensation degree in resonant earthed networks, the variance of the current density function can be presented as follows:

$$\frac{(1+n)\sigma_0^2}{3} \le \sigma_{1U}^2 \le \frac{(1+200n)\sigma_0^2}{3} \tag{26}$$

The lower boundary is equal to the variance determined for the unearthed network.

4.4 Prototype system

The practical implementation of the method requires a close integration of the substation SCADA with modern relays, which are designed to be used for protection and control of the distribution network. A close connection to the

remote terminal units in the line locations is needed as well. PC based prototype version for the high impedance earth fault indication and location was developed for testing and simulation purposes, and it was coded with C-language. The system based on the network configuration, which is presented in Fig. 19, where the measurable variables are also presented. The relay functions were modelled as procedures. The procedures read the network parameters and the current and voltage samples from files as input data.

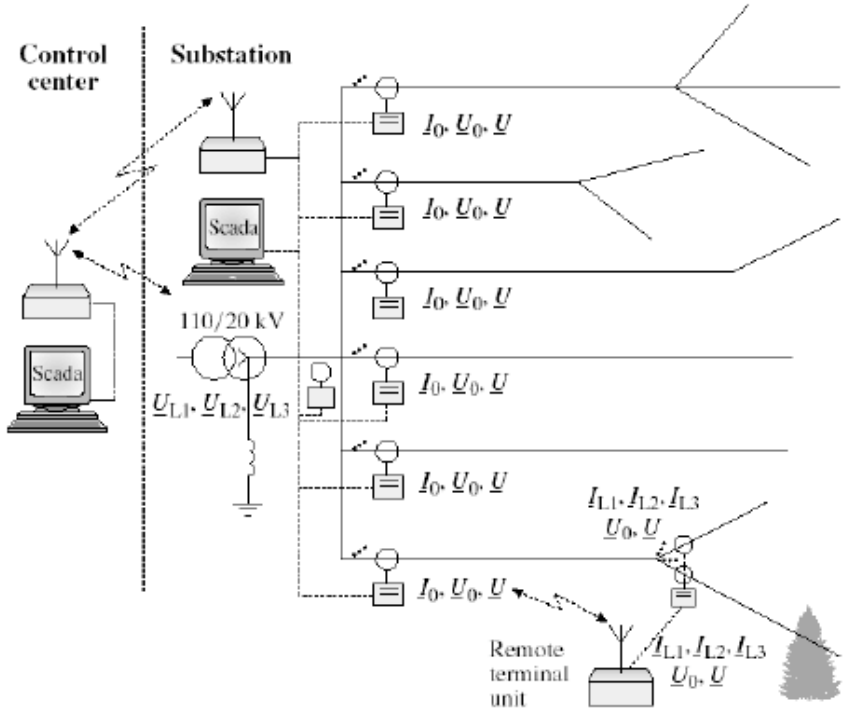

Figure 19. High resistance indication and location system.

The main functions of the prototype system consisted of the following procedures:

1. Measurement procedure in neutral voltage relay
2. Measurement procedure in feeder protection relays
3. Measurement procedure in disconnector substation

Program components in substation SCADA-computer

1) Procedure, which process the measurements and switching actions
2) Procedure, which updates the zero sequence impedances of the network and each feeder.

The computation uses the phasor form for currents, voltages and impedances. These parameters are computed as one second mean values and ten minutes sliding values. Without going to details, the high resistance indication and location system is intended to work briefly in the following way. The neutral voltage algorithm runs continuously in neutral voltage relay. It computes, among other things, the values of fault impedance, neutral voltage and its sliding mean value and the faulty phase. Also the residual current function runs continuously in each feeder protection relay and computes among other things the value of the sum current and the highest changes of the sum current and the neutral voltage during the last ten minutes. The same parameters are also computed in the disconnector terminal unit, if the feeder is equipped with remote controlled and readable disconnector. The time stamps of all measurements are also stored.

If the resistive part of the fault impedance is below the alarm or fault limit, the neutral voltage relay sends an event to the SCADA computer, which reads the value of fault impedance and the changes of neutral voltage and sum currents from each feeder and remote terminal unit. In this phase, the states of switches and connections are checked and stored. In the case of high resistive fault, the procedure of SCADA computer calculates the compensated sum current values for each feeder and if needed, for feeder branches. Using these current values, the faulty feeder or faulty branch is located based on the probabilistic method or on the magnitudes of the compensated sum currents.

In the case of auto-reclosure or permanent low resistance fault, the changes of neutral voltage and sum current of each sound feeder are stored during the fault. The SCADA procedure uses these values for updating the zero sequence impedances of the feeders and the whole network. These impedances must be also updated if the connection of network changes. Table 1 and Papers C and D show some computed results, when the earth fault test data from Kitee substation were used as an input data. The results showed that the method is able to detect and locate resistive earth faults up to a resistance of at least 220 kΩ. The first column of the Table 1 contains the exact values of the fault resistances (R_f) and

the phase to which the fault resistance was connected in the tests. The second column shows the complex phasors of the fault impedances ($\underline{Z}_f$), which were calculated from Eq. (18) using the voltage measurement values during the earth faults. The column titled ΔI_{0i} shows the compensated residual currents of the five feeders. These current values were determined by Eq. (20) and in the next column, I_f is the fault current obtained by Eq. (19).

Table 1. Detailed results for detection of the failed feeder with two alternative probabilistic method in the case of high resistance earth fault with the fault resistances 180–220 kΩ.

Phase, R_f [kΩ]	**$\underline{Z}_f$ [Ω]**	**ΔI_{0i} [A]**	**I_f [A]**	**$Pr(i\|x)_I$**	**$Pr(i\|x)_{II}$**	**Deviations**
L1 180	132970.45 - j*57056.70	0.0338 **0.1413** 0.0105 0.0350 0.0285	0.115	0.000524 0.998335 0.000179 0.000558 0.000403	0.000115 0.999673 0.000013 0.000128 0.000070	σ_o = 0.0325 σ_{om} = 0.0379 σ_{1C} = 0.0551 σ_{1U} = 0.0535 σ_{1Um} = 0.1778
L1 200	149451.84 - j*36034.95	0.0445 **0.1427** 0.0192 0.0601 0.0555	0.109	0.026388 0.881241 0.012957 0.042515 0.036899	0.006102 0.952745 0.000410 0.024173 0.016570	σ_o = 0.0538 σ_{om} = 0.0538 σ_{1C} = 0.0671 σ_{1U} = 0.0761 σ_{1Um} = 0.1545
L1 220	165731.73 - j*78135.77	0.0312 **0.1247** 0.0095 0.0307 0.0270	0.091	0.000749 0.997669 0.000254 0.000730 0.000597	0.000220 0.999419 0.000016 0.000209 0.000136	σ_o = 0.0297 σ_{om} = 0.0331 σ_{1C} = 0.0476 σ_{1U} = 0.0468 σ_{1Um} = 0.1556
L2 200	122712.48 - j*15709.50	0.0500 **0.2091** 0.0203 0.0592 0.0643	0.135	0.001931 0.991718 0.000886 0.002526 0.002939	0.001149 0.993298 0.000107 0.002248 0.003199	σ_o = 0.0581 σ_{om} = 0.0581 σ_{1C} = 0.0795 σ_{1U} = 0.0822 σ_{1Um} = 0.1778

These ones were calculated from the current and voltage values, which were measured in the beginning of the feeders at the Kitee substation. Faulty feeder is marked in bold. The column $Pr(i|x)_I$ shows the fault probability for each feeder determined by the point probability method. The corresponding probabilities $Pr(i|x)_{II}$, determined by the overall probability method, are in the following column. The last column shows the estimated deviations. The deviations σ_{0m} and σ_{1Um} are determined by iterating according to Paper D, if the initial values for the deviations were too small.

4.5 Discussion of the indication and location methods

A review of the existing techniques shows that many methods have been proposed for dealing with the high impedance fault detection problem. Several of these techniques have been implemented, either at the prototype level or at the production level; others have only been suggested. There are two distinct, competing parts to the high impedance fault problem: reliability and security. Reliability defines an algorithm's ability to detect faults sensitively, while security defines its ability to be immune from false detection when encountering a wide variety of other distribution system events. Security is at least as difficult to achieve as reliability.

Harmonic analysis cannot satisfactorily distinguish the disturbances of arcing faults from many switching events. A neural network approach, which trains the behaviour of the harmonic algorithm, still cannot successfully discriminate arcing faults and capacitor bank switching events. When encountering different disturbances, the neural network structure needs to be reorganised, plus the training process must be performed again. The reason for only partial success in discrimination is that when there is a disturbance, except in a few cases, the frequency domain information of the disturbance contains almost all the harmonic components. Thus it is not easy to find the one or two essential harmonic components that will discriminate one disturbance from another (Kim & Russell 1995). In Fourier transform based approaches where a window is used uniformly for spread frequencies, the wavelet uses short windows at high frequencies and long windows at low frequencies. In other words, by utilising wavelets, both time and frequency information can be obtained. However, the effectiveness of this method is highly dependent on the selection of a suitable

basis function. Poor selection of the basis function may inversely degrade the performance. The problems with radio waves are that the signals are greatly influenced by noise and interference from the surrounding area. In addition, the methods based on the harmonic analysis have been tested only in networks that are grounded via a small resistor.

According to experience gained from field tests in a 20 kV distribution system, the methods presented in Papers C and D are able to detect and locate resistive earth faults up to a resistance of at least 220 kΩ. The results clearly showed that in all cases, the highest fault probability was computed for the feeder where the earth fault really was. It would be possible to develop the method further to monitor the isolation state of a network continuously. From the practical point of view, the algorithms are also possible to implement to the modern numerical relays.

The problems of the algorithms, proposed in Papers C and D, are similar to those mentioned above. The drawback is that normal system activity and intermittent disturbances may cause changes to the neutral voltage and residual currents similar to the real faults in the feeders. Examples of these are normal switching actions, thunderstorms and snowfall. Thunderstorms and snowfalls can be discriminated by the fact, that they usually affect several feeders simultaneously. Using longer duration average measurements for comparison can mitigate the switching action problem, when identifying the faulty feeder or line section.

When applying the probabilistic methods, difficulties may arise if the sound feeder current distribution $f_0(x)$ is very narrow due to the small deviation. In these cases, the maximum feeder current value observed (I_{max}) does not fit the distribution, and the point probability is zero, $f_0(I_{\max}) = 0$. Problems may also occur if the deviation is too great. This is especially the case in the compensated network, where the variance σ_{1U}^2 may be too broad for the successful location of the failed feeder.

5. Low resistance earth fault distance estimation based on initial transients

One of the prime objectives when developing the automation of the distribution networks is the indication and location of earth faults. In this chapter, the fault distance estimation in radial operated networks is discussed based on charge transients. The existing solutions are first reviewed. Next, the signal pre-processing is described. The developed differential equation, wavelet and two different artificial neural network methods are then described. At the end of the chapter, the estimation accuracy of the methods is compared and the possible error sources are analysed.

5.1 Review of the fault distance estimation methods

Methods based on the calculation of the faulty line impedance, on the fault generated travelling waves, and on the Artificial Neural Networks are very promising, when the fault distance is estimated using current and voltage measurements derived from the substation in radial operated networks. In the travelling wave method, information about the fault position can be determined from the time difference between the incident travelling wave and its reflections. Bo et al. (1999) and Liang et al. (2000) have used transient voltage signals, and Xinzhou et al. (2000) have applied current travelling waves and wavelet transform. The main restrictions are the need of a very high sampling rate, in the range of MHz, and the difficulty to analyse the travelling waves and then extract the fault information if the feeder has several branches (Abur & Magnago 2000).

Ground fault initial charge transients can be utilised for line impedance estimation. Schegner (1989) presented a very promising differential equation algorithm. The second proposed technique employed Fourier-transform methods, which solve the line impedance in the frequency domain. The reactance of the faulty line length is obtained directly as the imaginary part of the impedance calculated from the corresponding frequency spectrum components of the voltage and current (Igel 1990, Igel et al. 1991). Lehtonen (1992) developed a least-squares fitting method, which uses a modification of Prony's method for estimation of the transient parameters. The average error in

field tests is reported to be a little more than 1 km when the fault resistance is 0 Ω, and the sampling rate is 10–20 kHz (Lehtonen 1995). Eickmeyer (1997) applied the neural network method trained by the transient samples of current and voltage signals. However, the accuracy of that method was tested only by simulated data.

In the following sections, four new algorithms are described. The aim of these methods is that they allow online calculations in numerical relays. The main advantage is the numerical stability and relatively small computation burden using the sampling rate of 5 kHz. The differential equation method is essentially an impedance relay algorithm and therefore, it is suitable for this purpose. The wavelet algorithm and the ANN algorithms also provide a fast response. In addition, a second ANN algorithm is proposed, which needs only one measurement per primary transformer.

5.2 Signal pre-processing

The fault distance estimation algorithms are intended to work in the feeder protection relays, in spite of the second ANN algorithm, so called ANN Uo-algorithm, which is intended to work in the zero sequence overvoltage relay. In the first mentioned case, some network periods of phase voltages and phase currents are needed to measure before and during the fault including the transient. In the case Uo-algorithm, some network periods of zero sequence voltage have to be measured. The measured voltage signal contains in addition to the fundamental both its harmonic components and the transient components. The current signal contains the following components (Lehtonen 1992):

– fundamental (50 Hz) component of the load current and its harmonics
– fundamental (50 Hz) component of the fault current and its harmonics
– charge transient component
– discharge transient component
– interline compensating transient component
– a decaying DC-transient of the suppression coil circuit.

The charge component has a lower frequency than the discharge component and it dominates the amplitudes of the composite transient. The signal pre-processing covers the extraction of the dominating transient component from the other signal parts in the following steps:

1) removal of the fundamental frequency component
2) spectrum analysis for estimating the charge transient frequency
3) low-pass filtering in order to remove the higher frequency components

For the fundamental frequency removal a straightforward technique is used: $g(t) = f(t) - f(t + T)$, where $g(t)$ is the output of the filter, $f(t)$ is the original signal and T is the period of the fundamental frequency. The spectrum analysis is performed by a Fourier algorithm, which covers only a 20 ms window, starting from the beginning of the transient. The frequency band used is from 100 Hz to 833 Hz, corresponding to a 5 kHz sampling frequency. The highest amplitude spectrum component is assumed to be the one corresponding to the charge transient frequency. The cut-off frequency of the low-pass Bessel filter is set 400 Hz higher than the estimated charge transient frequency (Schrüfer 1990). The measured signals are processed in a reversed order. Similar signal pre-processing is applied to all the algorithms considered.

5.3 Differential equation method

Differential equation algorithms solve the line inductance directly in the time domain, if three equally spaced pairs of phase current and voltage samples are available as follows (Phadke & Thorp 1990):

$$L = \frac{\Delta t}{2}\left[\frac{(i_{k+1}+i_k)(u_{k+2}+u_{k+1})-(i_{k+2}+i_{k+1})(u_{k+1}+u_k)}{(i_{k+1}+i_k)(i_{k+2}-i_{k+1})-(i_{k+2}+i_{k+1})(i_{k+1}-i_k)}\right] \tag{27}$$

The above equation yields the total inductance of the faulty line length, which in the case of a single phase to earth fault is composed of a series connection of zero-, positive- and negative-sequence inductances.

$$L = \frac{1}{3}\left(L_1^{'} + L_2^{'} + L_0^{'}\right) \cdot l \tag{28}$$

In this study, the differential equation algorithm is used in its basic form as described in Eq. 27, see Paper E. The computation is made first for a window of 12 subsequent samples. In this phase, Equation (27) is applied for 10 different three sample sets, and the average value and statistical deviation is computed for the inductance estimates. This procedure is repeated for 20 time, shifting the starting point gradually forward. The final estimate of the inductance is the one having the smallest deviation.

5.4 Wavelet method

The distance estimation is based on the computation of the wavelet coefficients for voltage and current transients, see Paper E. The discrete wavelet transform was used to find the complex wavelet coefficients W_s. Let us call Δt the sampling period, k and n are integers, and f_c is the estimated charge transient frequency. For a chosen frequency f and for a "location" of wavelet $k\Delta t$:

$$W_s(k\Delta t, f) = \sum_n s(n\Delta t) \cdot \sqrt{f / f_c} \cdot \overline{\Psi}\left[(f / f_c) \cdot (n\Delta t - k\Delta t)\right] \cdot \Delta t \tag{29}$$

After examination of several kinds of wavelet (Chui 1992, Rioul & Vetterli 1991, Weiss 1994), the following complex "mother wavelet" $\Psi(t)$ was chosen (Chaari et al. 1996):

$$\Psi(t) = \left(1 + \sigma|t| + \frac{\sigma^2}{2}t^2\right) e^{-\sigma|t|} e^{i\omega \cdot t} \tag{30}$$

The earth fault distance can be estimated by first calculating the inductance as follows:

$$L = \frac{1}{\omega}\mathrm{Im}\left[\frac{U_w(k\Delta t, f)}{I_w(k\Delta t, f)}\right] = \frac{1}{3}\left(L_1^{'} + L_2^{'} + L_0^{'}\right) \cdot l \tag{31}$$

The algorithm first determines the maximum wavelet coefficient of the current including the amplitude, frequency and location of the wavelet. Using this frequency with different time translations, the equivalent fault inductances are calculated with equation (31). The 2 ms inductance interval, corresponding to 10 subestimates, is then determined with the smallest standard deviation. The mean value of the inductance, which is calculated in this interval, is finally used to determine the fault distance.

The differential equation and wavelet algorithms were about one and a half years in trial use on one feeder on two substations. There occurred altogether 8 permanent earth faults for which the fault distance could be computed. The results are in Table 2. In this case the sampling frequency was only 3.7 kHz, due to the limitations of the recorders.

Table 2. Calculated fault distances in the case of real earth faults, MEK= mean absolute error in kilometers.

			Diff. equation algorithm	Wavelet algorithm
Network grounding	Exact fault distance	Fault resistance	Error	Error
	[km]	[Ω]	[km]	[km]
Compensated network	9.5	19.8	–2.4	–1.9
Compensated network	22.2	30.2	–0.1	+0.8
Compensated network	18.5	96.2	–5.2	+7.5
Unearthed network	5.8	36.7	–0.3	–4.3
Unearthed network	13.6	104.8	+3.1	–0.1
Unearthed network	4.9	27.4	–0.2	+5.6
Unearthed network	13.8	27.7	+2.7	+0.6
Unearthed network	1.1	10.9	+3.2	–0.1
			MEK = 2.2	MEK = 2.6

5.5 Artificial neural network methods

The application of Artificial Neural Network (ANN) computing to power systems has a relatively short time span of about 10 years. The applications for

protective relays are still at an exploratory stage concerning fault distance estimation in distribution networks. So far applications have been developed for fault detection and classifications (Dalstein & Kulicke 1995), distance and direction detection (Sidhu et al. 1995), autoreclosure (Yu & Song 1998) and fault location (Bo et al. 2000) in transmission systems. The survey of ANN applications to protective relaying (Kezunovic 1997, Dillon & Niebur 1996) shows that almost all the applications use the multilayer perseptron type of the architecture with the basic three layers being a typical choice. The supervised learning with the Backpropagation learning rule was selected most often with few exceptions.

When applying ANN methods for fault distance estimation a result that can be predicted is desirable. The output of the ANN is a linear knowledge of the fault distance when real measured signals are used as input values. This means that the estimating fault distance is in the range of 0 km to the length of the longest feeder presented in kilometres. Due to these facts, the supervised learning of the ANN is the most suitable for this purpose. In the case of supervised learning for real signals, the most effective learning algorithm is the Backpropagation algorithm (Eickmeyer 1997), which is also used in this study. The optimal structure of ANN, concerning the number of hidden layers, the number of neurons in a layer and the size of the input and out put vectors, can only be determined empirically.

In Papers F and G, two transient based ANN algorithms are discussed. The ANN-structure called Multilayer Perceptron is used. It consists of the input vector, one hidden layer and the output layer. Haykin (1994) has proved that in general one hidden layer is sufficient for representing any given input-output transformation. Using more than one hidden layer is necessary if the pattern recognition task seems to be quite sophisticated and if there is a large number of input neurons. The number of hidden neurons n_j was varied in the range [$10 \leq n_j \leq 30$] for different neural networks. An example for choosing the optimal number of hidden neurons empirically is presented in Fig. 20.

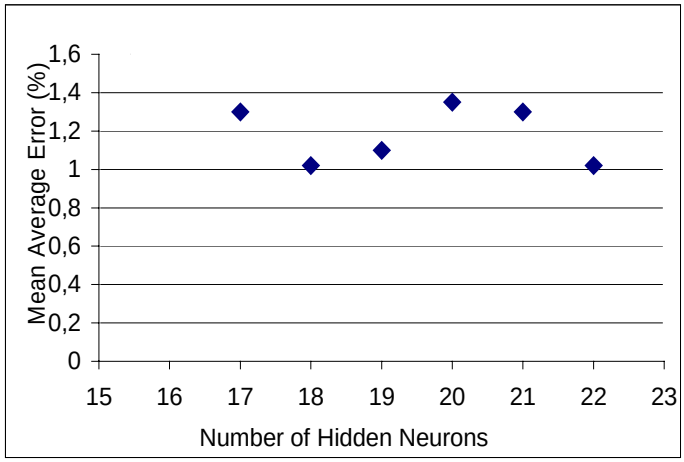

Figure 20. Mean average error in distance estimation for different numbers of hidden neurons for the network size of 300 km.

The algorithm in Paper F uses either the phase voltage or the phase voltage and current samples as input data. The second algorithm in Paper G uses the harmonic components of the neutral voltage transients as input data. As an output value, the fault distance is given by the activation of one single output neuron. The Backpropagation training algorithm provides a fast and stable training and a sufficient error decrease for the ANN. For implementation, training and verification of the ANN, the software MATLAB and its ANN toolbox were applied.

For training and testing of the ANN a large data set of voltage and current samples is necessary. The affecting parameters are varied within an appropriate range to provide the ANN with all the important features.

– fault distance: 1–40 km
– network size: 100–600 km
– load: 0–100 A
– load angle, cosΦ: 0.8–1
– network grounding: unearthed, compensated
– entrance angle: 0–90°
– fault resistance: 0.1–15Ω
– Phase: *L*1, *L*2.

Earth faults were simulated by the common simulation tool "Alternative Transients Program" (ATP-EMTP). The basic 20 kV overhead lines were modelled using the Line Constants ATP-EMTP Program and taking into account the real geometrical and electrical values.

A fault distance estimation system must be able to work properly in networks of different sizes, and under different load conditions and fault entrance angles; i.e. the phase to ground voltage angle that exists when the fault occurs. Paper F shows that, although good general performance is achievable, there was a small span in frequency and entrance angles where the ANN produced very exact results. The network size affects both the charge frequency and the amplitude of the transients. To decrease the huge training process different scaling methods were developed for the cases where input data adaptation is needed. In Paper F, the ANNs are trained either by phase voltage or phase voltage and current samples of transients, the network sizes being 150 km and 300 km for compensated and unearthed networks. The purpose of the time scaling is to move the actual frequency into the trained frequency band. Stretching or shortening the cycle period accomplishes the scaling of the frequency. For this kind of curve fitting a Pascal program that utilises the Newton method was developed. The transient current amplitude increases with enlargement of the power distribution network, but the amplitude of the transient voltage remains almost constant. The amplitude scaling factors for voltage and for current were determined by testing a number of simulated and measured data.

In Paper G, two different ANNs were trained for the network sizes of 300 km and 420 km, respectively. The purpose of the frequency scaling is to move the actual frequency into the trained frequency band. The network size and fault distance can be taken into account by utilising a linear function. The scaling factor (SF) for the spectrum of the harmonic components can be obtained as follows:

$$SF = \frac{f_0 - f_{30}}{f'_0 - f'_{30}} \tag{32}$$

The harmonic frequencies are multiplied by the scaling factor SF, meaning that the spectrum is stretched or shrunk while the amplitudes remain unchanged. The

scaled harmonic spectrum for the distance computation is finally determined by interpolation due to the fact that the harmonic frequencies must be the same as used for the ANN training.

5.6 Discussion of the distance estimation methods

It is possible to calculate an estimate for the position of single phase to earth faults. If the faulty feeder has several branches, there are also several possible fault locations. In this case, remotely read fault current indicators can complement the fault location system. In high impedance earthed networks, the charge frequency of the transient varies approximately in the range 100 to 800 Hz, and the amplitude can be as much as 15 times that of an uncompensated steady state fault current. This component is suitable for fault location purposes (Lehtonen 1992).

Four different algorithms were developed. The differential equation algorithm, the wavelet algorithm and the ANN algorithm trained by current and voltage samples require simultaneous measurements of the phase currents and voltages in the faulty feeder. The ANN algorithm, which uses the harmonic components of the neutral voltage transients, needs only one measurement per primary transformer. The developed methods were tested with the same field test data. In addition, the differential equation and wavelet algorithms were one and a half years in trial use in real network circumstances, see Table 2. Comparison of the conventional algorithms shows that both algorithms worked equally if all staged field tests are taken into account. In the case of real earth faults, the differential equation algorithms gave slightly more accurate results. Considering different earthing systems, the differential equation algorithm is more accurate in the partially compensated and unearthed networks, whereas the wavelet algorithm is better in the compensated case. The likely reason is, that transients are more oscillatory and the form of the wavelet used is more similar to the real transient in the compensated systems than in the other ones. On the other hand, the presence of the decaying DC component in the compensated network may have more influence on the calculation accuracy of the differential equation algorithm than on the accuracy of the wavelet algorithm.

The performance of the ANN methods was comparable to that of the conventional algorithms. Regarding only the earth faults with very low fault resistance, the ANN methods gave even better results, see Table 3. The mean error in absolute terms was about 1.0 km for ANN methods and about 2.0 km for the conventional algorithms in the staged field tests. The ANN with single voltage input samples reached an absolute mean error of 3.7 km. The conventional algorithms worked better with higher fault resistances. The ANN methods are also sensitive to the scaling in cases where input data adaptation is needed due to different network sizes. The usable results were achieved when the input data adaptation was small, i.e. when the scaling factor was in the range of 0.85 to 1.15.

Table 3. Comparison of different ANN methods using field test data. The errors are absolute mean values computed from the repeated earth fault tests.

Network earthing	Exact fault distance (km)	Fault resistance (Ω)	ANN methods		
			Voltage	Voltage/ current	U_0-spectrum
			error (km)	error (km)	error (km)
Compensated	0.76	0	2.4	0.7	1.7
Compensated	10.4	0	13.8	0.7	0.9
Compensated	14.2	0	2.7	1.3	0.2
Partially compensated	25.4	0	1.3	1.3	0.2
Partially compensated	36.0	0	0.9	1.0	2.5
Unearthed	13.3	47	7.9	5.9	5.0
Unearthed	20.0	47	13.8	15.2	5.8

The most important causes of errors in transient based fault distance estimation are parameter identification inaccuracy, measurement transformer errors, line model simplifications, line inductance variation and load impedances. If damping of the transient is small, the total error due to parameter identification is typically less than 2%. Fault resistance and resistive loads increase the attenuation, with a corresponding increase in the errors. In the tests, the highest fault resistance that allowed for reliable distance estimation was 50 Ω. Standard

current transformers have a good fidelity in the frequency range of transients. Unfortunately this is not always the case for voltage transformers. The errors of the line model simplifications primarily include the effect of ignored capacitances at the fault location and behind it. The maximum error due to these is, in typical overhead line networks, about 2%. One of the two major error sources is the variation of line inductances. The zero sequence inductances of an overhead line vary with the soil type and frequency. Perhaps the largest errors are, however, due to low voltage loads. Usually, neither the load devices nor their impedances during the transients are known well enough. The loads can cause large errors, especially in the case of distant faults and for fault resistances higher than zero.

The practical implementation of the algorithms requires the measurement of the neutral voltage in the case of the ANN U_0-spectrum algorithm, and the measurements of the phase currents and voltages of the feeder in the case of the other algorithms. ANN algorithms are sensitive to the changes of the network size for example due to the changes in connections of the network. Small changes are possible to manage with input data adaptation, but for bigger changes several ANNs are needed to train. For the time being, the practical implementation to the numerical relays is restricted by the sampling rate of the relays. The sampling rate of the numerical protection relays is 2 kHz nowadays. It should be 5 kHz for transient based methods at least.

6. Summary

The contribution of this thesis is to determine the characteristics of real earth faults in Finnish distribution network circumstances. Based on these characteristics new methods of earth fault indication and location were developed. Implementing these methods as new functions in distribution automation can decrease outage times.

In unearthed networks, more than a half of the disturbances were arcing faults. These can lead to overvoltages higher than double the normal phase to ground voltage. Only a few arcing faults occurred in compensated networks. Especially in the unearthed systems, the maximum currents that allowed for autoextinction were, in spite of the use of surge arresters, clearly smaller than had previously been believed. Fault resistances fell into two major categories, one where the fault resistances were below a few hundred ohms and the other where they were in the order of thousands of ohms. In the first category, faults are most often flash-overs to the grounded parts of the network. Distance computation is possible for these faults. In the second category, the majority of the faults disappeared of their own accord. However, a part of these faults evolve to the lower range of fault resistance, whereupon early detection is important.

Faults evolving gradually are, for example, caused by a broken pin insulator, snow burden, downed conductor or tree contact. Using the neutral voltage and residual current analysis with the probabilistic method, it is possible to detect and locate resistive earth faults up to a resistance of 220 kΩ. Practical implementation of the method requires a close integration of the substation SCADA with modern numerical relays. The location means the determination of the faulty feeder or line section. The field test results showed that in all cases, clearly the highest fault probability was computed for the feeder where the earth fault really was. The neutral voltage and residual current algorithms, developed during this study for high resistive fault indication and location, are possible to implement to the numerical relays.

This work also contributed to the development of new applications of the transient based differential equation, wavelet and neural network methods for fault distance estimation. The performance of the ANN methods was comparable to that of the conventional algorithms. It was also shown that the ANN trained

only by harmonic components of the neutral voltage transients is applicable for earth fault distance computation. The benefit of this method is that only one measurement per primary transformer is needed. Regarding only the earth faults with very low fault resistance (0 Ω), the ANN methods gave even better results than the other methods. The mean error in absolute terms was about 1.0 km for the ANN methods and about 2.0 km for the conventional algorithms in the staged field tests. The differential equation and wavelet algorithms were also in pilot use with a 3.7 kHz sampling rate in real network circumstances, where the differential equation algorithms gave slightly more accurate results. The restriction for transient based methods was that the highest fault resistance allowing reliable distance estimation was about 50 Ω. The drawbacks of the ANN methods were that they gave the best results when trained specifically for the one network size for which they were primarily intended. Small variations are possible to manage with input data adaptation, but for bigger changes of the network, several ANNs are needed to train. Therefore, from the techniques tested in this thesis, the differential equation algorithm seems to be the most promising alternative for transient based fault distance estimation. For the time being, the practical implementation of the transient based methods to numerical relays is restricted by the sampling rate of 5 kHz, which is needed.

This thesis has indicated several subjects worthy of further study:

- To avoid unnecessary auto-reclosings, the methods should be developed to discriminate arcing faults from permanent ones.

- The probabilistic method concerning the indication and location of high resistance faults should be developed further to monitor the isolation state of the network continuously.

- The signal pre-processing methods for fault distance estimation should be developed so that the transient effects of the filter itself do not affect the measured signals.

- The applicability of the differential and wavelet methods to fault distance estimation using only the measurements of the primary transformer supply bay should be analysed.

References

ABB. 1995. Fault indicator SPEF 3A2 C. Vaasa: ABB Network Control & Protection. 26 p.

ABB. 1997. SPAA 341 C Feeder Protection Relay. User's manual and technical description. Vaasa: ABB Network Partner. 149 p.

Abur, A. & Magnago, F.H. 2000. Use of time delays between modal components in wavelet based fault location. Electrical Power & Energy Systems. Elsevier Science Ltd. Pp. 397–403. (Vol. 22.)

Atwell, E.A., Shaffer, A.W., Jerrings, D.I. & Linders, J.R. 1990. Performance testing of the Nordon high impedance ground fault detector on a distribution feeder. 1990, Rural electric power conference. Paper presented at the 34th annual conference. NY, USA: IEEE. Pp. C6/1–7. (Cat. No.90CH2823-3.)

Aucoin, B.M. & Jones, R.H. 1996. High impedance fault detection implementation issues. IEEE Transaction on Power Delivery. IEEE. Pp. 139–144. (Vol. 11. No. 1, January.)

Benner, C., Carswell, P. & Russell, B.D. 1989. Improved algorithm for detection arcing faults using random fault behavior. EPSR (Electric Power Systems Research), Switzerland. Pp. 49–56. (Vol. 17, No. 1, July.) ISBN 0378-7796

Benner, C.L. & Russell, B.D. 1997. Practical high-impedance fault detection on distribution feeders. IEEE Transactions on Industry Applications. USA: IEEE. Pp. 635–640. (Vol. 33, No. 3, May/June.) ISBN 0093-9994

Blackburn, J.L. 1993. Symmetrical Components for Power Systems Engineering. New York, USA: Marcel Dekker, Inc. 427 p. ISBN 0-8247-8767-6

Bo, Z.Q., Weller, G. & Redfern, M.A. 1999. Accurate fault location technique for distribution system using fault-generated high-frequency transient voltage signals. IEE Proceedings – Generation, Transmission and Distribution. IEE. Pp. 73–79. (Vol. 146, January.)

Bo, Z.Q., Jiang, F., Chen, Z., Dong, X.Z., Weller, G. & Redfern, M.A. 2000. Transient based protection for power transmission systems. Proceedings of 2000 IEEE Power Society Winter Meeting. 23–27 January 2000. Singapore: IEEE. 6 p. (CD-ROM, 00CH37077C.) ISBN 0-7803-5938-0

Box, G.E.P. & Tiao, G.C. 1973. Bayesian Inference in Statistical Analysis. Addison-Wesley, Reading, MA. 588 p. ISBN 0-201-00622-7

Brandes, W. & Haubrich, H.J. 1983. Sterbpunktverlagerung durch mehrfach-leitungen in erdschlußkompensierten 110-kV-Netzen. Betriebliche erfahrungen und Abhilfemaßnahmen. Elektrizitätswirtschaft. Frankfurt: VDEW. Pp. 400–405. (Jg. 82, Heft 11.) ISBN 0013-5496

Butler, K.L., Momoh, J.A. & Sobajic, D.J. 1997. Field studies using a neural-net-based approach for fault diagnosis in distribution networks. IEE Proceedings – Generation, Transmission and Distribution. IEE. Pp. 429–436. (Vol. 144, No. 5, September.)

Chaari, O., Meunier, M. & Brouaye, F. 1996. Wavelts: A new tool for the resonant grounded power distribution systems relaying. IEEE Transactions on Power Delivery. USA: IEEE. Pp. 1301–1308. (Vol. 11, No. 3, July.) ISBN 0885-8977-96

Chilard, O., Morel, L. & Renon, D. 1999. Compensated grounded medium voltage network protection against resistive phase to ground faults. Proceedings of CIRED'99, 15th International Conference and Exhibition on Electricity Distribution, 1–4 June 1999, Nice, IEE, 4 p. (CD-ROM)

Christgau, G. & Wolfenstetter, W. 1982. Zuverlässige Ortungs und Melde-methode bei Erdschlüssen im Mittelspannungsnetz. In: Elektrizitätswitrschaft. Frankfurt: VDEW. Pp. 804–810. (Jg. 82, Heft 23.) ISBN 0013-5496

Chui, C.K. 1992. An introduction to wavelets. San Diego, USA: Academic Press, Inc. 264 p.

Claudelin, P. 1991. Compensation of the earth fault current in a MV distribution network. Earth fault problems in MV Systems. Helsinki: INSKO. Pp. 1–38. (INSKO 157-91.) (In Finnish)

Crucius, M. & Kries, G. 2001. Fehlersensoren – ereignisorientierte Wartung in Mittelspannungsnetzen. ETZ Electrotechnik + Automation. Berlin: VDE Verlag. Pp. 22–25. (Heft 3–4)

Dalstein, T. & Kulicke, B. 1995. Neural network approach to fault classification for high speed protective relaying. IEEE Transactions on Power Delivery. IEEE. Pp. 1002–1011. (Vol. 10, No. 2, April.) ISBN 0885-8977-95

Dillon, T.S. & Niebur, D. 1996. Neural networks applications in power systems. London: CRL Publishing Ltd. 404 p. ISBN 0-9527874-0-7

Eickmeyer, D. 1997. Einsatz kunstlicher neuronaler Netze bei der Ortung von Erdschlussen. Dissertation TU Berlin: 136 p.

Girgis, A.A., Chang, W. & Makram, E.B. 1990. Analysis of high-impedance fault generated signals using a Kalman filtering approach. IEEE Transactions on Power Delivery. USA: IEEE. Pp. 1714–1722. (Vol. 5, No. 4, November.)

Haase, H. & Taimisto, S. 1983. New Finnish Equipment for compensation of earth fault current. Sähkö, Electricity and Electronics. Pp. 48–51. (Vol. 56, 12. December.) (In Finnish)

Haykin, S. 1994. Neural networks – A comprehensive foundation. New York: MacMillan, Prentice Hall International Editions. 696 p.

Huang, S.J. & Hsieh, C.T. 1999. High-impedance fault detection utilizing a Morlet wavelet transform approach. IEEE Transactions on Power Delivery. USA: IEEE. Pp. 1401–1410. (Vol. 14, No. 4, October.) ISBN 0885-8977-99

Huang, S.J. & Hsieh, C.T. 2001. Feasibility of fractal-based methods for visualization of power system disturbances. Electrical Power & Energy Systems. Elsevier Science Ltd. Pp. 31–36. (Vol. 23.)

Hubensteiner, H. 1989. Schutztechnik in elektrischen Netzen. Offenbach/Berlin: VDE-Verlag. 282 p.

Igel, M. 1990. Neuartige Verfahren für den Erdschlußdistanzschutz in isoliert and kompensiert betriebenen Netzen – Signale und Algorithmen im Frequenzbereich. Dissertation. Universität des Saarlandes, Saarbrücken, Germany. 181 p.

Igel, M., Koglin, H.-J. & Schegner, P. 1991. New algorithms for earth fault distance protection in insulated and compensated networks. ETEP (European Transaction in Electrical Power). VDE Verlag. Pp. 253–259. (Vol. 1, No. 5, September/October.)

Jeerings, D.I. & Linders, J.R. 1990. Unique aspects of distribution system harmonics due to high impedance ground faults. IEEE Transactions on Power Delivery. USA. Pp. 1086–1094. (Vol. 5. No. 2, April.) ISBN 0885-8977

Jota, F.G. & Jota, P.R.S. 1998. High-impedance fault identification using a fuzzy reasining system. IEE Proceedings – Genration, Transmission and Distribution. IEE. Pp. 656–662. (Vol. 145, No. 6, November.)

Kezunovic, M. 1997. A survey of neural net applications to protective relaying and fault analysis. Engineering Intelligent Systems. CRL Publishing Ltd. Pp. 185–192. (Vol. 5, No. 4, December.)

Kim, C.J., Russell, B.D. 1995. Analysis of distribution disturbances and arcing faults using the crest factor. EPSR (Electric Power Systems Research), Pp. 141-148. (Vol. 35, No. 2.) ISBN 0378-7796

Klockhaus, H., Poll, J. & Sauerbach, F.J. 1981. Sternpunktverlagerung und Erdschlußfehlerortsuche im Mittelspannungsnetz. Elektrizitätswirtschaft. Frankfurt: VDEW. Pp. 797–803. (Jg. 80, Heft 22.) ISSN 0013-5496

Ko, J.H., Shim, J.C., Ryu, C.W., Park, C.G. & Yim, W.Y. 1998. Detection of high impedance faults using neural nets and chaotic degree. Proceedings of EMPD '98. 1998 International Conference on Energy Management and Power Delivery. 3–5 March. Singapore: IEEE. Pp. 399–404. (IEEE Catalogue No. 98EX137.) ISBN 0-7803-4495-2

Lakervi, E. & Holmes, E.J. 1995. Electricity distribution network design. 2nd Edition. England: Peter Peregrinus Ltd. 325 p. (IEE Power Engineering series 21.) ISBN 0 86341 309 9

Lamberty, G. & Schallus, K. 1981. Betriebserfahrungen mit der Ortung von Erdschlussfehlern vei unterschiedlicher Sternpunktbehandlung im 10-kV-Mittelspannungsnetz. Elektrizitätswirtschaft. VDEW. Pp. 803–809. (Jg. 80, Heft 22.) ISSN 0013-5496

Lee, R.E. & Bishop, M.T. 1983. Performance testing of the ratio ground relay on a four-wire distribution feeder. IEEE Transactions on Power Apparatus and Systems. IEEE. Pp. 2943–2949. (Vol. PAS-102, No. 9.)

Lehtonen, M. 1992. Transient analysis for ground fault distance estimation in electrical distribution networks. Espoo: The Technical Research Centre of Finland. 181 p. (VTT Publications 115.) ISBN 951-38-4233-9

Lehtonen, M. 1995. Method for distance estimation of single-phase-to-ground faults in electrical distribution networks with an isolated or compensated neutral. ETEP (European Transaction in Electrical Power). VDE-Verlag. Pp. 193–198. (Vol. 5, No. 3, May/June.)

Lehtonen, M. 1998. A Method for detection and location of high resistance earth fault in electrical distribution networks. Pat. FI. No. 100922, ABB Transmit Oy, publ. 13.03.1998.

Lehtonen, M. 1999. A Method for detection and location of high resistance earth fault in electrical distribution networks based on current measurements. Pat. FI. No. 103217, ABB Transmit Oy, publ. 14.05.1999.

Lehtonen, M. & Hakola, T. 1996. Neutral earthing and power system protection. Earthing solutions and protective relaying in medium voltage distribution networks. Vaasa: ABB Transmit Oy. 118 p. ISBN 952-90-7913-3

Leitloff, V., Pierrat, L. & Feuillet, R. 1994. Study of the neutral-to-ground voltage in a compensated power systems. ETEP (European Transaction in Electrical Power). Pp. 145–153. (Vol. 4, No. 2, March/April.)

Leitloff, V., Pierrat, L. & Feuillet, R. 1997. Detection of resistive single-phase earth faults in a compensated power-distribution system. ETEP (European Transaction in Electrical Power). Pp. 65–73. (Vol. 7, No. 1, January/February.)

Liang, J., Elangovan, S. & Devotta, J.B.X. 2000. Application of wavelet transform in travelling wave protection. Electrical Power & Energy Systems. Elsevier Science Ltd. Pp. 537–542. (Vol. 22. No. 8.)

Lien, K.Y., Chen, S.L., Liao, C.J., Guo, T.Y., Lin, T.M. & Shen, J.S. 1999. Energy variance criterion and threshold tuning scheme for high impedance fault detection. IEEE Transactions on Power Delivery. IEEE. Pp. 810–817. (Vol. 14, No. 3, July.)

Mamishev, A.V., Russell, B.D. & Benner, C.L. 1996. Analysis of high impedance faults using fractal techniques. IEEE Transactions on Power Systems. USA: IEEE. Pp. 435–440. (Vol. 11, No. 1, February.) ISBN 0885-8950

Mörsky, J. 1992. Relay protection techniques. Second edition. Hämeenlinna: Otatieto Oy. 459 p. ISBN 951-672-175-3 (In Finnish)

Nikander, A. & Järventausta, P. 1998. Methods for earth fault identification and distance estimation in a compensated medium voltage distribution network. Proceedings of international conference on Energy Management and Power Delivery '98 (EMPD '98). Singapore: IEEE. Pp. 595–600. (IEEE Catalogue No. 98EX137.) ISBN 0-7803-4495-2

Nikander, A. & Lakervi, E. 1997. A philosophy and algorithms for extinguishing earth fault arcs in suppressed medium voltage networks. Proceedings of CIRED'97, 14th International Conference and Exhibition on Electricity Distribution, 2–5 June 1997. IEE. Pp. 4.20.1–4.20.6. (Conference Publication No. 438.)

Nikander, A., Järventausta, P. & Rissanen, P. 2000. Methods for identification and distance estimation of high impedance earth faults in medium voltage networks. In: Lehtonen, M. TESLA – Information technology and electric power systems. Technology Programme 1998–2002. Interim report 1999. VTT. 8 p. (Tesla NR 27/2000.)

Paulasaari, H., Järventausta, P., Verho, P., Kärenlampi, M., Partanen, J., Hakola, T. & Vähätalo, E. 1995. Methods to study earth fault phenomena by using a residual overvoltage relay module. Proceedings of IEEE/KTH Stockholm Power Tech. Conference, Stockholm, Sweden, June 18–22. 5 p.

Pettissalo, S., Sauna-aho, S. Hänninen, S. & Lehtonen, M. 2000. A novel application for fault location in distribution networks. Proceedings of Southern African Power System Protection Conference, Johannesburg, South Africa, 8.–9. November: ESKOM and TSI (Technology Services International). Pp. 117–121.

Phadke, A.G. & Thorp, J.S. 1990. Computer Relaying for Power Systems. England: Research Studies Press Ltd. 286 p.

Poll, J. 1981. Sternpunktverlagerung in gelöschten 110 kV-Netzen. Elektrizitäts-wirtschaft. Frankfurt: VDEW. Pp. 810–813. (Jg. 80, Heft 22.) ISSN 0013-5496

Poll, J. 1983. Auswertung der Störungsschreibraufzeichnungen von kurzzeitigen Erdschlüssen on kompensierten Netzen. Elektrizitätswirtschaft. Frankfurt: VDEW. Pp. 311–317. (Jg. 82, Heft 9.) ISSN 0013-5496

Poll, J. 1984. Löschung von Erdschlußlichtbögen. Elektrizitätswirtschaft. Frankfurt: VDEW. Pp. 322–327. (Jg. 83, Heft 7.) ISSN 0013-5496

Pundt, H. 1963. Untersuchungen der Ausgleichsvorgänge bei Erdschluss in Hochspannungsnetzen mit isoliertem Sternpunkt und induktiver Sternpunkt-erdung als Grundlage zur selektiven Erdschlusserfassung. TU Dresden. 167 p. + app. (Dissertation.)

Reason, J. 1994. Relay detects downed wires by fault-current harmonics. Electrical World. USA: Pp. 58–59. (Vol. 208, No. 12.) ISSN 0013-4457

Rioul, O. & Vetterli, M. 1991. Wavelets and signal processing. IEEE Signal Processing Magazine. New York, USA: IEEE. Pp. 14–38. (Vol. 8, No. 4, October.) ISBN 1053-5888

Roman, H. & Druml, G. 1999. Distance location of earth faults in compensated medium voltage networks. Proceedings of CIRED'99, 15th International Conference and Exhibition on Electricity Distribution, 1–4 June 1999, Nice, IEE, 5 p. (CD-ROM)

Russell, B.D. & Benner, C.L. 1995. Arcing fault detection for distribution feeders: Security assessment in long term field trials. IEEE Transactions on Power Delivery. Pp. 676–683. (Vol. 10, No. 2.) ISSN 0885-8977

Russell, B.D. & Chinchali, R.P. 1989. A digital signal processing algorithm for detecting arcing faults on power distribution feeders. IEEE Transactions on Power Delivery. USA: IEEE. Pp. 132–140. (Vol. 4, No. 1, January.) ISBN 0885-8977

Russell, B.D., Mehta, K. & Chinchali, R.P. 1988. An arching fault detection technique using low frequency current components – performance evaluation using recorded field data. IEEE Transaction on Power Delivery. USA. Pp. 1493–1500. (Vol. 3, No. 4.) ISBN 0885-8977

Schegner, P. 1989. Digitaler Erdschlssuniversalschutz. Konzept und erste Realisierung. Dissertation. Universität des Saarlandes Saarbrücken, Germany. 186 p.

Schrüfer, E. 1990. Signalverarbeitung. Numerische Verarbeitung digitaler Signale. Germany: Carl Hanser Verlag München Wien. 362 p. ISBN 3-446-15944-4

Shihab, S. & Wong, K.L. 2000. Detection of faulty components on power lines using radio frequency signatures and signal processing technigues. Proceedings of 2000 IEEE Power Society Winter Meeting. 23–27 January 2000. Singapore: IEEE. 4 p. (CD-ROM, 00CH37077C.) ISBN 0-7803-5938-0

Shiping, L. & Russell, B.D. 1991. Optimal arching fault detection using signal processing techniques. EPSR (Electric Power Systems Research). Switzerland: Pp. 121–128. (Vol. 21, No. 2.) ISBN 0378-7796

Sidhu, T.S., Singh, H. & Sachdev, M.S. 1995. Design, implementation and testing of an artificial neural networks based fault direction discriminator for protecting transmission lines. IEEE Transactions on Power Delivery. IEEE. Pp. 697–706. (Vol. 10, No. 2, April.) ISBN 0885-8977-95

Sultan, A.F., Swift, G.W. & Fedirchuk, D.J. 1992. Detection of hifh impedance arching faults using a multi-layer perceptron. IEEE Trancactions on Power Delivery. USA: IEE. Pp. 1871–1876. (Vol. 7, No. 4, October.) ISBN 0885-8677-92

Sultan, A.F., Swift, G.W. & Fedirchuk, D.J. 1994. Detecting arcing downed-wires using fault current flicker and half-cycle asymmetry. IEEE Transactions on Power Delivery. IEEE. Pp. 461–470. (Vol. 9, No. 1, January.) ISSN 0885-8977

Taimisto, S. 1993. Earth fault compensation in medium voltage distribution networks. Sähkö&Tele. Pp. 24–30. (Vol. 66, No. 1.) (In Finnish)

Taylor, H.M. & Karlin, S. 1984. An introduction to stochastic modeling. Orlando, USA: Academic Press Inc. 399 p. ISBN 0-12-684882-3

The Finnish Electricity Association Sener. 2000. Outage Statistics 1999. Helsinki, Sener. 21 p. (In Finnish)

Tungkanawanich, A., Abe, J., Kawasaki, Z.I. & Matsuura, K. 2000. Location of partial discharge source on distribution line by measuring emitted pulse-train electromagnetic waves. Proceedings of 2000 IEEE Power Engineering Society Winter Meeting. 23–27 January 2000, Singapore: IEEE. 6 p. (CD-ROM, 00CH37077C.) ISBN 0-7803-5938-0

Wai, D.C.T. & Yibin, X. 1998. A novel technique for high impedance fault identification. IEEE Transactions on Power Delivery. USA: IEEE. Pp. 738–744. (Vol. 13, No. 3, July.) ISSN 0885-8977

Warrington, A. R. van C. 1962. Protective relays, their theory and practice. Vol. 1. London: Chapman & Hall Ltd. 484 p.

Vaughan, M. & Moore, P.I. 2000. A non-intrusive power system arcing fault location system utilising the VLF radiated electromagnetic energy. Proceedings of 2000 IEEE Power Engineering Society Winter Meeting. 23–27 January 2000, Singapore: IEEE. 6 p. (CD-ROM, 00CH37077C.) ISBN 0-7803-5938-0

VDE 0228. 1987. Teil 2, Maßnahmen bei Beeinflussung von Fernmeldeanlagen durch Starkstromanlagen. Deutcshe Elektrotechnische Kommission im DIN und VDE (DKE).

Weiss, L.G. 1994. Wavelets and wideband correlation processing. IEEE Signal Processing Magazine. New York, USA: IEEE. Pp. 13–32. (Vol. 11, No. 1, January.) ISBN 1053-5888

Willheim, R. & Waters, M. 1956. Neutral earthing in high-voltage transmission. New York: Elsevier Publishing Co. 669 p.

Winter, K. 1988. Null point analysis – new method for detecting high resistance earth faults. ERA. Sweden: Pp. 18–20, 23–24. (Vol. 61, No. 5.) ISSN 0013-9939 (In Swedish)

Winter, K. 1993. Swedish distribution networks – A new method for earth fault protection in cable and overhead systems. DPSP'93. Fifth International Conference on developments in Power System Protection. Conference Publication No. 368, IEE. 4 p.

Xinzhou, D., Yaozhong, G. & Bingyin, X. 2000. Fault position relay based on current travelling waves and wavelets. Proceedings of 2000 IEEE Power Society Winter Meeting. 23–27 January 2000. Singapore: IEEE. 7 p. (CD-ROM, 00CH37077C.) ISBN 07803-5938-0

Yu, D.C. & Khan, S.H. 1994. An adaptive high and low impedance fault detection method. IEEE Transactions on Power Delivery. IEEE. Pp. 1812–1821. (Vol. 9, No. 4.) ISBN 0885-8977-94

Yu, I.K. & Song, Y.H. 1998. Wavelet analysis and neural network based adaptive singlepole autoreclosure scheme for EHV transmission systems. Electrical Power & Energy Systems. Great Britain: Elsevier Science Ltd. Pp. 465–474. (Vol. 20, No. 7.) ISBN 0142-0615-98

Appendix A

Reprinted with permission from the publisher
In: EPSR (Electric Power Systems Research) 1998. Vol. 44, No. 3, pp. 155-161.

APPENDIX A

Characteristics of earth faults in electrical distribution networks with high impedance earthing

Seppo Hänninen *, Matti Lehtonen

VTT Energy, Energy Systems, P.O. Box 1606, FIN-02044 VTT, Finland

Received 16 April 1997

Abstract

This paper presents an analysis and comparison of earth fault characteristics in the medium voltage distribution networks (20 kV) with high impedance earthing. The results presented are based on the evaluation of 476 real case data recordings, obtained from substations of distribution networks with an unearthed or a compensated neutral during the observation period of 3 years, 1994–1996. The networks were mainly of overhead construction, with a smaller share of underground cables. In the occurrence of disturbances, the traces of phase currents and voltages and neutral currents and voltages were recorded at two feeders at two substations. The study dealt with the clearing of earth faults, relation between short circuits and earth faults, arc extinction, arcing fault characteristics, appearance of transients and magnitudes of fault resistances. The results contribute to various developments of distribution automation and protection systems.

Keywords: Earth faults; Arc extinction; Arcing fault; Transients; Fault resistances

1. Introduction

Most of the medium voltage networks in Finland are operated with an isolated neutral point, but the compensation of the earth fault current with the Pedersen coil is also used in the substations where a reduction of fault current is needed. The feeders are radially operated. The most common fault type in the electrical distribution networks is the single phase to earth fault. According to earlier studies [1–3], for instance in Nordic countries, about 50–80% of all faults are of this type. To develop the protection and fault location systems, it is important to obtain real case data of disturbances and faults which occurred in the networks. Therefore, data of fault occurrences have been recorded and analyzed in the medium voltage distribution networks (20 kV) at two substations, of which one has an isolated and the other a compensated neutral. In the occurring disturbances, the traces of phase currents and neutral currents of two feeders and the traces of phase voltages and neutral voltage in the medium voltage busbar were recorded at each substation.

In addition to the measured data, other information of the fault occurrences was also collected (data of the line, cause and location of permanent faults, etc.).

2. Recorder installation

Disturbance recorders were installed at the Gesterby substation of Espoo Electricity, where the distribution network is isolated and at the Gerby substation of Vaasa Electricity, where the network is compensated. Substations, with mostly overhead feeders, were chosen, so that a significant number of circuit breaker operations, during adverse weather conditions, would be likely to occur. The length of overhead lines surveyed was 79.3 km and one of the cable lines was 4.2 km in the isolated neutral network and the corresponding lengths were 223.4 and 5.0 km in the compensated neutral network. For overvoltage protection, the former network has surge arresters and the latter network has spark gaps. In both cases, these are mounted at the medium voltage nodes of distribution transformers.

The recorder system was rack mounted and was provided with SPAA 322 and SPAC 531 relays and SPCR disturbance recorders. In both substations, the

* Corresponding author. Tel.: +358 9 4561; fax: +358 9 4566538.

0378-7796/98/$19.00
PII S0378-7796(97)01193-0

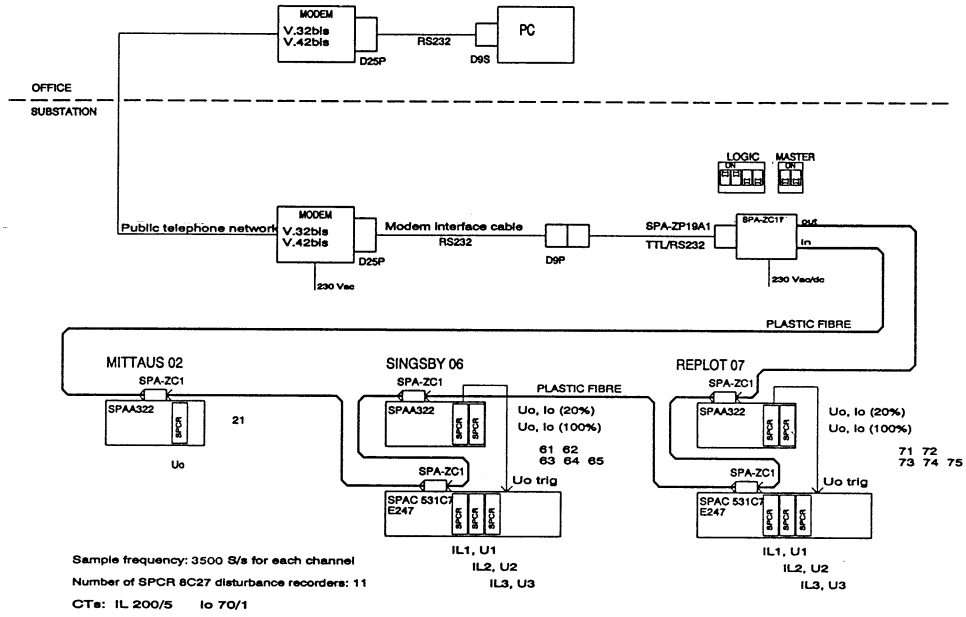

Fig. 1. Installation arrangement of the recorder system at the substation.

disturbance recorders were installed at two feeders including five SPCR recorder units for each feeder, three recorder units for the phase voltages and currents and two units for the residual or neutral current and voltage. In the latter case, one recorder unit was set with an increased sensitivity to ensure the identification of transients in the case of high fault resistance. One voltage and one current channel of each recorder unit was used. For neutral voltage, in addition to those mentioned above, one recorder unit was used, whose duration of each record was selected to be longer than the one of the other units.

Various triggering options are included within the recorder. In this case, if the predetermined threshold value of the neutral voltage was exceeded in one channel, this initiated the triggering of the other recorder units at the same feeder. The sample frequency was 3.5 kHz for each channel and the length of each recording was 0.5 s in the isolated neutral network and 0.7 s in the compensated neutral network. The sample set also contained some periods of data before the fault moment. If the fault on the feeder was sustained, the pause between successive recordings was 10 s. The recorders used the majority of their memory as a segmented cyclic buffer to store the sampled data. Once all the memory had been used, the recorder directed new data to the first segment of the buffer and the oldest recording in the memory was deleted.

The disturbance recorders were connected via modems and telephone networks to a PC in the office at VTT. The PC automatically monitored the recorders at selected intervals and if required, transferred the recorded files to the PC for further treatment. The communication software and the recorder equipment had been developed and supplied by ABB Transmit Oy. The schematic diagram of a recorder installation is shown in Fig. 1 [4].

3. Fault classification

An electrical fault can be defined as any abnormal condition which is caused by a reduction in the insulation strength between energized phase conductors, called a short circuit, or between a phase conductor and earth or any earthed part of an electrical system, called an earth fault. In addition to these two main categories, disturbances were further classified according to how they were cleared. The fault, which disappeared by itself and needed no function of a circuit breaker, was classified as ‘self extinguished’ (SE). In other cases, the clearing of the fault demanded the function of a circuit breaker. Many faults were cleared by auto-reclosing, high speed auto-reclosing (HSAR) or delayed auto-reclosing (DAR). Sometimes, the fault disappeared after the auto-reclosing during the time from the tripping of the circuit breaker to the time, when the circuit breaker was again closed manually with the aid of remote-control (RC). The remainder of the faults were permanent (P) and needed corrective actions in the terrain before the supply could be restored.

4. Data analysis

During the observation period of approximately 3 years at the substations of Gesterby and Gerby, altogether 476 recordings were obtained. This includes all disturbances in the substation busbar. Together 316 of the recordings were obtained from the feeders surveyed. Figs. 2 and 3 show the number of faults in the feeders divided into main fault categories and into the way of clearing.

In the compensated network, the division of faults into main categories was 53.8% for earth faults and 46.2% for short circuits. Here the disturbances, which extinguished themselves without any function of a circuit breaker (SE), were excluded. In the unearthed network, the corresponding numbers were 74.3 and 25.7%. Due to the difference in neutral earthing and also due to the longer delay of the HSAR sequence, a bigger share of faults were self extinguished in the compensated network than in the unearthed network. The analysis also showed that, if the function of the circuit breaker was needed, HSAR usually succeeded in clearing the fault. Since the recorder units were triggered by the rise of neutral voltage, all the faults analysed involved a ground contact. This material does not give the correct understanding of the ratio of one phase and multiphase fault frequencies. To mitigate this, the recorded fault data were also compared to the corresponding information acquired from a third power company [5]. Here the number of faults was acquired by the aid of numerical relays in the substations. The period surveyed was approximately 3 years. Only those disturbances, in which the clearing of the fault needed the function of the circuit breaker, were taken into account. Figs. 4 and 5 show that contrary to the former, the majority of the faults were short circuit faults. However, here also the share of earth faults was bigger in the isolated neutral substations than in the compensated neutral case.

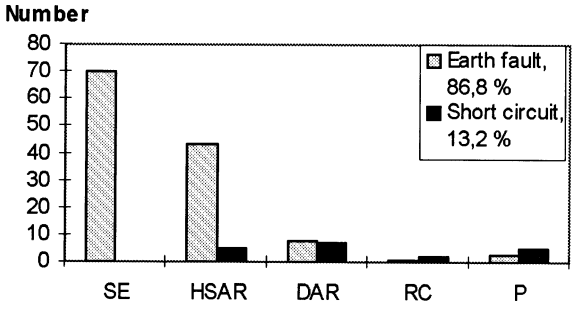

Fig. 2. Number of the disturbances classified by means of clearing in the unearthed network (SE, self extinguished; HSAR, high speed auto-reclose; DAR, delayed auto-reclose; RC, remote control; P, permanent fault).

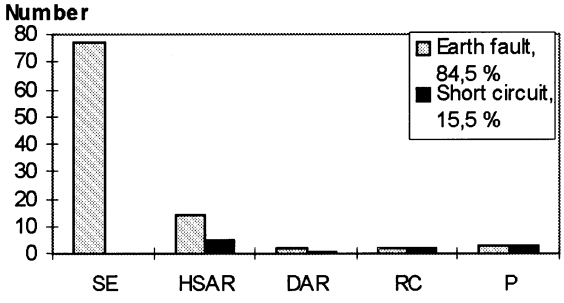

Fig. 3. Number of the disturbances classified by means of clearing in the compensated network.

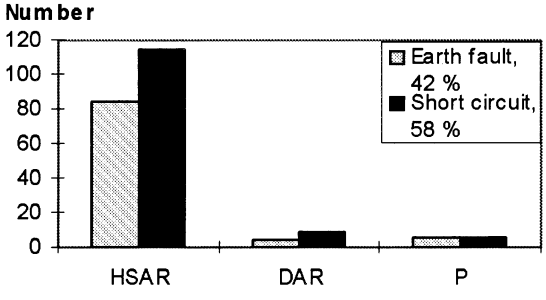

Fig. 4. Number of faults at one substation in North-Carelian Electricity (unearthed network).

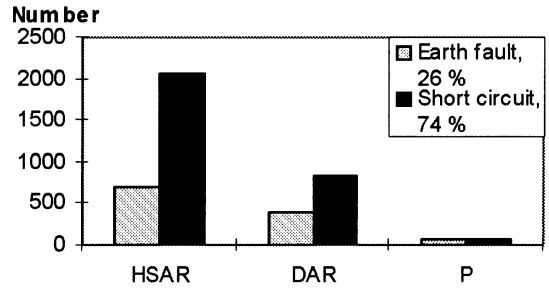

Fig. 5. Number of faults from eight substations in North-Carelian Electricity (compensated network).

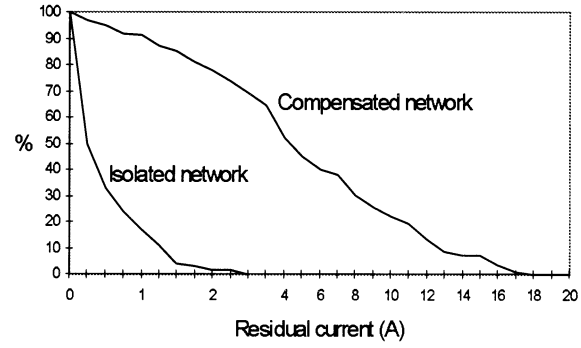

Fig. 6. Cumulative characteristic of faults which extinguished themselves versus maximum residual current.

4.1. Autoextinction

In some cases, an earth fault arc can extinguish itself without any auto-reclosing function and the interruptions can thus be avoided. The most significant factors,

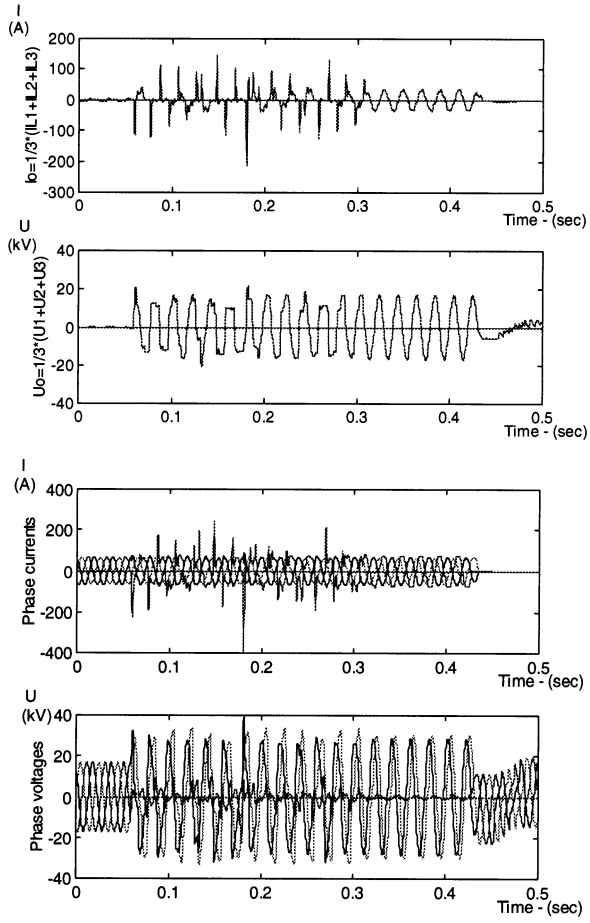

Fig. 7. Neutral current, neutral voltage, phase currents and phase voltages of an arcing fault in an isolated neutral network.

that determine whether the arc will disappear or not, are the recovery voltage and the residual fault current magnitude. During the observation period, the triggering level of the recorders was set a little below the function level of the feeder protection relays, so that disturbances which did not cause auto-reclosing functions could also be recorded.

The study showed (Figs. 2 and 3) that a larger share of disturbances disappeared by themselves in the compensated network than in the isolated network. In the

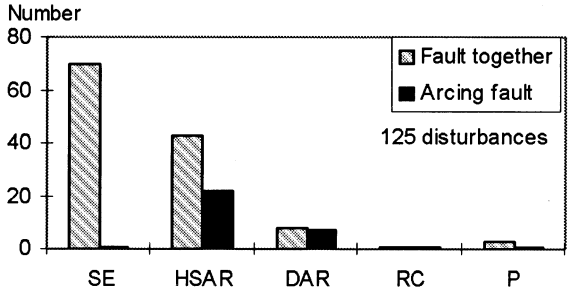

Fig. 8. Occurrences of arcing faults classified by means of clearing in the unearthed network

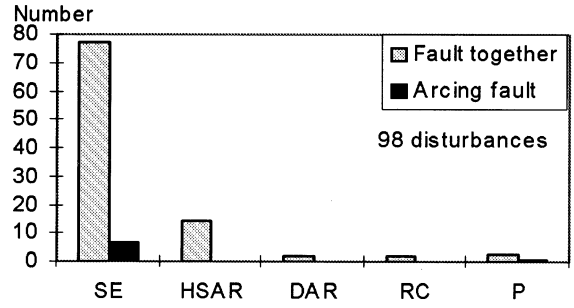

Fig. 9. Occurrences of arcing faults classified by means of clearing in the compensated network.

case of the autoextinction, the average residual current measured was 0.48 A and the maximum current 2.50 A in the unearthed network and correspondingly 5.96 A and 17.88 A in the compensated neutral network. The average duration of these faults was 0.34 s in the compensated network and 0.18 s in the isolated neutral network. Fig. 6 shows cumulatively the faults which extinguished themselves versus the maximum residual current. Especially in the unearthed systems, the maximum currents that allow for autoextinction are, in spite of surge arresters, clearly smaller than had been believed before.

4.2. Arcing faults

During the observation period, it was noticed, that the one phase earth fault was in many cases an arcing fault, especially in an unearthed network. In an arcing earth fault, the arc disappears at the current zero crossing, but is immediately re-established when the voltage rises. Fig. 7 shows the typical current and voltage curves of an arcing fault.

Fig. 8 shows that excluding the faults which extinguished themselves (case SE), about half of the disturbances were arcing faults in the isolated neutral network and Fig. 9 shows, that only few arcing faults occurred in the compensated network. The explanation for this is the factors which affect the arc extinction and its re-ignition. Among these, the amplitude and rising

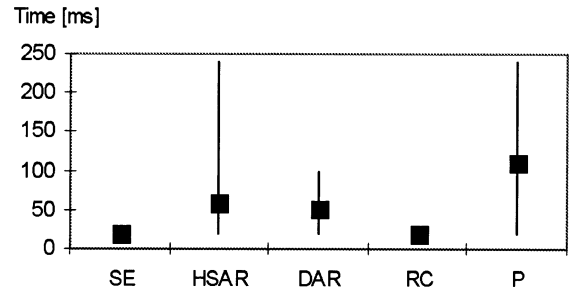

Fig. 10. The duration of arcing currents classified by means of clearing in the unearthed network, average value and range.

Table 1
The maximum and mean peak values of the phase voltage during the arcing fault in the unearthed network expressed in kV

Phase voltage	HSAR	DAR	RC	P
$U_{v,max}$	39.87	35.63	39.03	33.37
$U_{v,mean}$	37.04	34.62	39.03	33.23

Table 2
The maximum and mean peak values of the phase voltage during the arcing fault in the compensated network expressed in kV

Phase voltage	HSAR	DAR	RC	P
$U_{v,max}$	—	—	—	33.31
$U_{v,mean}$	—	—	—	33.31

speed of the recovery voltage and the residual capacitive fault current are the most important. The major reason, why the arc can strike more often in the isolated network than in the compensated network, is the rising speed of the recovery voltage, which is much higher in the isolated network [6].

A number of relay algorithms obtain the fundamental frequency components of both voltages and currents. The performance of these algorithms is dependent on obtaining accurate estimates of the fundamental frequency components of a signal from a few samples. In the case of an arcing fault, the signal in question is not a pure sinusoid and thus can cause errors in the estimated parameters [7].

Fig. 10 shows the average duration of arcing current and its range classified according to the means of fault clearing in the unearthed network. The arcing current occurred in all cases in the beginning of the disturbance and continued for some network periods prior to altering to a full earth fault or before the arc extinguished itself. According to Fig. 10, the average duration of the arcing current was about 60 ms in the isolated neutral network. The corresponding time was 80 ms in the compensated neutral network, but there occurred only eight arcing faults during the whole observation period.

The arcing faults can cause overvoltages, which in the worst case can be dangerous to human beings or destroy electrical equipment. Tables 1 and 2 show the maximum and mean peak value of the phase voltage, measured in the network during an arcing fault and classified according to how the faults were cleared. Table 2 is sparse, because so few arcing faults occurred in the compensated network. Table 1 shows that, in the isolated neutral network, the overvoltages were more than double the normal phase voltage.

4.3. Fault resistances

The fault resistance can be determined from the neutral voltage. In the unearthed networks we can use the following equation [8]:

$$R_f = \frac{\sqrt{U_1^2 - U_0^2}}{3\omega C_0 U_0} \quad (1)$$

Where R_f is the fault resistance; C_0 is the total phase to earth capacitance of the network; U_0 is the neutral voltage; and U_1 is the positive sequence voltage.

The corresponding equation for the compensated network is:

$$R_f = \frac{U_1 R_0 \sqrt{1 + \left(\frac{U_1^2 R_0^2 - U_0^2 R_0^2}{U_1^2}\right) * \left(3\omega C_0 - \frac{1}{\omega L}\right)^2} - U_0 R_0}{U_0 * \left[1 + R_0^2 \left(3\omega C_0 - \frac{1}{\omega L}\right)^2\right]} \quad (2)$$

Where R_0 is the parallel coupling of the system leakage resistances and the additional resistor of the compensation coil; and L is the inductance of the compensation coil.

The neutral voltage is equal to the phase voltage when the fault resistance is zero. When the fault resistance is low, the neutral voltage may even rise above

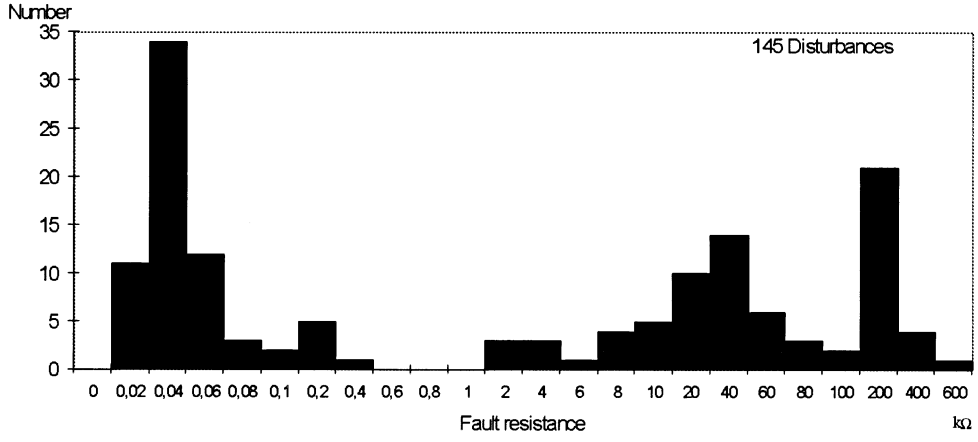

Fig. 11. The division of the fault resistances in the unearthed network.

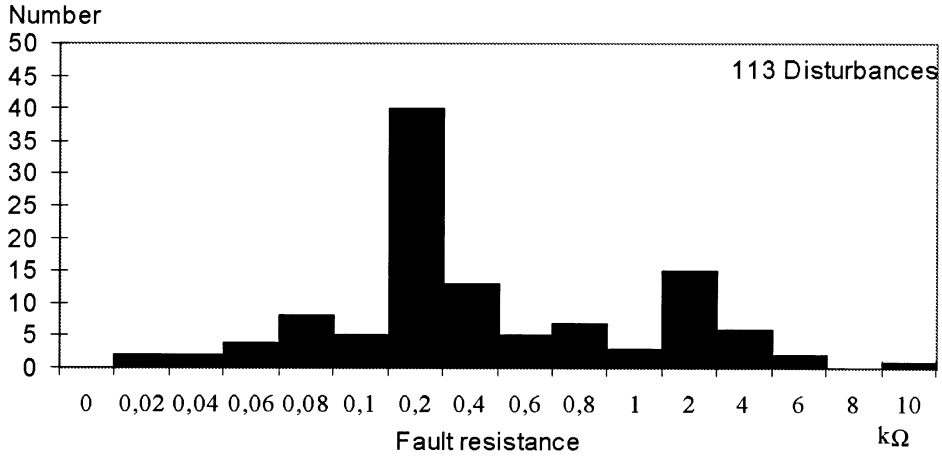

Fig. 12. The division of the fault resistances in the compensated network.

the phase voltage. Therefore in the case of low fault resistances, an approximative form of Eq. (3) was used. The resistance of the phase conductor from substation to fault point is included in this form, but it is usually only a few ohms.

$$R_f \approx \frac{U_{ph}}{I_0} \tag{3}$$

Where U_{ph} is the phase to earth voltage of the faulted phase during the earth fault; and I_0 is the sum current measured at the substation.

Figs. 11 and 12 show the division of the calculated fault resistances taking into account all disturbance recordings. According to these figures, there are clearly two major categories of earth faults. In the first category, the fault resistances are mostly below a few hundred ohms and circuit breaker tripping is required. In the other category, the fault resistances are in the order of thousands of ohms. In this case, the neutral potentials usually are so low, that continued network operation with a sustained fault is possible.

4.4. Transients

At the initial moment of the earth fault in high impedance earthed systems, the voltage of the faulty phase rapidly falls to, or close to zero, and the voltages of the sound phases rapidly increase (Fig. 13). The transient components of the voltages and currents are

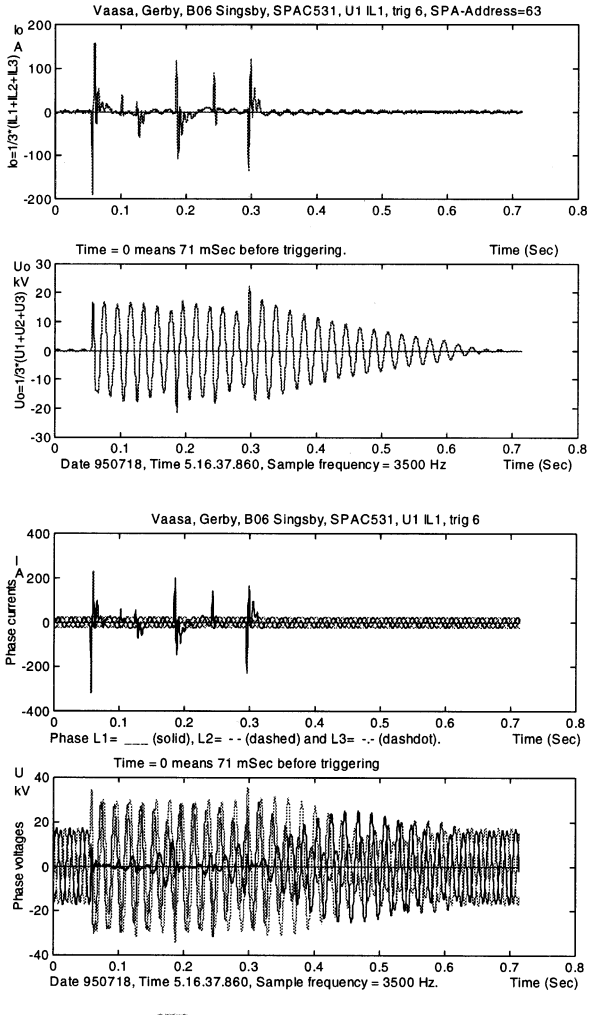

Fig. 13. Transient phenomenon in the neutral current, neutral voltage, phase current and voltage in the compensated network.

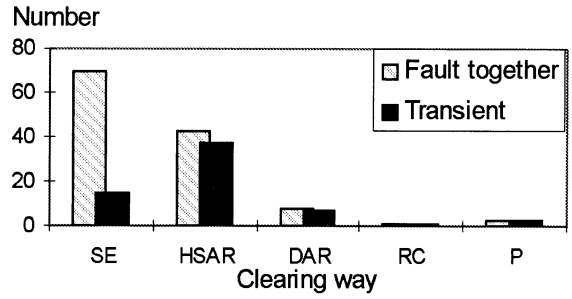

Fig. 14. Appearance of transients classified by means of fault clearing in the unearthed network.

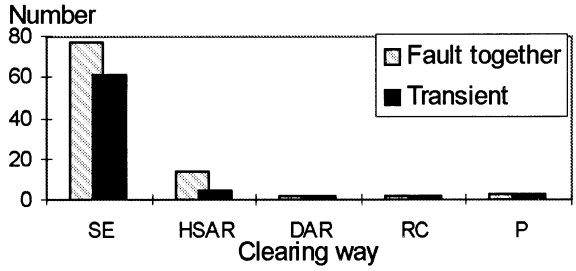

Fig. 15. Appearance of transients classified by means of fault clearing in the compensated network.

based on charging of the capacitances of the two healthy phases and discharging of the faulted phase capacitance [1]. Figs. 14 and 15 show that transients could be detected in nearly all fault occurrences which demanded the function of the circuit breaker. In addition, about 70% of the transients were oscillatory. These characteristics of the transient phenomenon can be made use of in the relay protection systems and in fault location [8].

4.5. Changing of an earth fault to a short circuit fault

The voltage rise of the sound phases during the earth fault can lead to a bolted short circuit between two phases. This kind of change could also be detected in some recorded faults of this study. The main causes for these faults were the contact of tree limb with phase conductors or birds on pole mounted transformers. During the observation period, only eight faults of this type were detected in the isolated neutral network and four in the compensated network. Average time for the fault to change was 0.16 s in both networks.

5. Summary

The results presented here are based on the evaluation of 476 real case data recordings, obtained from substations of medium voltage networks with high impedance earthing. The networks were mainly of overhead construction, with a smaller share of underground cables. In the unearthed network, about half of the disturbances were arcing faults. These can lead to overvoltages higher than double the phase to ground normal voltage. Only a few arcing faults occurred in the compensated network. An earth fault arc can extinguish itself without any auto-reclosing function and the interruptions can thus be avoided. The average residual current that allowed for autoextinction was 0.48 A and the maximum current 2.5 A in the unearthed network. The corresponding figures are 5.96 and 17.88 A, respectively in the compensated network. The average duration of these faults was 0.34 s in the compensated network and 0.18 s in the isolated network. Especially in the case of the unearthed system, the maximum current of autoextinction is much smaller than had been believed before. Fault resistances fell into two major categories, one where the fault resistances were below a few hundred ohms and the other where they were in the order of thousands of ohms. Transients could be detected in nearly all fault occurrences which demanded the function of the circuit breaker. In addition, about 70% of the transients were oscillatory. Characteristics of these phenomenon can be made use of in the relay protection systems and in fault location.

Acknowledgements

The authors wish to acknowledge the support of Tapio Hakola, Erkki Antila and Veikko Lehesvuo in ABB Transmit Oy, Vaasa, Jarmo Ström in Espoo Electricity, Espoo and Stefan Ingman in Vaasa Electricity, Vaasa.

References

[1] M. Lehtonen, Transient analysis for ground fault distance estimation in electrical distribution networks, VTT Publications No 115, Espoo, 1992, p. 16.
[2] H. Paulasaari, P. Järventausta, P. Verho, M. Kärenlampi, J. Partanen, T. Hakola, E. Vähätalo, Methods to study earth fault phenomena by using a residual overvoltage relay module, IEEE/KTH Stockholm Power Tech. Conference, Stockholm, Sweden, June 18-22, 1995, 5 pp.
[3] K. Winter, The earth fault problem and the treatment of the neutral in distribution network, ERA 2 (1987) 14–18 (Original in Swedish).
[4] M. Lehtonen (Ed.), EDISON-research programme on electricity distribution automation 1993–1997. Interim report 1996, VTT Research Notes No 1824, Espoo, 1997, pp. 21–32.
[5] S. Riikonen, Distribution network operation and protection; experiences with earth fault compensation, Symp. Relay Protection Distribution Networks, Assoc. Finn. Electr. Utilities, Helsinki, Finland, 1995, 4 pp.
[6] A. Nikander, E. Lakervi, J. Suontausta, Applications of transient phenomena during earth-faults in electricity distribution networks, IEEE Catalogue No. 95TM8130, 1995, pp. 234-239.
[7] A. G. Phadke, J.S. Thorp, Computer Relaying for Power Systems, Wiley, New York, 1988, p. 112.
[8] M. Lehtonen, T. Hakola, Neutral Earthing and Power System Protection. Earthing Solutions and Protective Relaying in Medium Voltage Distribution Networks, ABB Transmit Oy, Vaasa, 1996, pp. 11–19.

B

Appendix B

Reprinted with permission from the publisher.
In: Proc. of the IEEE PES SM2001, Vancouver, Canada, July 15–19, 2001,
CD-ROM 01CH37262C. 6 p.

Earth Faults and Related Disturbances in Distribution Networks

S. Hänninen
VTT Energy, Energy Systems,
Espoo, Finland

M. Lehtonen
Helsinki University of Technology,
Power Systems Laboratory,
Espoo, Finland

T. Hakola
ABB Substation Automation Oy,
Vaasa, Finland

Abstract: This paper describes the characteristics of the earth faults and related disturbances, recorded in medium voltage overhead distribution networks during the years 1998-1999. Altogether 316 real cases were analyzed. The use of subharmonic oscillation and harmonic distortion was investigated, as a means of anticipating of faults. Arcing faults made up at least half of all the disturbances, and were especially predominant in the unearthed network. Fault resistances reached their minimum values near the beginning of the disturbances. The maximum currents that allowed for autoextinction in the unearthed network were comparatively small.
Keywords: Power systems, overhead distribution lines, fault current.

I. INTRODUCTION

One of the prime objectives when developing the automation of the distribution networks is the indication and location of earth faults. The medium voltage, 20 kV, distribution networks in Finland are mainly of overhead construction with high impedance earthing, and they are radially configured. The previous recording project, carried out during the years 1994-1996, showed that a significant portion of outages in overhead line networks is caused by earth faults [1]. In many cases a developing, high-resistance earth fault can be detected and located before it sets off a triggering action in the protective relays. Therefore it is important to know how quickly the high-resistance faults would develop at a lower range of resistance.

In the first recording project, due to the size of the sample files and to the slowness of the telecommunication system, the detection sensitivity had to be set relatively low. Therefore, a large part of the high resistance faults was lost. In the new project, the current and voltage samples were analyzed at the substation immediately after their recording. The sensitivity of the triggering could be increased, resulting in a more comprehensive recording of the high resistance faults. This paper presents the main results of the survey with the emphasis on the characteristics of the high resistance disturbances.

II. RECORDING SYSTEM DESCRIPTION

Disturbance recorders were installed at the Gesterby substation of the Espoo Electricity Co., where the distribution network neutral is unearthed and at the Gerby substation of the Vaasa Electricity Co., where the network is compensated. The length of overhead and cable lines was 63.1 km and 3.4 km in the isolated neutral network, and 159.3 km and 5.0 km in the compensated neutral network respectively.

The whole recording system consisted of two subsystems, 1 and 2, and of the computers in the substations and in the office, see Fig. 1. The recorders for subsystem 1 were triggered regularly at 10-minute intervals, whereas the recorders for subsystem 2 were triggered when the neutral voltage exceeded a threshold value. The sample sets from the recording subsystem 1 were used to determine the network parameters in normal conditions. The recording system was rack mounted and was equipped with SPAA 322 and SPAC 531 relays, and SPCR disturbance recorders. In both substations, the disturbance recorders were installed at one feeder and they comprised five SPCR recorder units for each subsystem. One unit, for the phase voltages and the zero sequence current, was set to record 5.5 s of data and the other units 0.55 s of data, at a sampling rate of 3.7 kilohertz. The recordings included both pre-trigger and post-trigger data [2].

The PC in the substation automatically monitored the recorders at selected intervals, and analyzed the sample data using software developed for this purpose. In addition, the original sample files of the disturbances were compressed and stored so that the results could be verified afterwards. The PC on the substation was connected via modems and telephone networks to another PC in the office at VTT.

III. NUMBER AND CAUSES OF DISTURBANCES

The recorded disturbances were classified into two main categories; phase to phase faults, called a short circuit and phase to earth faults, called an earth fault. Disturbances were further classified, as either temporary or permanent faults, according to how they were cleared. A fault, which disappeared by itself and did not need the action of a circuit breaker, was classified as ”self extinguishing” (SE). In other cases, the clearing of the fault demanded the action of a circuit breaker. Many faults were cleared by auto-reclosing, high speed auto-reclosing (HSAR), or delayed auto-reclosing (DAR). The remainder of the faults is permanent (P) and required repair on location, before the supply could be restored.

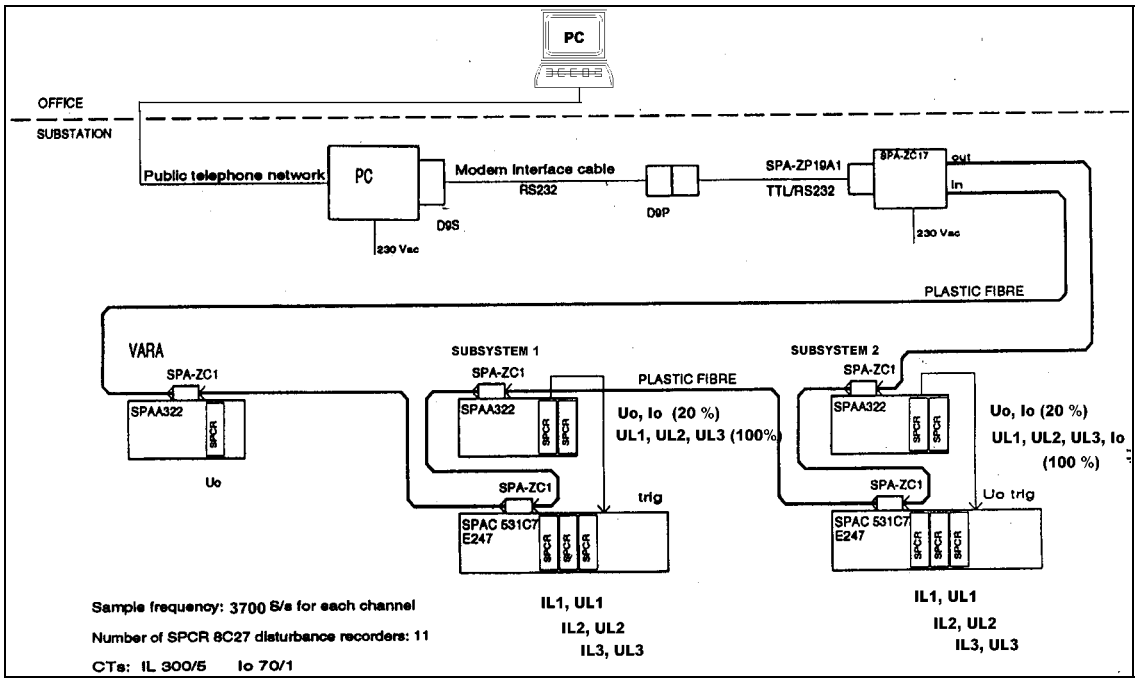

Fig. 1. Schematic diagram of the recorder system

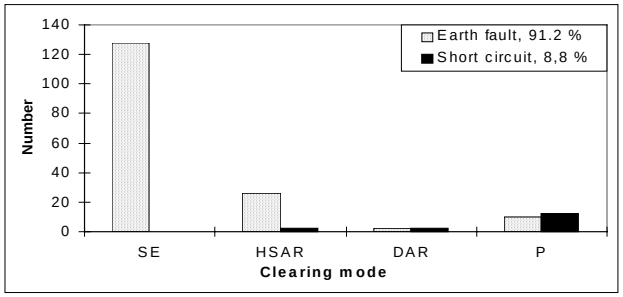

Fig. 2. Number of the disturbances classified by means of clearing in the unearthed network (SE = self extinguishing, HSAR = high speed auto-reclose, DAR = delayed auto-reclose, P = permanent fault)

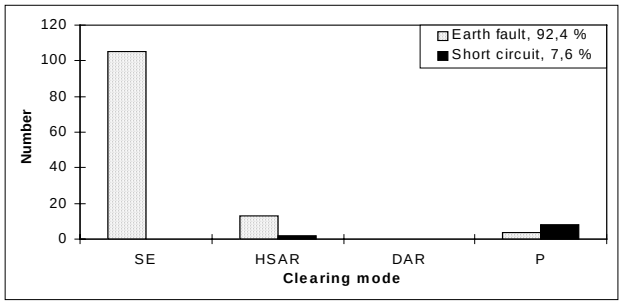

Fig. 3. Number of the disturbances classified by means of clearing in the compensated network

During the observation period of about one and a half years, altogether 424 recordings were obtained. This number includes all the disturbances on all the feeders of the substations concerned. Together 316 of the recordings were caused by events in the feeders under surveillance. Figs. 2 and 3 show the number of these disturbances divided into the main fault categories and the mode of clearing.

The delay of the high-speed auto-reclosing (HSAR) was 0.5 s in the unearthed network and 0.6 s in the compensated network. The analysis showed that HSAR was usually successful in clearing the fault. However, the majority of the disturbances disappeared of their own accord without any action from the circuit breaker. If these disturbances were to be excluded, the division of faults into earth faults and short circuits would be 70.4 % and 29.6 % in the unearthed network, and 62.9 % and 37.1 % in the compensated network. Considering all the faults, the division into the main categories and fault clearing modes was similar in both neutral earthing systems.

The causes of the disturbances could only be determined reliably for the permanent faults. About one half of the line surveyed was located in forests. The division of the fault causes was as follows; snow burden 35 %, fallen trees 27 %, boughs on pole transformers 9 %, diggers 6 %, lightning impulses 6 %. The rest of the faults (17 %) is probably caused by animals such as birds and squirrels, because the faults were cleared by an additional delayed reclosing. The causes of the disturbances cleared by auto-reclosing remained unknown. However, about one third of these events occurred during thunderstorms or windy weather. The same applied to the disturbances belonging to the SE (self-extinguishing) category. In the unearthed network, one third of the disturbances in the SE category were caused by control of the disconnecter in terrain. These 'self-inflicted' disturbances were ignored in the subsequent analysis.

IV. SUBHARMONIC OSCILLATION OF NEUTRAL VOLTAGE

When a temporary earth fault occurs, the charge stored in the earth capacitances of the faulted phase is removed. Because of the voltage rise in the two sound phases, their earth capacitances are charged. This charge dies out slowly causing subharmonic oscillation in the neutral voltage, initiated in the circuit formed by earth capacitances and voltage transformer inductance, see Fig. 4. The recurrent appearance of this subharmonic oscillation can be an indication of a developing earth fault. With higher amplitude values in the subharmonic oscillation, due to the saturation of voltage transformers, the 3rd harmonic component is also included in the neutral voltage. Comparative measurements with a resistive voltage divider have shown that the 3rd harmonic component does not exist on the primary side.

Figs. 5 and 6 show the amplitude and frequency of the subharmonic oscillation. The average of the amplitude was clearly higher in the unearthed network, whereas there was no clear difference in the frequency. The subharmonic oscillation could be detected in all the disturbances, which disappeared of their own accord. The zero sequence current was very low in these cases.

.

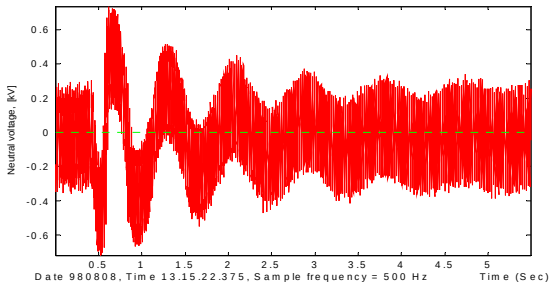

Fig. 4. Subharmonic oscillation of neutral voltage

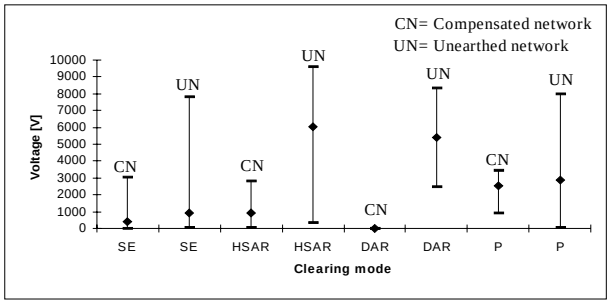

Fig. 5. Average magnitude and the range of subharmonic oscillation amplitude classified by means of fault clearing in the compensated and unearthed network

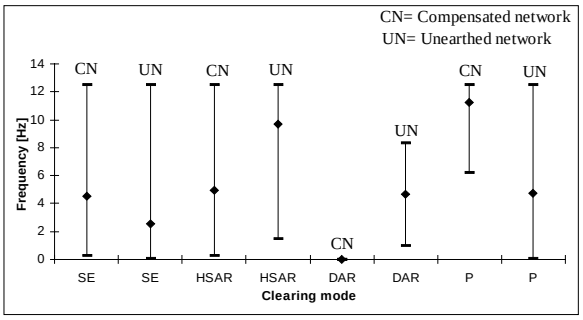

Fig. 6. Average value and the range of subharmonic oscillation frequency classified by means of fault clearing in the compensated and unearthed network

V. HARMONIC DISTORTION

An index known as total harmonic distortion (THD) is usually used to evaluate the power system quality [3]:

$$THD = \frac{\sqrt{\sum_{n=2}^{N} I_n^2}}{I_1} \times 100\ \% \qquad (1)$$

where I_1 is the fundamental, and I_n is the nth-order harmonic component. In this case, N was taken as 20 since the magnitudes of high-frequency harmonics were small and could be neglected. Two different indexes were computed. THD refers to harmonic components with n = 2-6 and, THD7 with n = 7-20. Tables 1 and 2 show the mean values of the harmonic distortions for zero sequence current and voltage. These values were computed during normal network conditions, in some network periods before and during a disturbance.

The THD of the zero sequence voltage was also high in the normal state, especially in the unearthed network. This was partially due to measuring inaccuracy, since the natural root-mean-square value of the neutral voltage was about 0.5 % of the phase voltage. The corresponding value was 6.5 % in the compensated network. In most cases, the distortion of zero sequence currents clearly increased before the fault occurred. Self extinguishing faults could also be detected by observing an increase in the neutral voltage distortion, especially in the case of an unearthed network [4].

VI. FAULT RESISTANCES

The fault impedances $\underline{Z}_f$ were determined in terms of the measured voltages and the zero-sequence impedance of the network $\underline{Z}_o$ as follows [5]:

$$\underline{Z}_f = \left(\frac{\underline{U}_v}{\underline{U}_0} - 1\right) \underline{Z}_0 \qquad (2)$$

Table 1. Mean total harmonic distortion values for zero sequence current (Io) and voltage (Uo), classified by means of disturbance clearing in the unearthed network

Fault clearing	Reference point	Io		Uo	
		THD [%]	THD7 [%]	THD [%]	THD7 [%]
	Normal state	5.0	2.0	41.0	6.0
SE	Before disturbance	22.0	15.2	65.0	14.8
SE	During disturbance	75.9	61.4	333.2	64.2
HSAR and DAR	Before disturbance	10.9	5.6	44.7	9.4
HSAR and DAR	During disturbance	42.6	14.2	14.0	2.8
P	Before disturbance	30.5	6.1	40.8	7.2
P	During disturbance	37.9	24.4	10.4	2.5

Table 2. Mean total harmonic distortion values for zero sequence current (Io) and voltage (Uo), classified by means of disturbance clearing in the compensated network

Fault clearing	Reference point	Io		Uo	
		THD [%]	THD7 [%]	THD [%]	THD7 [%]
	Normal state	5.0	4.0	0.7	0.1
SE	Before disturbance	20.2	14.3	1.2	0.5
SE	During disturbance	11.3	5.5	3.7	0.9
HSAR and DAR	Before disturbance	5.4	4.8	1.0	0.4
HSAR and DAR	During disturbance	44.7	12.5	9.0	1.1
P	Before disturbance	5.0	4.7	0.9	0.3
P	During disturbance	35.0	5.4	3.2	0.8

$\underline{U}_o$ represents the change in the phasor sum of the phase voltages and $\underline{U}_1$ is the positive sequence component of the phase voltage, measured at the moment considered. Applying (2) three times and using the following values for $\underline{U}_1$: $\underline{U}_1$, $a\underline{U}_1$ and $\underline{a}^2\underline{U}_1$, the faulted phase can also be determined. Here $\underline{a}$ is the phase shift operator, $\underline{a} = \underline{e}^{j120^o}$. From the three calculated values of $\underline{Z}_f$, the resistive part shows the highest value in the faulted phase. Fig. 7 shows an example of the change in fault resistance during the fault.

Fig. 8 shows the mean values of the fault resistances, which were taken as the minimum values from the 5 s records. The resistance value was about 0.5 kΩ for faults cleared by auto-reclosing. In the unearthed network, the fault resistances for self extinguished (SE) faults were mostly tens or hundreds of kilo-ohms, whereas the corresponding figure was some thousands of ohms in the compensated network, see Figs. 9-10. The average time and range of time from a fault initiation to the point when the fault resistance reached its minimum value, are shown in Fig. 11. The starting point for a disturbance was when the neutral voltage exceeded the triggering level. According to Fig. 11, the disturbances developed very quickly and, as a whole, the fault resistances reached their minimum values in the beginning of the disturbances.

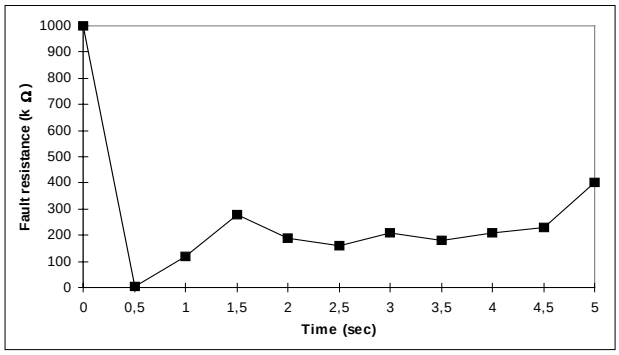

Fig. 7. The change in fault resistance during an earth fault which disappeared by itself

Table 3. The average duration for disturbances which extinguished themselves in different fault resistance classes

Neutral earthing	Average duration (sec)			
	<5kΩ	5-10 kΩ	10-100 kΩ	>100 kΩ
Unearthed network	0.10	0.09	0.14	0.27
Compensated network	0.67	0.29	1.95	3.68

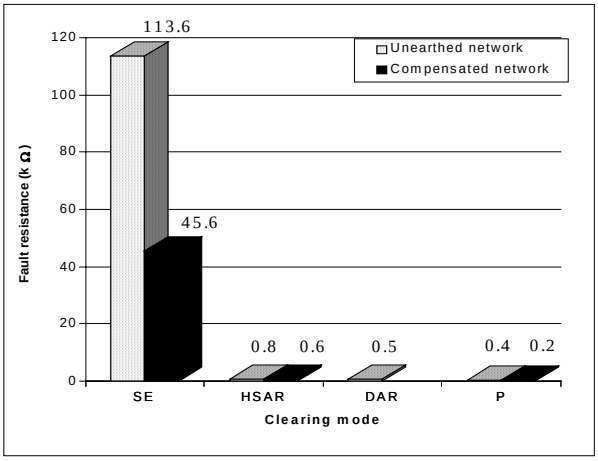

Fig. 8. Mean values of fault resistances classified by means of fault clearing in the compensated and unearthed networks

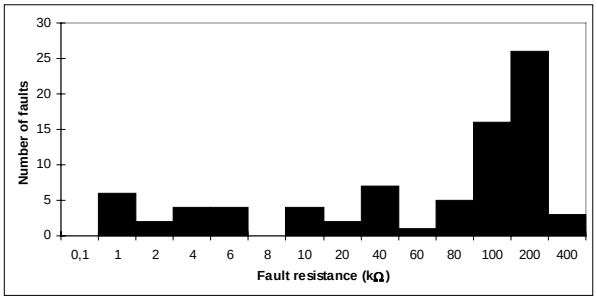

Fig. 9. The division of the fault resistances for self extinguishing faults in the unearthed network

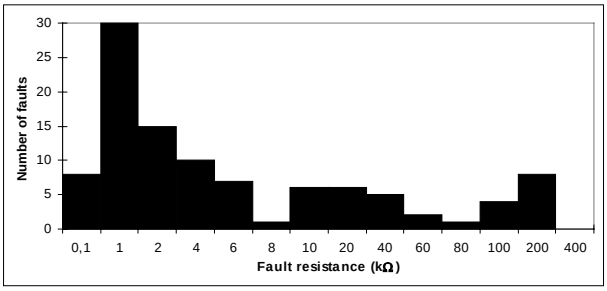

Fig. 10. The division of the fault resistances for self extinguishing faults in the compensated network

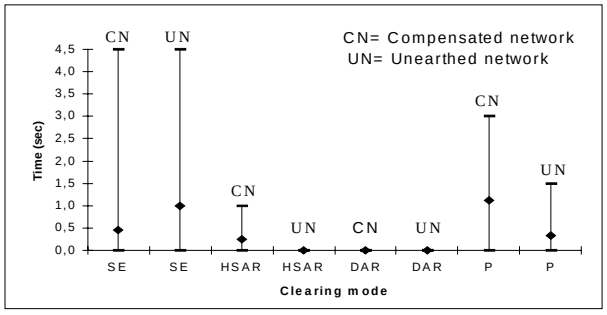

Fig. 11. Average time and range of time from fault initiation to the point when the fault resistance reached its minimum value, classified by means of fault clearing

VII. AUTOEXTINCTION

The triggering level of the recorders was set below the setting of the protection relays, so that disturbances without any auto-reclosing functions would also be recorded. Under normal conditions, the neutral voltage was about 0.5 % of the phase voltage value in the unearthed network and about 6.5 % in the compensated network. Fig. 12 shows cumulatively the faults, which extinguished themselves versus the maximum residual current. In the case of auto-extinction, the average and maximum measured residual currents were 0.9 A and 9.5 A in the unearthed network, and 5.7 A and 23.8 A in the compensated network, respectively. The average duration of these disturbances is shown in table 3. High-resistance faults disappeared noticeably more slowly in the compensated network. Fig. 12 confirmed our earlier results that, especially in the unearthed systems, the maximum currents that allowed for autoextinction were clearly smaller than had previously been believed [1]. The result is made even stranger by the fact that, in the unearthed network, surge arresters were used for overvoltage protection.

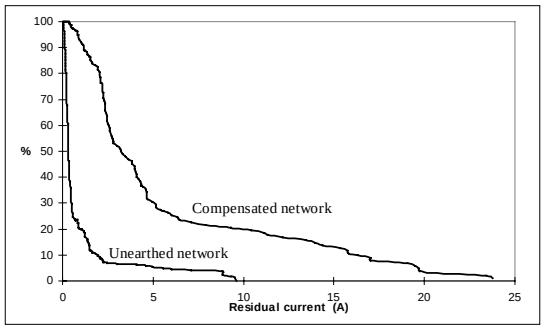

Fig. 12. Cumulative characteristic of faults which extinguished themselves versus maximum residual current

VIII. ARCING FAULTS

In an arcing earth fault, the arc disappears at the current zero crossing, but is immediately re-established when the voltage rises. Figs. 13 and 14 show the portions of arcing faults in the different neutral earthing cases. In the isolated neutral network, about 67 % of the disturbances were arcing faults, and the average duration of arcing current was approximately 60 ms. In the compensated network, the corresponding figures were 28 % and approximately 30 ms. The comparison of Tables 4 and 5 show that, the overvoltages in the unearthed network were higher than, and more than double the normal phase voltage.

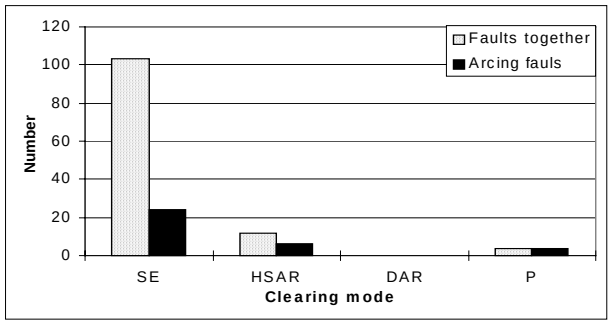

Fig. 13. Arcing faults classified by means of clearing mode in the compensated network

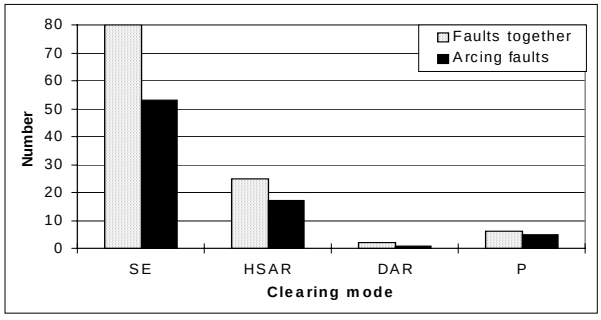

Fig. 14. Arcing faults classified by means of clearing mode in the unearthed network

0-7803-7031-7/01/$10.00 (C) 2001 IEEE

Table 4. The maximum, minimum and mean peak values of the phase voltage during an arcing fault in the unearthed network expressed in kV. The number of disturbances in each category is in brackets

Phase voltage	Voltage (kV)			
	SE /[53]	HSAR /[17]	DAR /[1]	P /[5]
$U_{v,min}$	16.88	18.62	35.39	17.06
$U_{v,max}$	37.02	38.91	35.39	40.12
$U_{v,mean}$	19.43	35.69	35.39	32.12

Table 5. The maximum, minimum and mean peak values of the phase voltage during an arcing fault in the compensated network expressed in kV. The number of disturbances in each category is in brackets

Phase voltage	Voltage (kV)			
	SE /[24]	HSAR /[6]	DAR /[0]	P /[4]
$U_{v,min}$	17.83	23.64	-	25.23
$U_{v,max}$	31.71	29.55	-	33.22
$U_{v,mean}$	22.33	26.37	-	30.71

IX. CONCLUSIONS

Disturbances in 20 kV distribution networks with high impedance earthing were recorded during years 1998-1999 on two substations. The analysis was based on the evaluation of 316 real case data recordings. Different parameters were computed which can be utilized in relay settings and in anticipation of faults. Subharmonic oscillation can indicate a developing earth fault and could be detected in all disturbances, which disappeared without intervention. The change in the total harmonic distortion of residual current and zero sequence voltage was clearly seen in both networks and could possibly be used for fault indication purposes. Especially in the unearthed systems, the maximum currents that allowed for autoextinction were, in spite of the use of surge arresters, clearly smaller than had previously been believed. The disturbances developed very quickly to the lower range of fault resistance, and as a whole the fault resistances reached their minimum values in the beginning of the disturbances. In the unearthed network, more than a half of the disturbances were arcing faults. These can lead to overvoltages higher than double the phase to ground normal voltage.

X. ACKNOWLEDGEMENTS

The authors would like to thank Veikko Lehesvuo in ABB Substation Automation Oy, Vaasa, Jarmo Ström in Espoo Electricity Co, Espoo and Stefan Ingman in Vaasa Electricity Co, Vaasa for the support of this project.

XI. REFERENCES

[1] S. Hänninen and M. Lehtonen, 'Characteristics of earth faults in electrical distribution networks with high impedance earthing,' EPSR, vol. 44, no. 3, 1998, pp. 155-161.

[2] J.A. Bright, R.O. Burnett, E.A. Baumgartner, T.W. Brandt, T.W. Cease, E.C. Fennell, C.W. Froman, R.F. Gustin, A.T. Howard, M. Kezunovic, M. Lefrancois, H.I. Mehta, R.J. Murphy, B.A. Picket, L.E. Smith and M.A.. Xavior, 'Fault and disturbance data requirements for automated computer analysis summary paper,' IEEE Trans. Power Delivery, vol. 13, no. 3, 1998, pp. 735-737.

[3] C.S. Moo, Y.N. Chang, 'Group-harmonic identification in power systems with nonstationary waveforms,' IEE Proceedings - Generation, Transmission and Distribution, vol. 142, no 5, 1995, pp. 517-522.

[4] M.B. Djuric, and V.V. Terzija, 'A new approach to the arcing faults detection for fast autoreclosure in transmission systems,' IEEE Trans. Power Delivery, vol. 10, no. 4, 1995, pp. 1793-1798.

[5] M. Lehtonen, 'A method for detection and location of high resistance earth faults in electrical distribution networks,' Pat. FI. no 100922, ABB Transmit Oy, publ. 13.03.1998, p. 12.

XII. BIOGRAPHIES

Seppo Hänninen (1956) has been with VTT Energy, Espoo, Finland since 1987. His current position is special research scientist in the research group, Electric Energy and IT. He received his Master's degree in Electrical Power Engineering from Tampere University of Technology in 1980 and Licenciate degree in Electromechanics from Helsinki University of Technology in 1991. His main fields of interest are earth fault problems, distribution automation in medium voltage networks and reliability engineering. (VTT Energy, P.O.Box 1606, FIN-02044 VTT, Finland, Tel. +358 9 4566759, Fax +358 9 4566538, E-mail: Seppo.Hanninen@vtt.fi)

Matti Lehtonen (1959) has been with VTT Energy, Espoo, Finland since 1987 and since 1999 with Helsinki University of Technology, where he is a Professor of IT applications in power systems. Matti Lehtonen received his Master's and Licenciate degrees in Electrical Engineering, both from Helsinki University of Technology, in 1984 and 1989 respectively, and the Doctor of Technology degree from Tampere University of Technology in 1992. The main activities of Dr. Lehtonen include earth fault problems, harmonic related issues and applications of information technology in distribution automation and distribution energy management. (Helsinki University of Technology, Power Systems Laboratory, P.O.Box 3000, FIN-02015 HUT, Finland, Tel. +358 9 4515484, Fax +358 9 460224, E-mail: Matti.Lehtonen@hut.fi)

Tapio Hakola (1947) has been employed by the Finnish electrotechnical company Oy Strömberg Ab, later ABB Oy, since 1973. He has worked as the research manager of the Relays and Network Control division of ABB Transmit Oy. His current position is the research manager of the Product Development division of ABB Substation Automation Oy. He gained his M. Sc. degree from the Tampere University of Technology in 1974 and he has now been working for over 25 years in the field of applied protection relaying. He is a specialist on practical methods of earth fault protection. Further, he is actively engaged in the specification and development of new protection relays. (ABB Substation Automation Oy, P.O.Box 699, FIN-65101 Vaasa, Finland, Tel.: +358 10 2241721, Fax: +358 10 2241599, E-mail: Tapio.Hakola@fi.abb.com)

C

Appendix C

Reprinted with permission from the publisher.
In: ETEP (European Transaction on Electrical Power) 1999.
Vol. 9, No. 5, pp. 285-291

Method for Detection and Location of Very High Resistive Earth Faults

S. Hänninen, M. Lehtonen

Abstract

A new method is presented for the detection and location of high resistive, permanent single-phase earth faults in medium-voltage (MV) distribution networks (20 kV). The systems considered are with unearthed or a compensated neutral and the fault resistances covered are in the range of 5 kΩ … 160 kΩ. The algorithms of the new method are based on the change of the neutral voltage and zero-sequence currents, measured at the MV substation and also at the distribution line locations.

1 Introduction

There are different ways of detecting and handling high impedance earth faults. The existing solutions can be classified as:

- direct measurement of the electric quantities of the power system [1–5],
- energy and randomness algorithms [6–7],
- harmonic analysis [8–9],
- artificial intelligence methods [10–11],
- neural networks [12],
- wavelet analysis [13–14] and
- chaotic pattern analysis [15].

This paper presents a new approach to the problem, based on the continuous monitoring of the changes of electric quantities, measured in the distribution system.

In the first part of the paper, the theory of earth faults in unearthed and compensated power systems is briefly presented. The main factors affecting high resistance fault detection are outlined and common practices for earth-fault protection in present systems are summarized.

The algorithms of the new method for high resistance fault detection and location are then presented. These are based on the changes of neutral voltage and zero-sequence currents, measured at the high-voltage /medium-voltage substation and also at the distribution line locations. The performance of the method is analyzed, and the possible error sources discussed. Among these are, for instance, switching actions, thunderstorms and heavy snowfall.

The feasibility of the method is then verified by an analysis based both on simulated data, which was derived using an EMTP-ATP simulator, and by real-system data recorded during field tests at three substations. For the error source analysis, some real-case data recorded during natural power-system events, is also used.

2 Networks with an Unearthed Neutral

In networks with an unearthed neutral, the currents of single-phase-to-ground faults depend mostly on the phase-to-ground capacitances of the lines. When the fault happens, the capacitance of the faulty phase is bypassed, and the system becomes unsymmetrical (**Fig. 1**). A model for the fault circuit can most easily

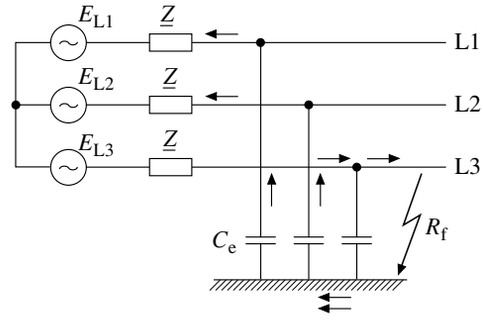

Fig. 1. Earth fault in a network with an unearthed neutral

be developed using *Thevenin*'s theorem. Before the fault, the voltage at the fault location equals the phase voltage E. The other impedances of the network components are small compared to those of the earth capacitances C_e, and can hence be neglected. This leads to the model in **Fig. 2**.

In the case where the fault resistance is zero, the fault current can be calculated as follows:

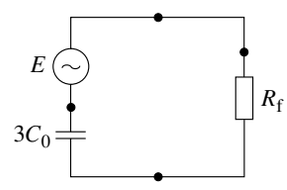

Fig. 2. Equivalent circuit for the earth fault in a network with an unearthed neutral

$$I_e = 3\omega C_e E, \qquad (1)$$

where $\omega = 2\pi f$ is the angular frequency of the network. The composite earth capacitance of the network C_e depends on the types and lengths of the lines connected in the same part of the galvanically con-

nected network. In radially operated medium-voltage distribution systems this is, in practice, the area supplied by one HV/MV substation transformer.

In earth faults there is usually some fault resistance R_f involved, the effect of which is to reduce the fault current:

$$I_{ef} = \frac{I_e}{\sqrt{1+\left(\frac{I_e}{E}R_f\right)^2}}, \quad (2)$$

where I_e is the current obtained from eq. (1). In unearthed systems this does not, in practice, depend on the location of the fault. However, the zero-sequence current of the faulty feeder, measured at the substation, includes only that part of the current that flows through the capacitances of the parallel sound lines. The zero-sequence voltage U_0 is the same that the fault current causes when flowing through the zero-sequence capacitances:

$$U_0 = \frac{1}{3\omega C_0} I_{ef}. \quad (3)$$

Using eqs. (1) and (2) this can also be written in the following form:

$$\frac{U_0}{E} = \frac{1}{\sqrt{1+(3\omega C_0 R_f)^2}}, \quad (4)$$

which states, that the highest value of neutral voltage is equal to the phase voltage. This value is reached when the fault resistance is zero. For higher fault resistances, the zero-sequence voltage becomes smaller. In networks with an unearthed neutral, the behaviour of the neutral voltage during the earth fault is of extreme importance, since it determines the overall sensitivity of the fault detection. Depending on the case, the highest fault resistance that can be detected using conventional relays is typically some kΩ.

3 Networks with a Compensated Neutral

The idea of earth-fault compensation is to cancel the system earth capacitances by an equal inductance connected to the neutral (**Fig. 3**), with a corresponding decrease in earth-fault currents. The equivalent circuit for this arrangement is shown in **Fig. 4**. The circuit is a

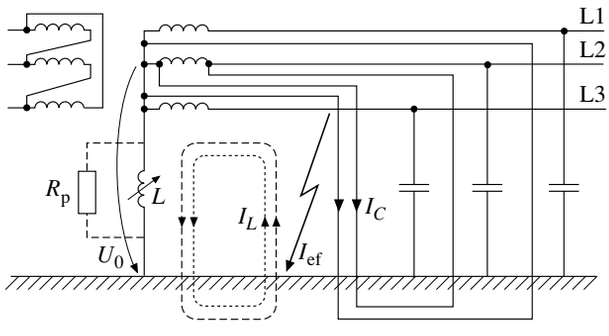

Fig. 3. Earth fault in a network with a compensated neutral

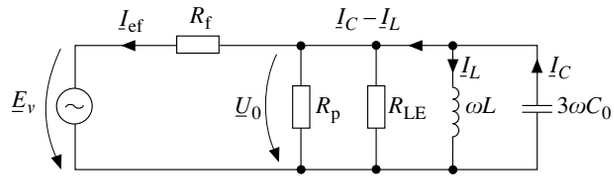

Fig. 4. Equivalent circuit for the earth fault in a network with a compensated neutral

parallel resonance circuit and if exactly tuned, the fault current has only a resistive component. This is due to the resistances of the coil and distribution lines together with the system leakage resistances (R_{LE}). Often the earthing equipment is complemented with a parallel resistor R_p, the task of which is to increase the ground fault current in order to make selective relay protection possible.

The resistive current is, in medium-voltage networks, typically from 5 % to 8 % of the capacitive current of the system. In totally cabled networks the figure is smaller, about 2 % to 3 % [16], whereas in networks with overhead lines solely, it can be as high than 15 % [17].

Using the equivalent circuit of Fig. 4, we can write for the fault current:

$$I_{ef} = \frac{E\sqrt{1+R_{LE}^2\left(3\omega C_0 - \frac{1}{\omega L}\right)^2}}{\sqrt{(R_f+R_{LE})^2 + R_f^2 R_{LE}^2\left(3\omega C_0 - \frac{1}{\omega L}\right)^2}}. \quad (5)$$

In the case of complete compensation, the above can be simplified as follows:

$$I_{ef} = \frac{E}{R_{LE}+R_f}. \quad (6)$$

The neutral voltage U_0 can be calculated correspondingly:

$$U_0 = \frac{I_{ef}}{\sqrt{\left(\frac{1}{R_{LE}}\right)^2 + \left(3\omega C_0 - \frac{1}{\omega L}\right)^2}}, \quad (7)$$

which in the case of complete compensation, is reduced to the following form:

$$\frac{U_0}{E} = \frac{R_{LE}}{R_{LE}+R_f}. \quad (8)$$

For the above equations it was assumed that no additional neutral resistor R_p is used. If needed, the effect of R_p can be taken into account by replacing R_{LE} in eqs. (5) to (8) by the parallel coupling of R_{LE} and R_p.

As in the case with an unearthed neutral, the highest zero-sequence voltage equals the phase voltage of the system. During earth faults, the neutral voltages are substantially higher in the systems with a compensated neutral than in the case with an unearthed one. Hence a more sensitive indication for high-resistance faults can be gained in the former case.

4 Present Techniques for Earth-Fault Detection

4.1 Earth-Fault Protection of MV feeders

The best result for earth-fault protection of MV lines in high-impedance earthed systems is gained by directional relays. In networks with an unearthed neutral, the phase shift between the earth-fault current of the faulty line and the current at the sound lines is about 180°. Hence, the selectivity is based on the measurement principle whereas the relay settings, neutral voltage and zero-sequence current, primarily affect the sensitivity of the protection only. In this case, the tripping is permitted, if the following conditions are met:

- the zero sequence current I_0 exceeds the setting, and
- the neutral voltage U_0 exceeds the setting, and
- the phase shift between I_0 and U_0 is in the range of $\varphi_0 + \Delta\varphi$ (where $\varphi_0 = 90°$ and $\Delta\varphi = \pm 80°$).

A more modern characteristic is the reactive current measurement, which is met in numerical relays. In this case the tripping is initiated, if neutral voltage and reactive current $I \sin\varphi$ both exceed the threshold value. However, in unearthed systems, there is practically no difference between the performance of the two relay characteristics, since the phase angle of the neutral voltage compared to the sum current is usually fairly close to –90°.

In resonant earthed systems, the protection cannot be based on the reactive current measurement, since the current of the compensation coil would disturb the operation of the relays. In this case, the selectivity can be based on the measurement of the active current component. Often the magnitude of this component is very small, and must be increased by means of a parallel resistor in the compensation equipment. The typical characteristics of the directional relays for compensated systems are similar to those used in unearthed networks. The only difference is that the characteristics are turned by –90°.

4.2 Use of Zero-Sequence Overvoltage Relays

In high-impedance earthed systems, the neutral voltage caused by an earth fault is practically the same in the whole supply area of the substation transformer. Also, its magnitude does not depend practically on the location of the fault. Consequently, a general detection of earth faults can be gained by means of a zero-sequence overvoltage relay.

In overhead line networks, faults with very high resistance can appear due to trees leaning against a conductor, for instance. These faults tend to evolve gradually into a fully established earth fault. A sensitive detection of such a fault can, to some degree, be achieved by neutral voltage relays. In this case, the voltage threshold should be as low as possible. The lowest limit depends on the neutral voltage present during the normal operating state. In unearthed systems this usually is very small, typically around 1 % of the nominal phase voltage, whereas in completely compensated networks higher values are encountered. In the latter case, the neutral voltage can be kept low by careful transposing of lines and by an appropriate setting of the compensation reactor. If the normal value varies below 2 %, a recommended relay setting is 3 %. In addition, a long time delay, up to 5 min, is needed. According to [18], these settings allow for the fault-detection sensitivity given in **Tab. 1**. It should be noted, however, that the settings in the example are applicable for alarm only.

U (in kV)	I_C (in A)	I_R (in A)	R_f (in kΩ)
6.6	5	5	13
11	5	5	22
22	10	10	22
33	20	10	24
44	20	10	32
55	20	10	40

Tab. 1. Sensitivity of earth-fault detection based on the zero-sequence overvoltage relay in a compensated system (U nominal voltage; I_C capacitive fault current after compensation; I_R resistive current of the system; R_f fault resistance value for which a fault can be detected [18])

The typical resistance of a tree is in the range of 20 kΩ … 80 kΩ. These figures apply in the seasons when the earth is not frozen. In the winter time much higher resistances, ranging up to several hundred kΩ are encountered. As can be noticed from Tab. 1, most faults of this type are beyond the reach of the zero-sequence overvoltage relays.

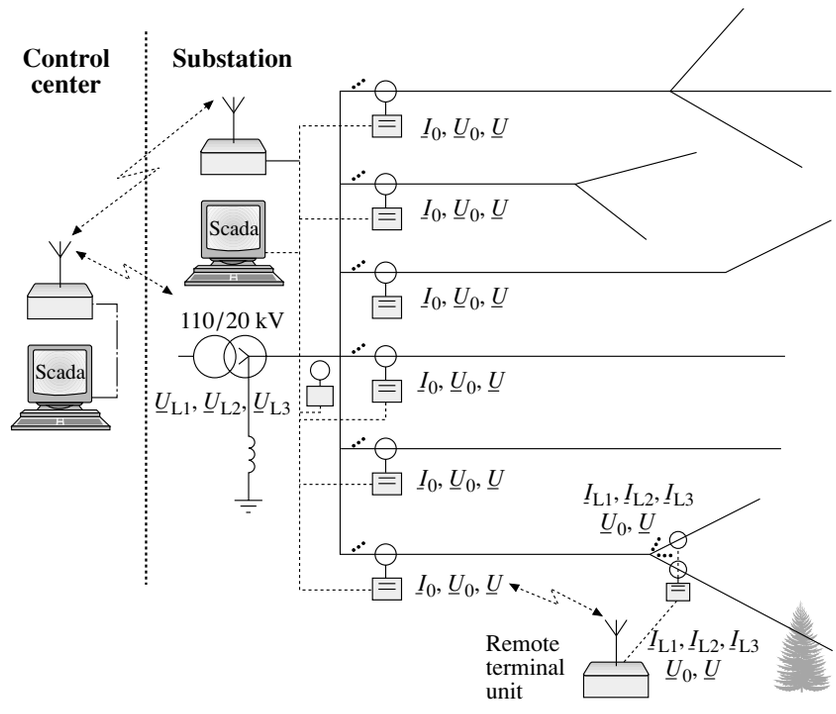

Fig. 5. High resistance fault-detection and location system

5 New Method for High Resistance Fault Detection

A new method for high resistance fault detection and location, based on the change of neutral voltage and zero-sequence currents, is presented in this section. The method consists of two independent and redundant algorithms, called neutral-voltage analysis and residual current analysis. The practical implementation of the method requires a close integration of the substation Scada with modern relays which are designed to be used for protection and control of the distribution network. A close connection is needed to the remote terminal units in the line locations as well (**Fig. 5**).

5.1 Neutral Voltage Analysis

The neutral voltage analysis algorithm can be explained by the simplified equivalent circuit for the one-phase earth fault (**Fig. 6**).

Using the equivalent circuit, the fault impedance $\underline{Z}_f$ can be determined in terms of the measured voltages and the zero-sequence impedance of the network as follows:

$$\underline{Z}_f = \left(\frac{\underline{U}_1}{\underline{U}_0} - 1 \right) \underline{Z}_0 . \qquad (9)$$

$\underline{Z}_0$ can be determined from the equivalent circuit of **Fig. 7**. In the unearthed network (Fig. 7a) it is the parallel connection of the phase-to-ground capacitances and phase-to-ground resistances, the so called "leakage resistances". For systems earthed via a Petersen coil, the circuit must be complemented with parallel connection of the coil impedance (Fig. 7b).

For the detection of a high resistance earth fault it is essential to determine the resistive part of the fault impedance. In eq. (9), $\underline{U}_0$ represents the phasor sum of the phase voltages and $\underline{U}_1$ is the positive sequence component of the phase voltage, measured at the moment considered. Applying eq. (9) for three times and using for $\underline{U}_1$ the following values: $\underline{U}_1$, $\underline{a}\,\underline{U}_1$ and $\underline{a}^2\underline{U}_1$, the faulted phase can also be determined. Here $\underline{a}$ is the phase shift operator, $\underline{a} = e^{j120°}$.

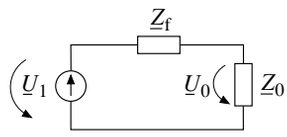

Fig. 6. Simplified equivalent circuit for an earth fault in a distribution network

From the calculated three values of $\underline{Z}_f$, the resistive part shows the highest value in the faulted phase. Because the fault impedance must be resistive, the calculated resistive parts of $\underline{Z}_f$ for the other two "healthy" phases are negative. The triggering level of the algorithm is set so that a high resistive earth fault is indicated, if the calculated maximum real part of $\underline{Z}_f$ is smaller than the fixed threshold value and is at least four times the magnitude of the imaginary part of the corresponding $\underline{Z}_f$.

The detection of very high fault resistances is difficult due to the neutral voltage present in the normal network conditions. This is mainly caused by the natural unbalances of the feeders. The sensitivity of the method can be improved by using the change of the neutral voltage which is determined as a difference of the real neutral voltage in the network at the moment being considered and of the corresponding mean value of the last 10 min [19].

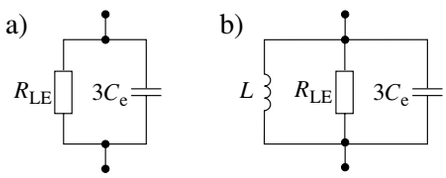

Fig. 7. Equivalent circuits
a) Zero-sequence network for the unearthed system
b) Compensated system

5.2 Residual Current Analysis

The faulted feeder is most often localised by the comparison of the residual current magnitudes. The indication is considerably more sensible, if the influence of the natural unbalances is eliminated by using the changes of the residual currents rather than the currents themselves. [4] introduces a method which uses the variations of the residual currents, neutral-to-ground voltage, phase-to-ground voltages and the values of the global phase-to-ground admittances of the feeders. It yields an estimate of the fault resistance and of the faulty phase correctly up to 100 kΩ.

The new algorithm presented in this paper utilises the simultaneous changes of neutral voltages and residual currents (**Fig. 8**). The idea of the algorithm is to compensate the effect of the earth capacitances using the measured change of the neutral voltage and the known zero-sequence impedance of the feeder considered (eq. (10)):

$$\Delta\underline{I}_{0j} = \Delta\underline{I}_{0jm} - \frac{\Delta\underline{U}_{0m}}{\underline{Z}_{0j}} . \qquad (10)$$

Depending on the measuring accuracy, the resulting compensated current of a healthy feeder is nearly zero and in the case of the faulty feeder, it corresponds to one third of the earth fault current at the fault point. This method can also be used to discriminate the faulty line section, if the disconnector stations are provided with modern remote terminal units.

This method requires accurate knowledge about the zero-sequence impedances of each feeder. An advantage of the method is that, in the case of autoreclosure, the modern relays restore the values of the neutral volt-

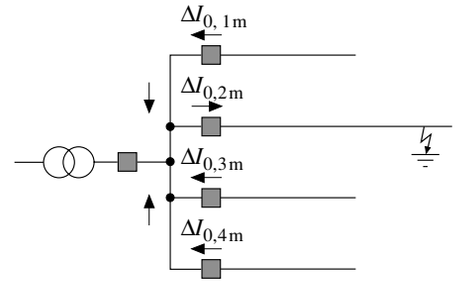

Fig. 8. Flows of the zero-sequence currents in the case of the earth fault

age and zero-sequence currents in the healthy feeders. These values can be used to update the zero-sequence impedance data.

After calculation of the fault resistance, the fault current can also be determined using the equivalent circuit of Fig. 6. When combining this information with the knowledge of the compensated zero-sequence currents and of the faulty phase, a very powerful means for detecting the faulty feeder, and further the faulty branch of the line, can be implemented.

6 Feasibility of the Method and Error Sources

In order to expose the detection algorithms to a wide range of field conditions, the algorithms were tested with naturally occurring faults, intermittent disturbances, staged faults and normal system activity. The feasibility of the method was also verified by an analysis based on simulated data, derived using an EMTP-ATP based network model. In the simulations, the sampling rate was 500 Hz and the sampling period was 1 s. Using simulated data, earth faults up to 500 kΩ could be detected. In order to evaluate the accuracy of the algorithm, we must keep in mind, that the simulated data did not include error factors. Among these are: the noise of the measured quantities produced by the power system itself, the accuracy of the measurement transducers, the properties of the electrical circuits of the measuring system, etc. [20].

The field tests with staged faults were carried out in the normal network conditions at the Lammi substation of Häme Electricity and at the Maalahti substation of Vaasa Electricity, where the distribution networks are unearthed and at the Kitee substation in North-Carelian Electricity, where the network is compensated. The networks are mainly of overhead construction. **Tab. 2** to **Tab. 4** show some results of the earth fault test.

Tab. 2 shows the fault resistances determined by the neutral voltage algorithm from the field measurements at three substations and **Tab. 5** gives some corresponding values for the real case faults before they developed into a permanent fault. Especially in the compensated network, residual currents of the feeders are very low in the case of high-resistance earth faults. Tab. 3 shows the measured changes of the residual currents in the beginning of the feeders at the Kitee substation and at the disconnector location. The faulty feeder is marked in boldface. Tab. 4 shows some experimental results for detection of the faulty feeder in the compensated network obtained by the residual current algorithm. Our experience has shown that these algorithms are able to detect resistive earth faults reliably up to a resistance of 160 kΩ in a 20-kV distribution system.

Staged fault		**Lammi**		**Maalahti**		**Kitee**	
R_f (in kΩ)	Ph.	R_{fc} (in kΩ)	arg ($\underline{Z}_f$)	R_{fc} (in kΩ)	arg ($\underline{Z}_f$)	R_{fc} (in kΩ)	arg ($\underline{Z}_f$)
20	L1	15.9	8.6°	20.5	11.3°	17.0	−7.2°
40	L2	39.8	7.6°	41.7	2.1°	26.4	−10.1°
60	L3	71.2	1.8°	62.2	10.5°	46.8	−2.9°
80	L2	83.0	7.6°	80.5	−1.1°	50.2	−10.1°
100	L1	111.8	6.9°	131.3	5.5°	81.5	−14.8°
160	L3	179.5	−7.6°	120.0	18.7°	142.4	−3.0°
180	L3	177.0	−33.6°	141.6	17.2°	156.6	−0.9°
220	L3	178.1	−40.6°	223.3	27.0°	194.4	−2.4°
Tree	L1	174.4	9.4°	–	–	–	–
Tree	L1	207.1	7.0°	–	–	–	–
Tree	L2	281.9	33.3°	–	–	–	–
Tree	L3	237.8	−32.0°	–	–	–	–

Tab. 2. Experimental results obtained by the neutral voltage algorithm (R_f real fault resistance: Ph. faulty phase in the field test; R_{fc} calculated fault resistance (real part of the fault impedance); arg ($\underline{Z}_f$) argument of the fault impedance (in degrees))

Staged fault		**Substation**					**Disc.**
R_f (in kΩ)	Ph.	$3\Delta I_{01m}$ (in A)	$3\Delta I_{02m}$ (in **A**)	$3\Delta I_{03m}$ (in A)	$3\Delta I_{04m}$ (in A)	$3\Delta I_{05m}$ (in A)	$3\Delta I_{0m}$ (in **A**)
20	L1	0.284	**0.467**	0.227	0.599	0.569	**0.318**
40	L3	0.157	**0.421**	0.149	0.384	0.390	**0.228**
60	L2	0.108	**0.284**	0.091	0.248	0.239	**0.141**
80	L3	0.082	**0.152**	0.062	0.175	0.170	**0.099**
100	L2	0.054	**0.105**	0.069	0.182	0.178	**0.090**
120	L3	0.045	**0.069**	0.042	0.109	0.097	**0.054**
160	L1	0.010	**0.093**	0.043	0.137	0.139	**0.090**
180	L2	0.039	**0.036**	0.047	0.134	0.127	**0.084**
200	L1	0.034	**0.063**	0.047	0.125	0.110	**0.042**
220	L1	0.021	**0.049**	0.025	0.057	0.055	**0.069**

Tab. 3. Changes of the measured residual currents in the beginning of the feeders at the Kitee substation and at the disconnector location (faulted feeder is marked in boldface)

Staged fault		**Substation**					
R_f (in kΩ)	Ph.	$3\Delta I_{01}$ (in A)	$3\Delta I_{02}$ (in **A**)	$3\Delta I_{03}$ (in A)	$3\Delta I_{04}$ (in A)	$3\Delta I_{05}$ (in A)	$3\Delta U_{0m}$ (in V)
20	L1	0.047	**0.561**	0.010	0.019	0.017	1 350
40	L3	0.053	**0.545**	0.019	0.047	0.056	866
60	L2	0.029	**0.345**	0.056	0.025	0.027	574
80	L3	0.036	**0.191**	0.006	0.015	0.014	422
100	L2	0.015	**0.197**	0.012	0.034	0.032	365
120	L3	0.010	**0.095**	0.007	0.027	0.018	242
160	L1	0.027	**0.157**	0.010	0.026	0.028	201
180	L2	0.035	**0.114**	0.022	0.064	0.061	204
200	L1	0.050	**0.120**	0.026	0.069	0.059	154
220	L1	0.006	**0.072**	0.005	0.003	0.001	130

Tab. 4. Some experimental results for detection of the faulted feeder in a compensated network obtained by the residual current algorithm (faulted feeder is marked in boldface)

Substation	**Fault cause**	R_f (in kΩ)
Honkavaara	Broken insulator	20.0
Honkavaara	Broken insulator	108.0
Honkavaara	Broken insulator	110.0
Honkavaara	Transformer fault	29.8
Honkavaara	Snow burden	29.2
Honkavaara	Snow burden	104.0
Kitee	Downed conductor	228.0
Lammi	Downed conductor	223.0
Renko	Tree contact	95.5

Tab. 5. Fault resistances detected by the neutral voltage algorithm before the fault developed into a permanent one

	Unearthed network			Compensated network		
	$R_{f,min}$ (in kΩ)	$R_{f,max}$ (in kΩ)	$R_{f,mean}$ (in kΩ)	$R_{f,min}$ (in kΩ)	$R_{f,max}$ (in kΩ)	$R_{f,mean}$ (in kΩ)
Switching action	43	199	93	10	218	53
Thunder-storm	85	116	93	–	–	–
Snowfall	199	268	233	46	318	136

Tab. 6. Fault resistances detected by the neutral voltage algorithm in the case of some intermittent disturbances in the network

The drawback of the algorithms is that the normal system activity and intermittent disturbances may cause changes to the neutral voltage and residual currents similar to the real faults in the feeders. **Tab. 6** shows the calculated resistances which correspond to the recorded changes of the neutral voltages in the case of normal switching actions, thunderstorms and snowfalls. These results are based on the continuous monitoring and recording of the neutral voltages at four substations during the period of one and a half years. For discrimination of the intermittent disturbances, the algorithms use 1 s mean values of the currents and voltages and for calculations of the corresponding changes, mean values of the last 10 min are used as a reference level. Thunderstorms and snowfalls can be discriminated by the fact, that they usually affect several feeders simultaneously.

7 Conclusions

A new method was presented for the single-phase-to-earth fault detection and location in high impedance earthed distribution systems. The method is able to detect faults up to 160 kΩ. The drawback of the method is that the normal system activity and intermittent disturbances may cause changes to the neutral voltage and residual currents similar to the real faults in the feeders. Examples of these are normal switching actions, thunderstorms and snowfall. This problem can be mitigated by using longer time average measurements for comparison when identifying the fault feeder or line section. The algorithms were verified by field tests and the first trial system implemented in modern relays and substation Scada will be installed during the autumn of 1999.

8 List of Symbols and Abbreviations

8.1 Symbols

$\underline{a}$, $\underline{a}^2$	complex rotation operators
C_e	phase-to-ground capacitance of the system
C_0	zero-sequence capacitance
E	phase-to-ground voltage at fault location
$E_{L1,L2,L3}$	fault moment phase-to-ground voltage
I_C	capacitive fault current
I_e	earth fault current
I_{ef}	earth fault current reduced by fault resistance
I_R	resistive current
$\Delta\underline{I}_{0j}$	compensated zero-sequence current of the feeder j
$\Delta\underline{I}_{0mj}$	measured change of zero-sequence current of the feeder j
L	coil inductance
R_{LE}	phase-to-ground resistance of the system
R_f	fault resistance
R_p	parallel resistor
U	nominal voltage (phase-to-phase voltage)
U_1	positive-sequence component of the phase-to-ground voltage
$U_{L1,L2,L3}$	phase-to-ground voltages
U_0	neutral voltage (zero-sequence voltage)
$\Delta\underline{U}_{0m}$	measured change of neutral voltage (zero-sequence voltage)
$\underline{Z}_0$	zero-sequence impedance of the network
$\underline{Z}_{0j}$	zero-sequence impedance of the feeder j
$\underline{Z}_f$	fault impedance
ω	rated angular frequency

8.2 Abbreviations

EMTP-ATP	electromagnetic transients program-alternative transients program
HV/MV	high voltage/medium voltage (substation)
Scada	supervision control and data acquisition

References

[1] *Aucoin, B. M.; Jones, R. H.:* High Impedance Fault Detection Implementation Issues. IEEE Trans. on Power Delivery PWRD-11 (1996) no. 1, pp. 139 – 148

[2] *Winter, K.:* Nollpunktsanalysis – ny metod att detektera högohmiga jordfel. ERA Electricitetens Rationella Använding (Sweden) (1988) no. 5, pp. 18 – 20 and 23 – 24

[3] *Leitloff, V.; Pierrat, L; Feuillet, R.:* Study of the Neutral-to-Ground Voltage in a Compensated Power System. ETEP Eur. Trans. on Electr. Power 4 (1994) no. 2, pp. 145 – 153

[4] *Leitloff, V.; Feuillet, R.; Griffel, D.:* Detection of Resistive Single-Phase Earth Faults in a Compensated Power-Distribution System. ETEP Eur. Trans. on Electr. Power 7 (1997) no. 1, pp. 65 – 73

[5] *Kim, C. J.; Russel, B. D.:* Analysis of Distribution Disturbances and Arcing Faults Using the Crest Factor. Electr. Power Syst. Res. 35 (1995) no. 2, pp. 141 – 148

[6] *Li, S.; Russel, B. D.:* Optimal Arching Fault Detection Using Signal Processing Techniques. Electr. Power Syst. Res. 21 (1991) no. 2, pp. 121 – 128

[7] *Benner, C.; Carswell, P.; Russel, B. D.:* Improved Algorithm for Arching Faults Using Random Fault Behavior. Electr. Power Syst. Res. 17 (1989) no. 1, pp. 49 – 56

[8] *Russel, B. D.; Mehta, K.; Chinchali, R. P.:* An Arching Fault Detection Technique Using Low Frequency Current Components – Performance Evaluation Using Recorded Field Data. IEEE Trans. on Power Delivery PWRD-3 (1988) no. 4, pp. 1 493 – 1 500

[9] *Jeerings, D. I.; Linders, J. R.:* Unique Aspects of Distribution System Harmonics Due to High Impedance Ground Faults. IEEE Trans. on Power Delivery PWRD-5 (1990) no. 2, pp. 1 086 – 1 094

[10] *Russel, B. D.; Chinchali, R. P.:* A Digital Signal Processing Algorithm For Detecting Arcing Faults on Power Distribution Feeders. IEEE Trans. on Power Delivery PWRD-4 (1989) no. 1, pp. 132 – 140

[11] *Russel, B. D.; Benner, C. L.:* Arcing Fault Detection for Distribution Feeders: Security Assessment in Long Term Field Trials. IEEE Trans. on Power Delivery PWRD-10 (1995) no. 2, pp. 676 – 683

[12] *Sultan, A. F.; Swift, G. W.; Fedirchuk, D. J.:* Detection of High Impedance Faults Using a Multi-Layer Perceptron. IEEE Trans. on Power Delivery PWRD-7 (1992) no. 4, pp. 1 871 – 1 876
[13] *Chaari, O.; Meunier, M.; Brouaye, F.:* Wavelets: A New Tool for the Resonant Grounded Power Distribution Systems Relaying. IEEE Trans. on Power Delivery PWRD-11 (1996) no. 3, pp. 1 301 – 1 308
[14] *Yinin, X.; Li, Q.; Wai, D. C. T.:* DSP Implementation of a Wavelet Analysis Filter Bank for High Impedance Fault Detection. Int. Conf. on Energy Managem. and Power Delivery (EMPD'98), Singapore, Proc. IEEE Cat. no. 98EX137, pp. 417 – 421
[15] *Ko, J. H.; Shim, J. C.; Ryu, C. W.; Park, C. G.; Yim, W. Y.:* Detection of High Impedance Faults Using Neural Nets and Chaotic Degree. Int. Conf. on Energy Managem. and Power Delivery (EMPD'98), Singapore, Proc. IEEE Cat. no. 98EX137, pp. 399 – 404
[16] *Hubensteiner, H.:* Schutztechnik in elektrischen Netzen. Offenbach · Berlin/Germany: VDE VERLAG, 1989
[17] *Claudelin, P.:* Compensation of the earth fault current in a MV distribution network. INSKO Insinöörijärjestöjen Koulutuskeskus 157-91 (Earth- Fault Problems in MV Systems), Helsinki/Finland 1991, Proc. pp. 1 – 38 (in Finnish)
[18] Känsliga jordfelsskydd: Bortkoppling av högresistiva jordslutningar i icke direkt jordade distributions- och transmissions system. Stockholm/Sweden: Svenska Eleverksföreningen, 1990
[19] *Lehtonen, M.:* A method for detection and location of high resistance earth faults in electrical distribution networks. Pat. FI. no 100922, ABB Transmit Oy, publ. 13.03.1998
[20] *Lehtonen, M.:* Transient analysis for ground fault distance estimation in electrical distribution networks. Espoo/Finland: VTT Publ. No 115, 1992

Manuscript received on April 6, 1998

The Authors

Seppo Hänninen (1956) has been with VTT Energy, Espoo, Finland, since 1987. His current position is research scientist in the research group, Electricity Distribution. He received his Master's degree in Electrical Power Engineering from Tampere University of Technology in 1980 and Licenciate degree in Electromechanics from Helsinki University of Technology in 1991. His main fields of interest are earth fault problems, distribution automation in medium voltage networks and reliability engineering. (VTT Energy, P.O. Box 1606, FIN-02044 VTT, Finland, Phone: +35 89 /456 67 59, Fax: +35 89 /456 65 38, E-mail: Seppo.Hanninen@vtt.fi)

Matti Lehtonen (1959) has been with VTT Energy, Espoo, Finland, since 1987 and since 1999 with Helsinki University of Technology, where he is a Professor of IT applications in power systems. He received his Master's and Licenciate degrees in Electrical Engineering, both from Helsinki University of Technology, in 1984 and 1989, respectively, and the Doctor of Technology degree from Tampere University of Technology in 1992. His main activities include earth fault problems, harmonic related issues and applications of information technology in distribution automation and distribution energy management. (Helsinki University of Technology, Power Systems Laboratory, P.O. Box 3000, FIN-02015 HUT, Finland, Phone: +35 89 /451 54 84, Fax: +35 89 /460 2 24, E-mail: Matti.Lehtonen@hut.fi)

Appendix D

D

ELSEVIER

Preprinted with permission from the publisher.
In: EPSR (Electric Power Systems Research. Vol. 54, No. 3, pp. 199-206

ELECTRIC POWER SYSTEMS RESEARCH

www.elsevier.com/locate/epsr

A probabilistic method for detection and location of very high resistive earth faults

Seppo Hänninen [a,*], Matti Lehtonen [a], Urho Pulkkinen [b]

[a] *VTT Energy, Energy Systems, PO Box 1606, FIN-02044 VTT, Finland*
[b] *VTT Automation, Industrial Automation, PO Box 1301, FIN-02044 VTT, Finland*

Received 12 January 1999; received in revised form 24 March 1999; accepted 15 September 1999

Abstract

A probabilistic method is presented for the detection and location of very high resistive, permanent single-phase earth faults in medium voltage, radial operated distribution networks (20 kV). The systems considered have an unearthed or a compensated neutral and the fault resistances covered are in the range 5–220 kΩ. The algorithms of the method are based on the change of the neutral-voltage and zero-sequence currents, measured at the MV substation and also at the distribution line locations. The feasibility of the method was verified by an analysis based on system data recorded during field tests in real power systems.

Keywords: Earth faults; Probabilistic methods

1. Introduction

In high-impedance earthed distribution systems, conventional relaying solutions are able to detect earth faults selectively up to 4–5 kΩ, but not for higher impedances. However, there is a class of permanent faults which typically starts with very high phase-to-earth resistance, and only gradually evolves to a fully established fault, causing relay tripping. Examples of these faults are a tree leaning on an overhead line conductor, or a broken overhead-line pin insulator.

It is clear that the identification of these faults before they cause any permanent outage would be extremely useful. This need has been widely recognised, and there has been active research in several institutes to find the solutions needed. A short review of the algorithms for high resistive fault detection and location is given in Refs [1,2]. In the same references, two algorithms are proposed, based on the changes of neutral-voltage and zero-sequence currents — measured at the high-voltage/medium-voltage substation. In this paper, these algorithms are developed further and two alternative probabilistic approaches are proposed for faulty feeder and line-section identification. Uncertainties related to current and voltage measurements and to network components are discussed. The feasibility of the methods is verified by an analysis based on real system data recorded during field tests at one medium-voltage substation.

2. High resistance earth fault detection

The method for high resistance fault detection and location consists of two independent algorithms, called neutral-voltage analysis and residual-current analysis. The practical implementation of the algorithms requires a close integration of the substation SCADA with modern relays used for protection and control of the distribution network. A close connection is needed to the remote terminal units in the line locations as well (see Fig. 1).

2.1. Neutral voltage analysis

The neutral-voltage analysis algorithm can be explained by the simplified equivalent circuit for an earth fault (see Fig. 2).

* Corresponding author.

0378-7796/00/$ - see front matter
PII: S0378-7796(99)00084-X

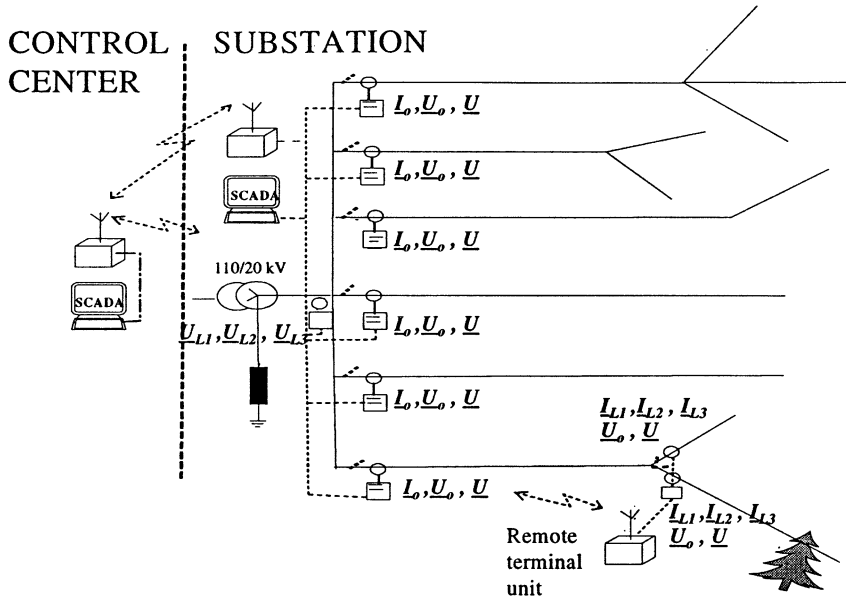

Fig. 1. The high resistance fault detection and location system.

Using the equivalent circuit, the fault impedance $\underline{Z}_f$ can be determined in terms of the measured voltages and the zero-sequence impedance of the network as follows:

$$\underline{Z}_f = \left(\frac{\underline{U}_L}{\underline{U}_0} - 1\right) * \underline{Z}_0 \quad (1)$$

where $\underline{Z}_0$, is obtained from the equivalent circuit of Fig. 3. In an unearthed network (see Fig. 3a) it is a parallel connection of the phase-to-ground capacitances and phase-to-ground resistances, the so-called 'leakage resistances'. For systems earthed via a Petersen coil, the circuit must be complemented with a parallel connection of the coil impedance (see Fig. 3b).

Of the other terms in Eq. (1), $\underline{U}_0$, represents the phasor sum of the phase voltages and $\underline{U}_L$ is the positive sequence component of the phase voltage, measured at the moment considered. Eq. (1) is applied three times using for $\underline{U}_L$ the following values: $\underline{U}_L$, $\underline{a}\underline{U}_L$ and $\underline{a}^2\underline{U}_L$ ($\underline{a}$ is the phase shift operator, $\underline{a} = 1/\underline{120}°$).

From the calculated three values of $\underline{Z}_f$ the resistive part shows the highest value in the failed phase. Because the fault impedance must be resistive, the calculated resistive parts of $\underline{Z}_f$ for the other two 'healthy' phases are negative. The triggering level of the algorithm is set so that an earth fault is indicated, if the calculated maximum real part of $\underline{Z}_f$ is smaller than a fixed threshold value and is at least four times the magnitude of the imaginary part of the corresponding $\underline{Z}_f$.

The detection of very high fault resistances is difficult due to the neutral voltage present in the normal network conditions. This is mainly caused by the natural unbalances of the feeders. The sensitivity of the method can be improved by using for $\underline{U}_0$ the change of the neutral voltage, determined as a difference between the last measured value and the mean value of the last 10 min [1].

After calculation of the fault impedance $\underline{Z}_f$, and supposing that the fault resistance is very much higher than the network zero-sequence impedance $\underline{Z}_f \gg \underline{Z}_0$, the earth fault current can be solved as follows

$$\underline{I}_f \cong \frac{\underline{U}_L}{\underline{Z}_f} \quad (2)$$

where $\underline{U}_L$, positive-sequence component of the phase voltage in failed phase; $\underline{Z}_f$, fault-impedance.

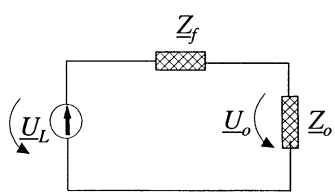

Fig. 2. Simplified equivalent circuit for an earth fault in a distribution network.

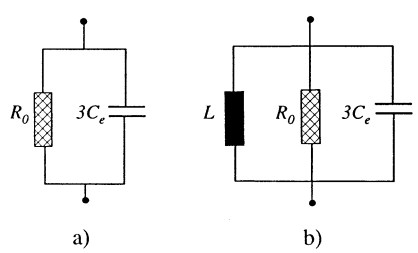

Fig. 3. Equivalent circuit of the zero-sequence network for the unearthed system (a) and for the compensated system (b).

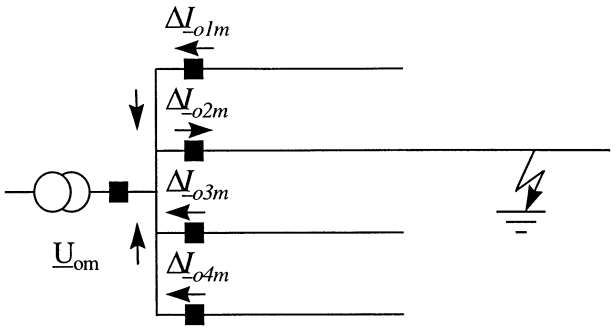

Fig. 4. Flows of the zero-sequence currents in the ease of the earth fault.

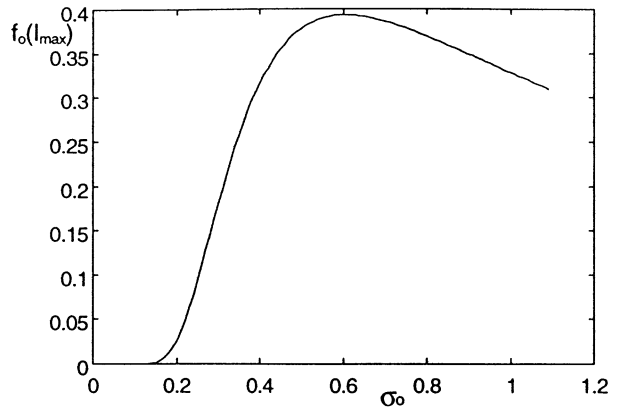

Fig. 6. Values of the normal distribution function versus deviation when $I_{max} = 0.615$ A and $\mu_0 = 0$ A.

2.2. Residual current analysis

The residual current analysis algorithm utilises the simultaneous changes of neutral voltages and residual currents (see Fig. 4). The idea is to compensate the effect of the earth capacitances of the feeder considered as follows:

$$\underline{I}_{0i} = \underline{I}_{0i\mathrm{m}} - \frac{\underline{U}_{0\mathrm{m}}}{\underline{Z}_{0i}} \quad (3)$$

where $\underline{I}_{0i}$, compensated zero-sequence current of the feeder i; $\underline{I}_{0i\mathrm{m}}$, measured change of zero-sequence current of the feeder i; $\underline{U}_{0\mathrm{m}}$, measured change of neutral voltage (zero-sequence voltage); $\underline{Z}_{0i}$, zero-sequence impedance of the feeder i (includes earth capacitance and leakage resistance.

In the case of absolute measuring accuracy, the resulting compensated current of a healthy feeder is zero and that of the faulty feeder corresponds to one third of the earth fault current at the fault point.

For the discrimination of intermittent disturbances, the algorithm uses 1 s mean values of the currents and voltages and when computing the corresponding changes, mean values of the last ten minutes are used as a reference level. For example, thunderstorms and snowfalls can be discriminated by the fact that they usually affect several feeders simultaneously.

When combining the information of the fault current, obtained by the neutral-voltage analysis Eq. (2), with the knowledge of the compensated zero-sequence currents, a very powerful means for location of the faulty feeder and the faulty line section can be implemented [2,3].

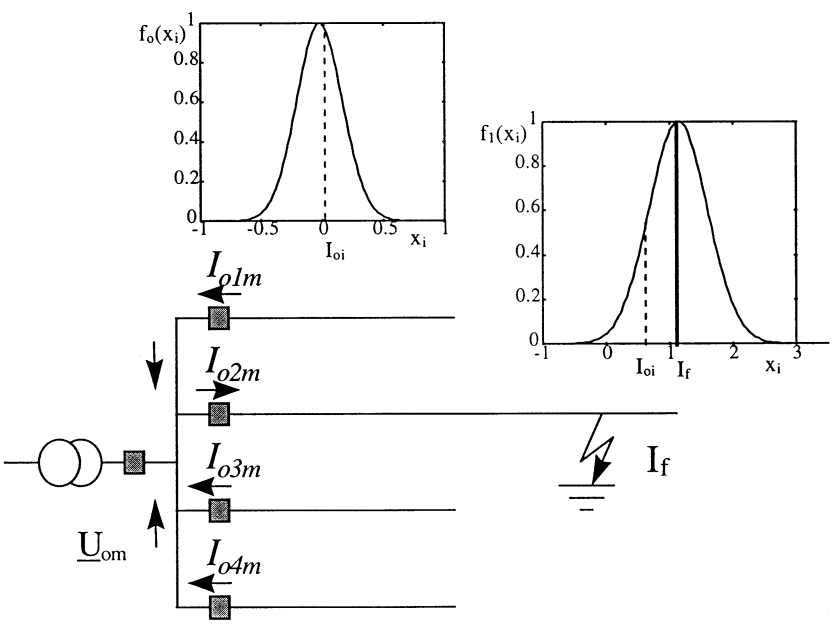

Fig. 5. A principle scheme of the current point probabilities; $f_0(x)$ is the probability density function of a current in a 'healthy' feeder and $f_1(x)$ is the corresponding function in a 'faulty' feeder.

3. Probabilistic approach

3.1. General

In the case of a low fault resistance, the faulty feeder can simply be identified by a straight comparison of the compensated current magnitudes of the feeders. Normally, the failed feeder indicates the highest current magnitude. However, in the case of very high fault resistance, the magnitudes of the compensated feeder currents are small and there is a risk of malfunction. This is due to the inaccuracies of the current and voltage measurements and to the errors of the network component values. Therefore, instead of direct comparison, it is more reasonable to quantify a probability estimate that the feeder concerned is failed.

The compensated current values of the feeders and the estimated fault current are later regarded as random variables. These are assumed to be independent and identically distributed random variables obeying Normal distributions with parameters $\mu =$ mean and $\sigma^2 =$ variance [4]. In what follows, two different probabilistic methods are presented, called point probability method and overall probability method. The principle of point probability method is illustrated in Fig. 5.

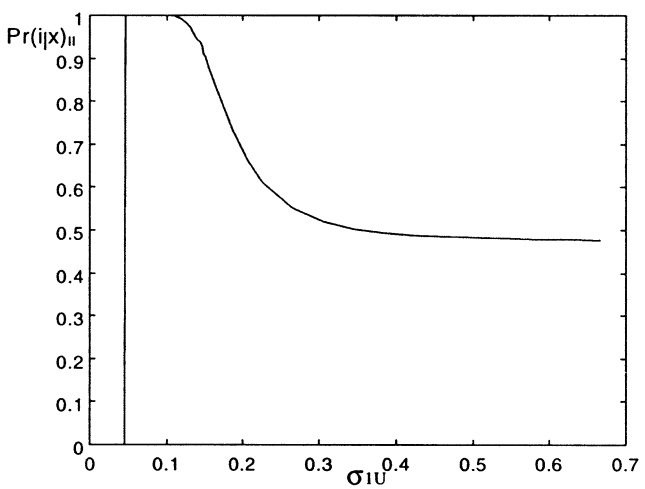

Fig. 7. Probability $\Pr(i\,|x)_{II}$ as a function of the deviation.

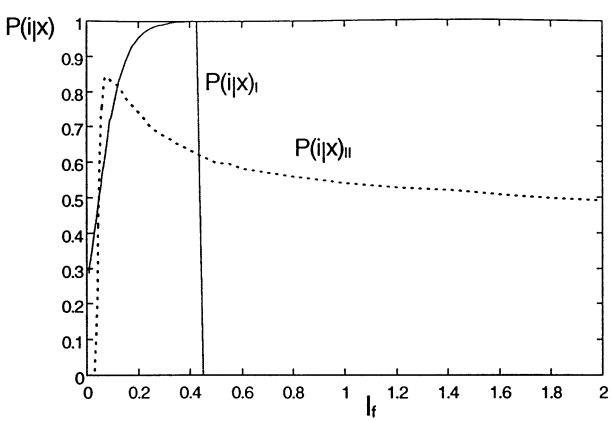

Fig. 8. Outputs of the two earth fault detection methods as a function of the fault current I_f which is expressed in amperes.

3.2. Point probability method

In the case of point probability method, the expected fault current is modelled by a fixed value I_f (Eq. (2)). For the method, two different probability density functions are defined. Let $i = 1,\ldots, n$ denote feeders at the substation and variables $x_1,\ldots, x_n$ the possible compensated current values. Now, the current density function of a 'healthy' feeder is denoted by $f_0(x)$ Since the compensated current values of sound feeders should be zeros, the mean of $f_0(x)$ is also taken zero, $\mu_0 = 0$. The second probability density function is that of the faulty feeder, denoted by $f_1(x)$. In this case, the mean value should be equal to the expected fault current, $\mu_1 = I_f$.

Our problem is now formulated so that one of the feeders is faulty, and we have to define the probability that it is the feeder i. What is given is the observed compensated feeder currents (Eq. (3)). To calculate the probability Pr(feeder i is failed $|I_{01},\ldots, I_{0n}$) we use the Bayesian theorem [5].

We must first determine the conditional probability that we observe measurements $I_{01},\ldots, I_{0n}$ given that the ith feeder is faulty. This can be calculated from the equation:

$$\Pr(I_{01},\ldots,I_{0n}|\text{feeder } i \text{ is failed}) = f_1(I_{0i})\prod_{\substack{j\neq 1\\ j=1}}^{n} f_0(I_{0j}) \quad (4)$$

The probability that feeder i is failed is now, according to the Bayesian theorem:

$$\Pr(\text{feeder } i \text{ is failed}|I_{01},\ldots,I_{0n}) = \frac{f_1(I_{0i})\prod_{\substack{j\neq i\\ j=1}}^{n} f_0(I_{0j})}{\sum_{i=1}^{n}\left[f_1(I_{0i})\prod_{\substack{j\neq i\\ j=1}}^{n} f_0(I_{0j})\right]} = \frac{\dfrac{f_1(I_{0i})}{f_0(I_{0i})}}{\sum_{i=1}^{n}\dfrac{f_1(I_{0i})}{f_0(I_{0i})}} \quad (5)$$

The point probabilities in the cases of healthy and faulty feeders are obtained by substituting the compensated current values I_{0i} to the normal distribution density functions $f_0(x)$ or $f_1(x)$ correspondingly. When considering the middle term of Eq. (5), the numerator gives the probability that feeder i is failed and the other feeders are sound. It is obtained by multiplying the corresponding point probabilities with each other. The denominator in Eq. (5) gives the total probability that one of the feeders is failed, and it is needed to scale the sum of the feeder fault probabilities to unity. Probabilities calculated by the point probability method are denoted later by $\Pr(i\,|x)_I$.

Table 1
Detailed results for detection of the failed feeder with two alternative probabilistic method in the case of fault resistances 180–220 kΩ

Phase, R_f (kΩ)	$\underline{Z}_f$ (Ω)	I_{0I} (A)	I_f (A)	$\Pr(i\|x)_I$	$\Pr(i\|x)_{II}$	Deviations
L1	132 970.45 −	0.033805	0.115678	0.000524	0.000115	$\sigma_0 = 0.032574$
180	j*57 056.70	**0.141373**		0.998335	0.999673	$\sigma_{0m} = 0.037900$
		0.010505		0.000179	0.000013	$\sigma_{1C} = 0.055169$
		0.035044		0.000558	0.000128	$\sigma_{1U} = 0.053599$
		0.028502		0.000403	0.000070	$\sigma_{1Um} = 0.177839$
L1	149 451.84 −	0.044551	0.109045	0.026388	0.006102	$\sigma_0 = 0.053818$
200	j*36 034.95	**0.142706**		0.881241	0.952745	$\sigma_{0m} = 0.053818$
		0.019256		0.012957	0.000410	$\sigma_{1C} = 0.067157$
		0.060116		0.042515	0.024173	$\sigma_{1U} = 0.076111$
		0.055593		0.036899	0.016570	$\sigma_{1Um} = 0.154523$
L1	165 731.73 −	0.031237	0.091345	0.000749	0.000220	$\sigma_0 = 0.029740$
220	j*78135.77	**0.124786**		0.997669	0.999419	$\sigma_{0m} = 0.033139$
		0.009564		0.000254	0.000016	$\sigma_{1C} = 0.047657$
		0.030766		0.000730	0.000209	$\sigma_{1U} = 0.046866$
		0.027038		0.000597	0.000136	$\sigma_{1Um} = 0.155673$
L2	122 712.48 −	0.050008	0.135669	0.001931	0.001149	$\sigma_0 = 0.058189$
200	j*15 709.50	**0.209115**		0.991718	0.993298	$\sigma_{0m} = 0.058189$
		0.020947		0.000886	0.000107	$\sigma_{1C} = 0.079591$
		0.059288		0.002526	0.002248	$\sigma_{1U} = 0.082292$
		0.064360		0.002939	0.003199	$\sigma_{1Um} = 0.17783$
L2	130 907.93 −	0.058954	0.127205	0.010055	0.034151	$\sigma_0 = 0.068541$
220	j*15 369.23	**0.220466**		0.957908	0.797303	$\sigma_{0m} = 0.068541$
		0.021619		0.004913	0.001742	$\sigma_{1C} = 0.090510$
		0.073151		0.013649	0.084845	$\sigma_{1U} = 0.096932$
		0.072574		0.013476	0.081959	$\sigma_{1Um} = 0.163602$
L3	156 813.59 +	0.025678	0.107047	0.053210	0.019105	$\sigma_0 = 0.035195$
180	j*8 393.12	**0.057553**		0.614152	0.759752	$\sigma_{0m} = 0.035195$
		0.015143		0.024505	0.005120	$\sigma_{1C} = 0.038945$
		0.043936		0.212069	0.166489	$\sigma_{1U} = 0.049733$
		0.033559		0.096064	0.049534	$\sigma_{1Um} = 0.163524$
L3	179 715.16 +	0.030786	0.093130	0.074061	0.043724	$\sigma_0 = 0.033089$
200	j*22 125.86	**0.060891**		0.719326	0.823732	$\sigma_{0m} = 0.033089$
		0.004786		0.012044	0.002858	$\sigma_{1C} = 0.037488$
		0.037868		0.012436	0.089124	$\sigma_{1U} = 0.046795$
		0.030047		0.070203	0.040562	$\sigma_{1Um} = 0.166565$
L3	194 691.66 −	0.022260	0.086921	0.000425	0.000072	$\sigma_0 = 0.024581$
220	j*7 845.83	**0.114241**		0.998353	0.999697	$\sigma_{0m} = 0.030141$
		0.006114		0.000185	0.000009	$\sigma_{1C} = 0.044919$
		0.024136		0.000473	0.000091	$\sigma_{1U} = 0.042626$
		0.027103		0.000563	0.000130	$\sigma_{1Um} = 0.153461$

3.3. Overall probability method

In the second method, the expected fault current value I_f is no longer fixed, but it is assumed to be a random variable having a normal density function $f_{1U}(x)$. Let the normal density function of the compensated current value of the faulted feeder be $f_{1C}(x)$. The information of these two distributions can be combined, resulting in the expected value $\overline{f_1(x_i)}$ instead of the point probability value $f_1(x_i)$. If $f_{1C}(x)$ has the probability density function $f_{1U}(x)$, then the expected value $f_{1C}(x_i)$ is evaluated by the integration [4]:

$$\overline{f_1(x_i)} = \int_{-\infty}^{+\infty} f_{1C}(x_i) f_{1U}(x_i) \mathrm{d}x \tag{6}$$

which gives

$$\overline{f_1(x_i)} = \frac{1}{\sqrt{2\pi(\sigma_{1C}^2 + \sigma_{1U}^2)}} \mathrm{e}^{-\frac{1}{2}\left(\frac{\mu_{1C} - \mu_{1U}}{\sigma_{1C}^2 + \sigma_{1U}^2}\right)^2} \tag{7}$$

where, μ_{1C}, σ_{1C}^2 and μ_{1U}, σ_{1U}^2 are the corresponding parameters of the normal distribution functions of the feeder current and expected fault current. In this case, the mean values of the fault currents are supposed to be $\mu_{1U} = I_f$ and $\mu_{1C} = I_{0i}$, when Eq. (7) is substituted to Eq. (5). Probabilities calculated by the overall probability method are denoted later by $\Pr(i\,|x)_{II}$.

4. Parameter estimation of the probability density functions

4.1. Sound feeder current variance

The variance of the current density function $f_0(x)$ can be estimated by considering Eq. (3). The mean values of the compensated currents of the sound feeders should be zeros. Therefore, the deviations from zero are measuring errors, which can be used for the determination of the variance σ_0^2. Since there is no a priori knowledge about which of the feeders are sound, the maximum and minimum values of the compensated feeder currents observed (I_{max} and I_{min}) aren't taken into account. The variance is calculated as follows

$$\sigma_0^2 = \frac{1}{n-2} \sum_{i=1}^{n} (x_i - \mu_0)^2 \quad (8)$$

when $x_i \neq I_{max}$ and $x_i \neq I_{min}$ and $\mu_0 = 0$.

4.2. Failed feeder current variance

For the variance σ_{1C}^2 of the current density functions $f_1(x)$ and $f_{1C}(x)$, consider Eq. (3). If all the right hand terms vary by a small amount, the variation in the measured change of zero-sequence currents is given by

Table 2
Results for the detection of the failed feeder with two alternative probabilistic methods in the case of fault resistances 20–180 kΩ

Phase, R_f, (kΩ)	$\Pr(i\|x)_I$	$\Pr(i\|x)_{II}$	Phase, R_f, (kΩ)	$\Pr(i\|x)_I$	$\Pr(i\|x)_{II}$	Phase, R_f, (kΩ)	$\Pr(i\|x)_I$	$\Pr(i\|x)_{II}$
	0.001410	0.000300		0.000260	0.000091		0.000798	0.000092
L1	**0.994503**	**0.998861**	**L2**	**0.997637**	**0.998936**	**L3**	**0.997126**	**0.999691**
20	0.001317	0.000261	100	0.000151	0.000046	100	0.000454	0.000023
	0.001408	0.000299		0.000983	0.000468		0.000709	0.000070
	0.001361	0.000279		0.000969	0.000459		0.000913	0.000124
	0.000902	0.000122		0.000603	0.000044		0.000453	0.000045
L1	**0.996102**	**0.999424**	**L2**	**0.997832**	**0.999861**	**L3**	**0.998103**	**0.999780**
40	0.000891	0.000119	120	0.000434	0.000019	120	0.000243	0.000012
	0 001055	0 000169		0.000547	0.000035		0.000749	0.000119
	0.001049	0.000167		0.000584	0.000041		0.000452	0.000044
	0.000299	0.000040		0.000587	0.000107		0.000017	0.000015
L1	**0.998731**	**0.999816**	**L2**	**0.998130**	**0.999702**	**L3**	**0.999906**	**0.999917**
60	0.000215	0.000022	160	0.000239	0.000016	160	0.000010	0.000009
	0.000385	0.000063		0.000432	0.000059		0.000047	0.000042
	0.000371	0.000059		0.000612	0.000116		0.000020	0.000017
	0.003468	0.000749		0.020311	0.001432			
L1	**0.987269**	**0.997047**	**L2**	**0.855823**	**0.967093**			
160	0.000908	0.000042	180	0.014009	0.000498			
	0.003388	0.000716		0.057409	0.016957			
	0.004967	0.001446		0.052448	0.014020			
	0.000612	0.000663		0.002782	0.002483			
L2	**0.997445**	**0.997237**	**L3**	**0.988659**	**0.989848**			
20	0.000554	0.000602	20	0.002805	0.002507			
	0.000760	0.000818		0.002933	0.002638			
	0.000628	0.000679		0.002821	0.002524			
	0.000061	0.000096		0.001039	0.000099			
L2	**0.999722**	**0.999566**	**L3**	**0.995889**	**0.999611**			
40	0.000046	0.000074	40	0.000928	0.000075			
	0.000082	0.000126		0.001011	0.000093			
	0.000090	0.000137		0.001134	0.000121			
	0.000749	0.000066		0.000394	0.000064			
L2	**0.997139**	**0.999754**	**L3**	**0.998233**	**0.999683**			
60	0.000523	0.000029	60	0.000271	0.000033			
	0.000806	0.000078		0.000581	0.000120			
	0.000782	0.000073		0.000521	0.000101			
	0.000454	0.002207		0.000540	0.000018			
L2	**0.993948**	**0.980532**	**L3**	**0.997841**	**0.999928**			
80	0 000165	0.001093	80	0.000532	0 000017			
	0.003684	0.010288		0.000545	0.000019			
	0.001749	0.005879		0.000541	0 000018			

$$\Delta \underline{I}_{0i} = \frac{\partial \underline{I}_{0i}}{\partial \underline{I}_{0i\mathrm{m}}} \Delta \underline{I}_{0i\mathrm{m}} + \frac{\partial \underline{I}_{0i}}{\partial \underline{U}_{0\mathrm{m}}} \Delta \underline{U}_{0\mathrm{m}} + \frac{\partial \underline{I}_{0i}}{\partial \underline{Z}_{0i}} \Delta \underline{Z}_{0i} \quad (9)$$

By taking the partial derivatives, the greatest relative measuring error is approximated by

$$\left|\frac{\Delta \underline{I}_{0i}}{\underline{I}_{0i}}\right| \cong \left|\frac{\Delta \underline{I}_{0i\mathrm{m}}}{\underline{I}_{0i\mathrm{m}}}\right| + \left|\frac{\Delta \underline{U}_{0\mathrm{m}}}{\underline{U}_{0\mathrm{m}}}\right| + \left|\frac{\Delta \underline{Z}_{0i}}{\underline{Z}_{0i}}\right| \quad (10)$$

Assuming that these three terms are independent of each other, the current variance is proportional to the measuring errors as follows:

$$\sigma^2_{I0i} \cong \sigma^2_{I0i\mathrm{m}} + \sigma^2_{U0\mathrm{m}} + \sigma^2_{Z0i} \quad (11)$$

where σ^2_{I0i}, variance of the compensated current distribution; $\sigma^2_{I0i\mathrm{m}}$, variance of the measured current distribution; $\sigma^2_{U0\mathrm{m}}$, variance of the neutral voltage distribution; σ^2_{Z0i}, variance of the zero-sequence impedance distribution of the feeder i.

In the case of the sound feeders, the variances are small, and it is feasible to suppose that they are about equal $\sigma^2_{I0i\mathrm{m}} = \sigma^2_{U0\mathrm{m}} = \sigma^2_{Z0i}$. Eq. (11) can now be simplified as

$$\sigma^2_{I0i} \cong 3\sigma^2_{I0i\mathrm{m}} = \sigma^2_0 \quad (12)$$

The current measuring accuracy in modern relays depends on the measuring range. Therefore in the case of the failed feeder, the variance of the measured current distribution must be scaled taking into account the maximum compensated current value observed ($I_{\max}$). The variances $\sigma^2_{U0\mathrm{m}}$ and σ^2_{Z0i} are unchanged. The variance for the current distribution of the failed feeder based on the residual current analysis is reformed as

$$\sigma^2_{1C} \cong \frac{I_{\max}}{I_{\mathrm{ave}}} \sigma^2_{I0i\mathrm{m}} + \sigma^2_{U0\mathrm{m}} + \sigma^2_{Z0i} \quad (13)$$

where I_{ave} is the average value of the currents which are used to define the variance σ^2_0 in Eq. (8). By substituting Eqs. (12) and (13), the variance of the current distribution for the failed feeder is derived as

$$\sigma^2_{1C} \cong \left(\frac{I_{\max}}{3I_{\mathrm{ave}}} + \frac{2}{3}\right)\sigma^2_0 \quad (14)$$

The variance σ^2_{1U} of the current density function $f_{1U}(x)$, can be defined by error analysis from Eqs. (1) and (2). By substituting Eq. (1) into Eq. (2) and because $U_I \gg U_0$ in the case of high resistive earth faults, the following approximation is given by

$$\underline{I}_{\mathrm{f}} \cong \frac{\underline{U}_0}{\underline{Z}_0} \quad (15)$$

$\underline{U}_0$ is the zero-sequence voltage of the network. $\underline{Z}_0$ is the zero-sequence impedance of the network.

By taking partial derivatives of Eq. (15) the greatest relative measuring error in magnitude is simplified as

$$\left|\frac{\Delta \underline{I}_{\mathrm{f}}}{\underline{I}_{\mathrm{f}}}\right| \cong \left|\frac{\Delta \underline{U}_{0\mathrm{m}}}{\underline{U}_{0\mathrm{m}}}\right| + \left|\frac{\Delta \underline{Z}_0}{\underline{Z}_0}\right| \quad (16)$$

where the relative impedance error is obtained as a function of the compensation degree $\underline{Z}_C/\underline{Z}_1$ as

$$\left|\frac{\Delta \underline{Z}_0}{\underline{Z}_0}\right| = \left|1 - \frac{1}{1 + \frac{\underline{Z}_{\mathrm{c}}}{\underline{Z}_1}}\right| \cdot \left|\frac{\Delta \underline{Z}_1}{\underline{Z}_1}\right| + \left|1 - \frac{1}{1 + \frac{\underline{Z}_1}{\underline{Z}_{\mathrm{c}}}}\right| \cdot \left|\frac{\Delta \underline{Z}_{\mathrm{c}}}{\underline{Z}_{\mathrm{c}}}\right| \quad (17)$$

Z_1 is the parallel connection of the feeder impedances Z_{0i}; Z_{c} is the coil impedance.

The previous equation can in the case of unearthed network ($\underline{Z}_{\mathrm{C}} = \infty$) be written as follows:

$$\left|\frac{\Delta \underline{Z}_0}{\underline{Z}_0}\right| = \left|\frac{\Delta \underline{Z}_1}{\underline{Z}_1}\right| = \sum_{i=1}^{n} \left|\frac{\Delta \underline{Z}_{0i}}{\underline{Z}_{0i}}\right| \quad (18)$$

n is the number of the feeders.

Taking into account Eq. (12) and Eq. (16), the variance in the case of unearthed network is hence:

$$\sigma^2_{1U} \cong (1+n)\sigma^2_0/3 \quad (19)$$

In resonant earthed networks, in addition to the compensation degree, we have to take into account the system resistive residual current [6], [7]. Supposing that this is 5% of the capacitive current, the minimum and maximum values of the current measuring errors can be estimated as follows (0–100% compensation):

$$\left|\frac{\Delta \underline{U}_{0\mathrm{m}}}{\underline{U}_{0\mathrm{m}}}\right| + \left|\frac{\Delta \underline{Z}_{\mathrm{C}}}{\underline{Z}_{\mathrm{c}}}\right| \leq \left|\frac{\Delta \underline{I}_{\mathrm{f}}}{\underline{I}_{\mathrm{f}}}\right| \leq \left|\frac{\Delta \underline{U}_{0\mathrm{m}}}{\underline{U}_{0\mathrm{m}}}\right| + 10 \cdot \left|\frac{\Delta \underline{Z}_1}{\underline{Z}_1}\right| + 10 \cdot \left|\frac{\Delta \underline{Z}_0}{\underline{Z}_{\mathrm{c}}}\right| \quad (20)$$

Supposing that the errors of the components $\underline{Z}_1$ and $\underline{Z}_{\mathrm{c}}$ are equal, this can he simplified as follows

$$\frac{(1+n)\sigma^2_0}{3} \leq \sigma^2_{1U} \leq \frac{(1+200n)\sigma^2_0}{3} \quad (21)$$

where the lower boundary is equal to the variance determined for the unearthed network Eq. (19).

5. Sensitivity analysis

When applying the probabilistic methods, difficulties may arise if the sound feeder current distribution is very narrow due to the small deviation. In these cases, the maximum feeder current value observed ($I_{\max}$) doesn't fit the distribution, and the point probability is zero, $f_0(I_{\max}) = 0$. Fig. 6 shows an example. Here the minimum deviation that allows the fault identification is $\sigma_0 = 0.17$. To avoid this problem, the minimum deviation is selected so that $f_0(I_{\max}) \geq 0.01$.

Problems may occur also if the deviation is too big. This is the case especially in the compensated network, where the variance σ^2_{1U} may be too broad for the location of the failed feeder. Fig. 7 shows an example of this. The probabilities were calculated using the following data: $\sigma_{1C} = 0.038$, $\mu_{IU} = I_{\mathrm{f}} = 0.093$ and $\mu_{IC} = I_{\max} = 0.061$. Reliable fault location is possible only in the

range where the probability values $\Pr(i|x)_{II}$ are clearly higher than 0.5.

Fig. 8 shows the difference of the two methods $\Pr(i|x)_I$ and $\Pr(i|x)_{II}$ in failed feeder identification. The same data were used as for Fig. 7. The fault current value I_f was varied from 0.008–2 A. In this example case, the point-probability method $\Pr(i|x)_I$ is able to locate the right feeder in the range from $0.8I_{max}$ to $7I_{max}$. but the overall probability method $\Pr(i|x)_{II}$ in the range from $0.8I_{max}$ to $26I_{max}$. Hence, the overall probability method is far less sensitive to large measurement errors.

6. Field test results

Field tests with staged faults were carried out in the normal 20 kV network circumstances at the Kitee substation in North-Carelian Electricity, where the network is compensated and mainly of overhead construction. During the tests, fault resistances from 20 to 220 kΩ with 20 kΩ steps were connected to each phase of the three-phase system in turn at a distant line location. Altogether, 27 earth-fault tests were carried out. Simultaneously, the phase voltages, neutral voltage and residual currents of five feeders were recorded with 500 Hz sampling frequency. The sample set also contained some periods of data before the fault moment.

In Table 1, some detailed results are given for the cases, where fault resistances were 180–220 kΩ. The first column contains exact values of fault resistances (R_f) and the phase to which the fault was thrown. The second column shows the complex phasors of the fault impedances, calculated from Eq. (1). The column titled I_{0i} shows the compensated residual currents of the five feeders, determined by Eq. (3). Faulty feeder is marked in bold. In the next column, I_f is the fault current obtained by Eq. (2). The column $\Pr(i|x)_I$ shows the fault probabilities determined by the point probability method, and the column $\Pr(i|x)_{II}$, shows the results obtained by the overall probability method. The last column shows the estimated deviations. Table 2 shows summarised results of the earth fault tests with resistances 20–180 kΩ.

Tables 1 and 2 show that in all cases, both of these probabilistic methods gave clearly the highest fault probability to the feeder, where the earth fault really was. The overall probability method ($\Pr(i|x)_{II}$) gives a little higher probability values, but both methods are able to detect and locate resistive earth faults up to a resistance of 220 kΩ.

7. Conclusions

Probabilistic methods were presented for the detection and location of very high resistive earth faults. According to the experience with field tests in a 20 kV distribution system, the methods are able to detect and locate resistive earth faults up to a resistance of 220 kΩ. The results showed that in all cases, clearly the highest fault probability was computed for the feeder, where the earth fault really was. It is likely that by the theory developed, it is possible to identify and locate the failed feeder with fault resistances also above 220 kΩ. In the future, the methods will be developed further to monitor the isolation state of a network continuously.

Acknowledgements

The authors wish to acknowledge the support of Tapio Hakola, Erkki Antila and Veikko Lehesvuo in ABB Substation Automation Oy, Vaasa and Seppo Riikonen in North-Carelian Electricity, Joensuu, Finland.

References

[1] M. Lehtonen, A method for detection and location of high resistance earth faults in electrical distribution networks, Pat. Fl. No. 100922, ABB Transmit Oy, publ. 13-03-1998, 12 pp.
[2] S. Hänninen, M. Lehtonen, E. Antila, A Method for Detection and Location of High Resistance Earth Faults, International Conference on Energy Management and Power Delivery (EMPD'98), Singapore, Proceedings IEEE Catalogue No. 98EX137, 1988, pp. 495–500.
[3] V. Leitloff, R. Feuillet, D. Griffel, Detection of resistive single-phase earth faults in a compensated power-distribution system, ETEP Eur. Trans. Electr. Power 7 (1) (1997) 65–73.
[4] H.M. Taylor, S. Karlin, An Introduction to Stochastic Modeling, Academic Press, Orlando, FL, 1984, pp. 1–28.
[5] G.E.P. Box, G.C. Tiao, Bayesian Inference in Statistical Analysis, Addison-Wesley, Reading, MA, 1973, 588 pp.
[6] H. Hubensteiner, Schutztechnik in elektrischen Netzen, VDE Verlag, Berlin, 1989, 282 pp.
[7] M. Lehtonen, T. Hakola, Neutral Earthing and Power System Protection. Earthing Solutions and Protective Relaying in Medium Voltage Distribution Networks, ABB Transmit Oy, Vaasa, 1996, pp. 11–19.

Appendix E

E

Reprinted with permission from the publisher.
In: Proc. of the PSCC'99. 13th Power Systems Computations Conference,
Trondheim, Norway, June 28–July 2, 1999. Vol. 2. Pp. 801–807.

APPENDIX E

COMPARISON OF WAVELET AND DIFFERENTIAL EQUATION ALGORITHMS IN EARTH FAULT DISTANCE COMPUTATION

Seppo Hänninen	Matti Lehtonen	Tapio Hakola	Reijo Rantanen
VTT Energy	VTT Energy	ABB Transmit Oy	ABB Corporate Research Oy
P.O.Box 1606	P.O.Box 1606	P.O.Box 608	P.O.Box 608
FIN-02044 VTT	FIN-02044 VTT	FIN-65101	FIN-65101
Espoo, Finland	Espoo, Finland	Vaasa, Finland	Vaasa, Finland
Seppo.Hanninen@vtt.fi	Matti.Lehtonen@vtt.fi	Tapio.Hakola@fimit.mail.abb.com	Reijo.Rantanen@ficrc.abb.fi

ABSTRACT

This paper gives a comparison between wavelet analysis and a differential equation algorithm in transient based earth fault location in the 20 kV radial power distribution networks. The items discussed are earth fault transients, signal pre-processing and the performance of the proposed distance estimation algorithms. The networks considered are either unearthed or resonant earthed. The comparison showed that both algorithms were equal. The mean error in fault location was 12 % in the field tests using staged faults which were recorded in real power systems.

Keywords: Wavelet analysis; Signal processing; Earth fault transients

1. INTRODUCTION

In power systems with high impedance earthing, i.e. with unearthed neutral or compensated neutral, the currents initiated by single phase to earth faults usually are too small to allow for a reliable fault distance estimation. To mitigate this problem, methods which utilise the earth fault initial transients have been studied by several researchers. The solutions proposed include differential equation algorithms [1], Fourier analysis [2], curve fitting methods [3] and artificial neural networks [4].

A more recent solution to the problem is the wavelet transform [5,6,7], which initially was used for the analysis of seismic data. The attractive feature of wavelet is, that it imitates the decayed oscillating form of the transients, and hence seems to be a very promising tool in analyzing the practical transients met in real power systems.

This paper gives a comparison between wavelet analysis and a differential equation algorithm in transient based earth fault distance computation. The earth fault transients are first briefly discussed. Next, the signal pre-processing is described. This covers the extraction of the dominating transient component from the other signal parts. The techniques used include the removal of fundamental frequency as well as direct current components and an adaptive low pass filtering. For the latter, Fourier transform is first applied to the sample set in order to determine the cut off frequency of the filter. To make the comparison possible, similar signal pre-processing is used for both the distance computation algorithms.

The wavelet and differential equation algorithms used are then described in detail. The basic forms of the methods are presented and the selection of the sample sets used in the final phase of the fault distance computation is discussed. Finally the algorithms presented are tested using staged faults recorded in real power systems. Three different power systems are considered, having an unearthed, a compensated or a partially compensated neutral. The performance of the algorithms is analyzed and the pros and cons of the two different methods are outlined.

2. EARTH FAULT TRANSIENTS

When an earth fault happens, the voltage of the faulty phase falls and the charge stored in its earth capacitances is removed. This initiates the discharge transient. Because of the voltage rise of the two sound phases, another component, called charge transient, is created. The latter has a lower frequency and in most cases also a higher amplitude. Hence, it is the component best suitable for fault location purposes. Let us study the charge component using the simplified model of Fig.1. The angular frequency in the undamped conditions can be calculated as follows [8, 9]:

$$\omega_c = \frac{1}{\sqrt{L_{eq} C_{eq}}} = \frac{1}{\sqrt{3 L_T (C + C_E)}} \qquad (1)$$

where

$$L_{eq} = 1.5 L_T \quad ; \quad C_{eq} = 2(C + C_E) \qquad (2)$$

and where L_T is the substation transformer phase inductance, C is the phase to phase capacitance and C_E is the phase to earth capacitance of the network. If the fault

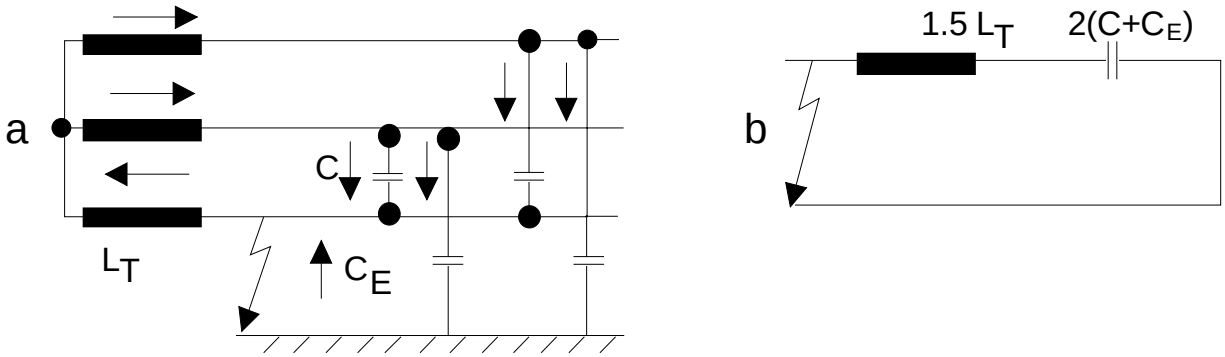

Fig. 1. The network model for the charge transient (a) and the corresponding equivalent circuit (b)

happens at the instantaneous voltage maximum, the transient amplitude is:

$$\hat{i}_c = \frac{C_{eq}}{3C_E}\frac{\omega_c}{\omega_f}\hat{J}_c \qquad (3)$$

where ω_f is the fundamental frequency and $\hat{J}_c$ is the uncompensated steady state earth fault current. The amplitude depends linearly on the frequency ω_c. Since it is not unusual for this to be 5000 rad/s, the maximum amplitudes can be even 10-15 times that of the uncompensated fundamental frequency fault current.

In real systems there is always some damping, which is mostly due to the fault resistance and resistive loads. Damping affects both frequencies and amplitudes of the transients. The critical fault resistance, at which the circuit becomes overdamped, is in overhead line networks typically 50...200 Ω, depending on the size of the network and also on the fault distance. If the resistive part of the load is large, damping is increased, and the critical resistances are shifted into a lower range.

In compensated networks there is, in addition to the charge and discharge transients, a decaying DC-transient of the coil circuit [3]. This component is usually at its highest, when the fault takes place close to voltage zero. If the coil is saturated, the current may also include harmonics.

Basically the distribution network is a multi-frequency circuit, since every parallel line adds a new pair of characteristic frequencies into the system. These additional components are, however, small in amplitude compared to the main components [3].

The earth fault transients have also been examined by field tests in real systems. According to the results, the amplitudes of charge transients agreed with equation (3). In the case of the discharge component the amplitude was typically 5 to 10 % of the amplitude of the charge component. The frequencies varied through a range of 500-2500 Hz and 100-800 Hz for discharge and charge components respectively.

3. SIGNAL PRE-PROCESSING

The key issue of signal pre-processing is to extract the charge transient, used for earth fault distance computation, from the other parts of the measured signals, i.e. phase voltages and phase currents. In order to make the comparison possible, a similar solution is used for both the distance computation algorithms. The signal pre-processing is made in the following steps:

1) removal of the fundamental frequency component
2) spectrum analysis for estimating the charge transient frequency
3) low-pass filtering in order to remove the higher frequency components

For the fundamental frequency removal a straightforward technique is used: $g(t)=f(t)-f(t+T)$, where $g(t)$ is the output of the filter, $f(t)$ is the original signal and T is the period of the fundamental frequency. The filter removes, in addition to the fundamental frequency, also its steady state harmonic components. Theoretically also the transients are affected, but since in real power system circumstances there always is some attenuation present, this effect is very small and can be ignored [3].

The spectrum analysis is made by a Fourier-algorithm, which covers only a 20 ms window, starting from the beginning of the transient. The frequency band used is from 100 Hz to 833 Hz, corresponding to a 5 kHz sampling frequency. The highest amplitude spectrum component is assumed to be the one corresponding to the charge transient frequency.

The cut-off frequency of the low-pass filter is taken 400 Hz higher than the estimated charge transient frequency. A second order Bessel filter is used. The attractive feature of this filter is a narrow transition band. However, because of the recursive nature, the transient effects of the filter itself are difficult to control. To mitigate this problem, the measured signals are processed in a reversed order.

4. THE WAVELET ALGORITHM

The wavelet transform of a time dependent signal, *s(t)*, consists in finding a set of coefficients $W_s(b,a)$. These coefficients measure the similarity between the signal *s(t)* and a set of functions $\Psi_{b,a}(t)$. All the functions, $\Psi_{b,a}(t)$, are derived from a chosen function $\Psi(t)$ called "mother wavelet" as follows:

$$\Psi_{b,a}(t) = \frac{1}{\sqrt{|a|}}\Psi\left(\frac{t-b}{a}\right) \qquad (4)$$

The only restriction on $\Psi(t)$ is that it must be short and oscillatory; i.e. it must have zero average and decay quickly at both ends. Each wavelet, $\Psi_{b,a}(t)$, is a scaled (compressed or dilated) and translated (shifted) version of the same original function $\Psi(t)$. In equation (4), "*a*" represents a time dilation and "*b*" a time translation and "$1/\sqrt{a}$" is an energy normalization factor, that keeps the energy of the scaled wavelets, $\Psi_{b,a}(t)$, the same as the energy of the "mother wavelet" [10].

In the case of the continuous wavelet transform, the coefficients $W_s(b,a)$ are defined by the inner product:

$$W_s(b,a) = \int_{-\infty}^{+\infty} s(t)\cdot\overline{\Psi}_{b,a}(t)dt \qquad (5)$$

where $\overline{\Psi}$ is the complex conjugate of Ψ.

For the choice of mother wavelet several functions have been proposed, for example the Morlet wavelet and the Daubechies wavelet. We have used the following complex "mother wavelet" introduced in Ref. [7]:

$$\Psi(t) = \left(1+\sigma|t|+\frac{\sigma^2}{2}t^2\right)e^{-\sigma|t|}e^{i\omega\cdot t} \qquad (6)$$

$\Psi(t)$ responds to the selection criteria mentioned above if the parameters are set so that $\omega = 2\pi f$ and $\sigma = \omega/\sqrt{3}$ and $a = f_c/f$, where f_c is the estimated charge transient frequency. An example of the wavelet of Eq. (6) is in Fig. 2.

To find the complex wavelet transform coefficients W_s with discrete and finite-length signals, the discrete wavelet transform is used. Let us call *T* the sampling period, and *k* and *n* are integers. For a chosen frequency *f*, and for a "location" of wavelet *b=kT*, the Eq. (5) becomes:

$$W_s(kT,f) = \sum_n s(nT)\cdot\sqrt{f/f_c}\cdot\overline{\Psi}\left[(f/f_c)\cdot(nT-kT)\right]\cdot T \qquad (7)$$

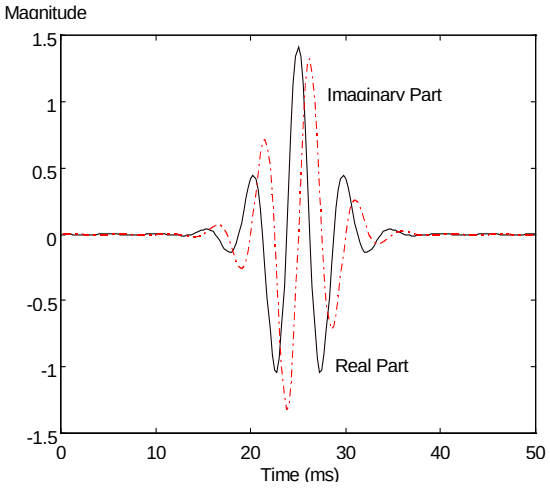

Fig.2. Real part and imaginary part of the complex wavelet. The wavelet has a frequency equal to 100 Hz

The maximum of the wavelet coefficient magnitudes yields the frequency and "location" of the wavelet that is closest to the original signal.

The complex wavelet coefficients are calculated for the pre-processed signals using a 20 ms analyzing window and frequencies from 100 Hz to 800 Hz. The computation is made starting from one half network period before the beginning of the transient and shifting the analyzing window from sample to sample forward.

After the computation of the wavelet coefficients for voltage and current transients, the earth fault distance can be estimated by first calculating the inductance as follows:

$$L_f = \frac{1}{\omega}\mathrm{Im}\left[\frac{U_w(kT,f)}{I_w(kT,f)}\right] = \frac{1}{3}\left(L_1' + L_2' + L_0'\right)\cdot l \qquad (8)$$

where *l* is the fault distance, L_1', L_2', L_0' are the inductances per unit length of the positive-, negative- and zero-sequence systems, L_f is the equivalent fault inductance, U_w and I_w are the complex wavelet coefficients of the voltage and current transients and $\omega = 2\pi f$.

The algorithm first determines the maximum wavelet coefficient of the current including the amplitude, frequency and location of the wavelet. Using this frequency with different time translations, the equivalent fault inductances are calculated with Eq. (8). The 2 ms inductance interval, corresponding to 10 subestimates, is then determined with the smallest standard deviation. The mean value of the inductance, calculated in this interval, is finally used to determine the fault distance.

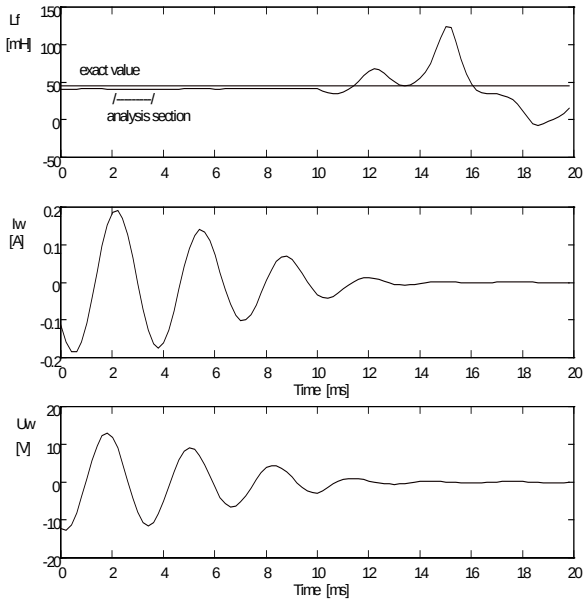

Fig. 3. Instantaneous values of the equivalent fault inductance L_f and the corresponding wavelet coefficients of current I_w and voltage U_w. Transient frequency is 163 Hz

The frequency dependence of the zero-sequence inductance is taken into account according to Carson's theory [3]. Fig. 3 shows an example of the fault inductance variation.

5. THE DIFFERENTIAL EQUATION ALGORITHM

Differential-equation algorithms solve the line inductance directly in time domain. Consider the first order model, which includes the series connection of the line resistance R and inductance L. The voltage and current of the faulty phase have the following relation:

$$u(t) = Ri(t) + L\frac{di(t)}{dt} \qquad (9)$$

which can be solved for inductance L, if three equally spaced pairs of samples are available. Since differentiation is sensitive to higher frequency noise, the solution is usually obtained by integrating the above. Using the trapezoidal rule we obtain:

$$L=\frac{\Delta t}{2}\left[\frac{(i_{k+1}+i_k)(u_{k+2}+u_{k+1})-(i_{k+2}+i_{k+1})(u_{k+1}+u_k)}{(i_{k+1}+i_k)(i_{k+2}-i_{k+1})-(i_{k+2}+i_{k+1})(i_{k+1}-i_k)}\right] \qquad (10)$$

The above equation yields the total inductance of the faulty line length, which in the case of a single phase to earth fault is composed of a series connection of zero-, positive- and negative-sequence inductances (compare Eq. 8).

The algorithm works in theory for all the voltage and current components which satisfy Eq. (9). The best result is, however, obtained if all the other frequencies are first filtered out, except the charge transient. In the prototype system described in reference [1] the accuracy of the method has been improved by using a larger number of samples. Also in the same reference a higher order model, which allows for the capacitances of the line, has been proposed. The model is based on higher order differential quotients, which are calculated during the signal preprocessing. Using the quotients as correction factors, the final calculation can be made using the first order line model.

In this study, the differential equation algorithm is used in its basic form as described in Eq. (10). The computation is made for a window of 12 subsequent samples. The Eq. (10) is applied for ten times, and the average value and statistical deviation is computed for the inductance estimates. Starting from the first sample of the transient, this procedure is repeated for 20 times, shifting the starting point gradually forward. The final estimate of the inductance is the one having the smallest deviation. Fig. 4 shows an example of the fault inductance variation.

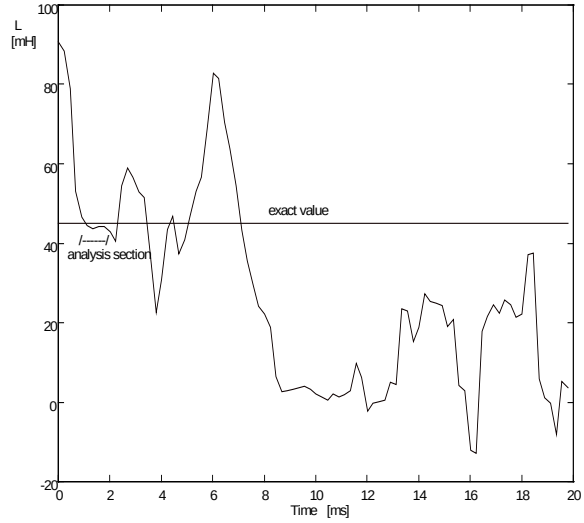

Fig. 4. Instantaneous values of the fault inductance L calculated with the differential equation algorithm. Transient frequency is 200 Hz.

6. COMPARISON OF THE ALGORITHMS

Field tests with staged faults were carried out in the normal network circumstances in South-West Finland Electricity where the distribution network is partially compensated, in Vaasa Electricity where the distribution network is compensated and in Espoo Electricity where the distribution network is unearthed. Tables I-III show the fault distances calculated with both algorithms to demonstrate their performance.

Table I. Calculated Fault Distances in the Partially Compensated Network

Exact fault distance [km]	Fault resistance [Ω]	**Differential equation algorithm** Fault distance [km]	Error [km]	**Wavelet algorithm** Fault distance [km]	Error [km]
25.4	0	27.2	1.8	31.9	6.5
25.4	0	32.0	6.6	29.8	4.4
25.4	0	22.7	-2.7	30.1	4.7
25.4	0	24.0	-1.4	27.8	2.4
25.4	0	25.2	-0.2	27.0	1.6
36.0	0	34.5	-1.5	33.7	-2.3
36.0	0	34.2	-1.8	32.2	-3.8
36.0	0	32.3	-3.7	29.7	-6.3

Table II. Calculated Fault Distances in the Compensated Network

Exact fault distance [km]	Fault resistance [Ω]	**Differential equation algorithm** Fault distance [km]	Error [km]	**Wavelet algorithm** Fault distance [km]	Error [km]
0.76	0	0.46	-0.30	0.36	-0.40
0.76	0	0.42	-0.34	0.36	-0.40
10.4	0	12.9	2.5	10.2	-0.2
10.4	0	12.6	2.2	10.1	-0.3
14.2	0	17.4	3.2	14.6	0.4
14.2	0	15.8	1.6	14.4	0.2
10.4	50	15.8	5.4	11.2	0.8
10.4	50	11.6	1.2	17.2	6.8
14.2	50	17.5	3.3	13.2	-1.0
14.2	50	9.7	-4.5	13.2	-1.0

Table III. Calculated Fault Distances in the Unearthed Network

Exact fault distance [km]	Fault resistance [Ω]	**Differential equation algorithm** Fault distance [km]	Error [km]	**Wavelet algorithm** Fault distance [km]	Error [km]
13.3	47	13.2	-0.1	12.0	-1.3
13.3	47	10.9	-2.4	11.3	-2.0
20.0	47	19.0	-1.0	19.9	-0.1
20.0	47	19.0	-1.0	18.3	-1.7

For comparison of the location accuracy of the both algorithms the mean error (*ME)* in percentage is calculated as follows:

$$ME = \frac{\sum |\Delta l|}{\sum l} \cdot 100 \qquad (11)$$

where $|\Delta l|$ is the absolute fault distance error and l is the exact fault distance in the field test. Table IV shows the summary of the comparison of the algorithms in each power system with different fault resistances.

Table IV. Comparison of the Algorithms. *MEK* is the Absolute Mean Error in Kilometers per Test and *ME* is the Mean Error in Percentage

	Differential equation algorithm		**Wavelet algorithm**	
	MEK [km]	*ME* [%]	*MEK* [km]	*ME* [%]
Partially compensated network, 0 Ω	2.5	8.4	4.0	13.6
Compensated network, 0 Ω	1.7	20.0	0.3	3.7
Compensated network, 50 Ω	3.6	29.3	2.4	19.5
Compensated network, 0 Ω and 50 Ω	2.5	24.6	1.2	11.5
Unearthed network, 47 Ω	1.1	6.7	1.3	7.6
Field tests with 0 Ω	2.1	10.4	2.4	11.8
Field tests with 47 Ω and 50 Ω	2.3	16.3	1.8	12.7
All field tests	2.2	12.1	2.2	12.1

Table IV shows that both algorithms work equally if all field tests are taken into account and the mean error in the absolute term is 2.2 km respectively. If only the earth fault tests with 0 Ω fault resistance are considered, the differential equation algorithm works a little better but if the fault resistance deviates from zero, the situation is opposite. Considering different earthing systems, the differential equation algorithm is more accurate in the partially compensated and unearthed networks whereas the wavelet algorithm is better in the compensated case. The likely reason is, that transients are more oscillatory and the form of the wavelet is more similar to the real transient in the compensated systems than in the other ones. On the other hand, the presence of the decaying DC component unfavourably affects the calculation accuracy of the differential equation algorithm in the compensated network, whereas the wavelet algorithm is less sensitive to the presence of aperiodic components.

The most important causes of errors in transient based fault distance estimation are parameter identification inaccuracy, measurement transformer errors, line model simplifications, line inductance variation and load impedances. If damping of the transient is small, the total errors due to parameter identification are typically less than 2 %. Fault resistance and resistive loads increase the attenuation, with the corresponding increase in the errors. In the tests, the highest fault resistance that allowed for reliable distance estimation was 50 Ω.

Standard current transformers have a good fidelity in the frequency range of transients. Unfortunately this is not always the case for voltage transformers, where the lowest resonant frequency can vary from 1 to 20 kHz. If the highest transient frequency is higher than about 10 % of this, the errors must be compensated for [3]. The errors of the line model simplifications include primarily, the effect of ignored capacitances at the fault location and behind it. The maximum error due to these is, in typical overhead line networks, about 2 %.

One of the two major error sources is the variation of line inductances. The zero sequence inductances of an overhead line vary with the soil type and frequency. Their values are based on simplified models, which are not necessarily in all cases accurate enough for fault location purposes. The inductances of underground cables vary with the frequency too. For cables, the problem is the proximity effect, which makes the estimation of both zero sequence and positive sequence inductances difficult.

Perhaps the largest errors are, however, due to the low voltage loads. Theoretically the load effects could be compensated for, but in practice there are some great difficulties. Usually neither the load devices nor their impedances during the transients are known well enough. The loads can cause large errors, especially in the case of distant faults and for fault resistances higher than zero.

6. CONCLUSIONS

By calculational means it is possible to produce an estimate for the distance of single phase to earth faults. If the faulty feeder has several branches, there are also several possible fault locations. In this case the fault location system can be complemented by remotely read fault current indicators.

In networks with an isolated or compensated neutral, fault distance estimation is not possible using the fundamental frequency signals. That is why transient based techniques have been studied. In high impedance earthed networks, the charge transient, which is due to the voltage rise of the two sound phases, is the most useful component for fault location purposes. Its frequency varies approximately in the range 100 to 800 Hz, and the amplitude can be even 15 times that of the uncompensated steady state fault current.

This paper gives a comparison of two transient based, earth fault distance estimation methods, the differential equation algorithm and the wavelet algorithm.

The comparison shows that both algorithms are equal and the mean error in the absolute term was 2.2 km for both algorithms in the field tests. Considering different earthing systems, the differential equation algorithm is more accurate in the partially compensated and unearthed networks, whereas the wavelet algorithm is better in the compensated case. The likely reason is, that transients are more oscillatory and the form of the wavelet used is more similar to the real transient in the compensated systems than in the other ones. On the other hand, the presence of the decaying DC component may have more influence on the calculation accuracy of the differential equation algorithm than on the accuracy of the wavelet algorithm in the compensated network.

The performance of earth fault location is in both cases restricted by the attenuation of the transients. In the field tests, the biggest fault resistance, that allowed for fault location, was 50 Ω.

REFERENCES

[1] P. Schegner, ”Digitaler Erdschlußuniversalschutz. Konzept und erste Realisierung”, Dissertation, Universität des Saarlandes, Saarbrücken, 1989, 186 pp.

[2] M. Igel, ”Neuartige Verfahren für den Erdschlußdistanzschutz in isoliert und kompensiert betriebenen Netzen. Signale und Algoritmen im Frequenzbereich”, Dissertation, Universität des Saarlandes, Saarbrücken, 1990, 181 pp.

[3] M. Lehtonen, ”Transient analysis for ground fault distance estimation in electrical distribution networks”, Dissertation, Technical Research Centre of Finland, Publications No 115. Espoo 1992, 181 pp + app.

[4] D. Eickmeyer, ”Einsatz künstlicher neuronaler Netze bei der Ortung von Erdschlüssen”, Dissertation, TU Berlin, 1997, 136 pp.

[5] O. Rioul and M. Vetterli, ”Wavelets and signal processing”, IEEE Signal Processing Magazine, vol. 8, no.4, pp 14-38, October 1991.

[6] L. G. Weiss, ”Wavelets and wideband correlation processing”, IEEE Signal Processing Magazine, vol. 11, no.1, pp 13-32, January 1994.

[7] O. Chaari, M. Meunier, and F. Brouaye, ”Wavelets: A new tool for the resonant grounded power distribution systems relaying”, IEEE Transactions on Power Delivery, vol. 11, no. 3, pp 1301-1308, July 1996.

[8] H. Pundt, ”Untersuchungen der Ausgleichsvorgänge bei Erdschluß in Hochspannungsnetzen mit isoliertem Sternpunkt und induktiver Sternpunkterdung als Grundlage zur selektiven Erdschlußerfassung”, Dissertation, TU Dresden, 1963, 167 pp + app.

[9] R. Willheim, M. Waters, ”Neutral earthing in high-voltage transmission”, Elsevier Publishing Co., New York, 1956, 669 pp.

[10] D. C. Robertson, O. I. Camps, J. S. Mayer and W. B. Gish, ”Wavelets and electromagnetic power transients”, IEEE Transactions on Power Delivery, vol. 11, no. 2, pp 1050-1058, April 1996.

Appendix F

F

Reprinted with permission from the publisher.
In: Proc. of the IEEE PES WM2000, Singapore, January 23–27, 2000,
CD-ROM 00CH37077C. 6 p.

APPENDIX F

Comparison of Artificial Neural Networks and Conventional Algorithms in Ground Fault Distance Computation

G. Eberl
University of Technology
in Dresden, Germany

S. Hänninen
VTT Energy, Espoo,
Finland

M. Lehtonen
Helsinki University of Technology
Finland

P. Schegner
University of Technology
in Dresden, Germany

Abstract: This paper gives a comparison between an artificial neural network method and a differential equation algorithm and wavelet algorithm in transient based earth fault location in the 20 kV radial power distribution networks. The items discussed are earth fault transients, signal pre-processing and the performance of the proposed distance estimation methods. The networks considered are either unearthed or resonant earthed. The comparison showed that neural network algorithm was better than the conventional algorithms in the case of very low fault resistance. The mean error in fault location was about 1 km in the field tests using staged faults, which were recorded in real power systems. With higher fault resistances, the conventional algorithms worked better.

Keywords: Neural networks, ground faults, relay algorithms

I. INTRODUCTION

In power systems with high impedance grounding, i.e. with ungrounded or compensated neutral, the currents of single-phase faults usually are too small for a reliable fault distance estimation. To mitigate this problem, methods which utilize the ground fault initial transients have been studied. The solutions proposed include differential equation algorithm [1], Fourier analysis [2] and curve fitting methods [3]. More recently also the use of wavelet transform has been proposed [4].

This paper gives a comparison between artificial neural network method (ANN) and more conventional algorithms in transient based ground fault distance computation. The other algorithms considered include the differential equation algorithm and wavelet transform. To make the different solutions comparable, a similar signal pre-processing is applied to all the cases considered. The signal pre-processing is first discussed. This covers the extraction of the dominating transient component from the other signal parts. The different alternatives for the ANN selection are then discussed. Special focus is also given to the scaling and adaptation of the input data, aiming to the high correlation in the training information and enabling one single ANN to estimate the fault distance in power distribution networks of different sizes. The wavelet and differential equation algorithms used for comparison are then briefly described and finally the algorithms presented are tested using staged faults recorded in real power systems.

II. SIGNAL PRE-PROCESSIG

The key issue of signal pre-processing is to extract the charge transient, used for earth fault distance computation, from the other parts of the measured signals, i.e. phase voltages and phase currents. In order to make the comparison possible, a similar solution is used for ANN, differential equation and wavelet algorithms. The signal pre-processing is made in the following steps:

1) removal of the fundamental frequency component
2) spectrum analysis for estimating the charge transient frequency
3) low-pass filtering in order to remove the higher frequency components

For the fundamental frequency removal a straightforward technique is used: $g(t)=f(t)-f(t+T)$, where $g(t)$ is the output of the filter, $f(t)$ is the original signal and T is the period of the fundamental frequency. The filter removes, in addition to the fundamental frequency, also its steady state harmonic components. Theoretically also the transients are affected, but since in real power system circumstances there always is some attenuation present, this effect is very small and can be ignored [3]. The spectrum analysis is made by a Fourier algorithm, which covers only a 20 ms window, starting from the beginning of the transient. The frequency band used is from 100 Hz to 833 Hz, corresponding to a 5 kHz sampling frequency. The highest amplitude spectrum component is assumed to be the one corresponding to the charge transient frequency.

The cut-off frequency of the low-pass filter is taken 400 Hz higher than the estimated charge transient frequency. A second order Bessel filter is used. The attractive feature of this filter is a flat transition band. However, because of the recursive nature, the transient effects of the filter itself are difficult to control. To mitigate this problem, the measured signals are processed in a reversed order. Due to the fact that transient decays very quickly and to shorten the training time of ANN, the ANN algorithm uses a 5 ms pre-processed data window. The distance computations with conventional algorithms are made for the pre-processed signals using 20 ms analyzing window.

III ARTIFICIAL NEURAL NETWORKS FOR EARTH FAULT DISTANCE ESTIMATION

A. ANN Structure

A very interesting alternative to the more conventional solutions for ground fault distance estimation is the use of artificial neural networks (ANN). ANN seems to be a very attractive tool for this problem, since it does not require the

0-7803-5938-0/00/$10.00 (c) 2000 IEEE

explicit formulation of the solution algorithm, but is able to implicitly utilise various dependencies in the training data [5].

Analysing the charge transient can be regarded as the evaluation of special characteristics (frequency, amplitude and damping) with respect to the information content of the fault distance. It is therefore a task of pattern recognition that corresponds to the abilities of the ANN. In this work the ANN-structure called Multilayer Perceptron was used. It consists of the input vector, one hidden layer and the output layer, see Fig. 1.

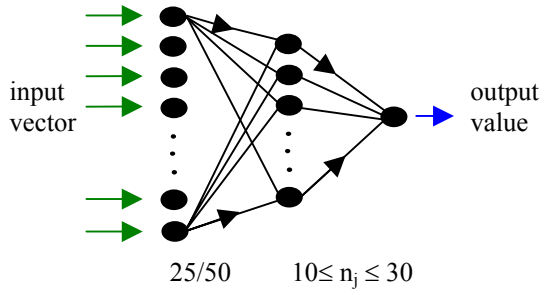

Fig.1 Structure of the Multilayer Perceptron.

B. Input Vector

The data window of 5 ms and a sampling frequency of 5 kHz determined the input data. For both voltage and current the resulting number of input values was 25. Using voltage and current as input data the length of the input vector was 50 samples. The input samples were scaled to the range [-1;1] due to their maximum.

C. Hidden Units

It has been proved that in general one hidden layer is sufficient for representing any given input-output transformation [6]. Using more than one hidden layer is necessary if the pattern recognition task seems to be quite sophisticated and if there is a large number of input neurons. For the fault distance estimation of this work the ANN consists of only one hidden layer. The number of hidden neurons n_j was varied in the range [$10 \le n_j \le 30$].

D. Output Vector

The fault distance is given by the activation of one single output neuron. In addition the estimation of other output parameters as the inductance and resistance of the faulty line as well as the fault resistance were investigated. Because the maximum activation of a neuron is 1, the output parameters were scaled to the maximal values occurred.

E. Training of ANN

Backpropagation algorithm (BPA) with adaptable learning rate η and momentum method provides a stable training process and a sufficient error decrease. Hence the BPA with gradient descent method was used for training the ANN. The training process was done several (50) times each with different initial values. This is due to that the error minimum depends on the random initial values of the weights and biases. The lowest training error that could be achieved was used for assessing the performance of the ANN. Training was done in the so-called "batch mode" or "offline training". This means all training patterns must be put through the ANN before the network parameters – the weights – are changed in one single step. Doing so the order of the training patterns has no importance to the weight changes and to the learning success [7].

F. Implementation

For implementation, training and verification of the ANN the software MATLAB5.2 and its ANN toolbox were applied. The training algorithm was implemented on a Cray Origin 2000 Computer. The training time depended on the amount of training data, the number of hidden neurons and the processor used, and it took up to 8 hours.

IV TRAINING DATA

For training and testing of the ANN a large data set of voltage and current samples is necessary. The affecting parameters must be varied within an appropriate range to provide the ANN with all the important features, see Table 1.

Table1. Variation of the network and fault parameters.

Parameter	**Varied range**	**Number of variations**
Fault distance d	1km …40km (Δd = 1km)	40
Network size s (busbar frequency F_0)	s F_0 100km → 750Hz 150km → 650Hz 250km → 550Hz 300km → 450Hz 600km → 350Hz	5
Load Load angle cosϕ	I_{Last} 0p.u. → 0A 0.2p.u. → 40A 0.5p.u. → 100A resistive; cosϕ = 1 resistive/inductive; cosϕ = 0.8	5
Grounding	Unearthed Compensated	2
Entrance angle	0°, 30° 45°;60°; 90°	5
Fault resistance	0.1Ω ;5Ω ;10Ω ;15Ω	4
Phase	R, S	2
Data sets		80000

0-7803-5938-0/00/$10.00 (c) 2000 IEEE

Earth faults were simulated by the common simulation tool "Alternative Electromagnetic Transients Program" (ATP/EMTP). The basic 20 kV overhead lines were modelled using the Line Constants ATP/EMTP Program and taking into account the real geometrical and electrical values.

V. TRAINING DATA PATTERNS

A. Network Size

The fault distance estimation system must be able to work properly in networks of different sizes, under different load conditions and entrance angles; i.e. phase to ground voltage angle when the fault occur. Three different training patterns were used, see Table 2. In the case of pattern C1, only one ANN was trained in a wide range of network size. For pattern CII one ANN was trained for each network size. The training pattern CIII included two ANN, and the input data covered different ranges of the entrance angles. It was found out that the ANN trained with high entrance angles (40° - 90°, 60° - 90°) are more powerful and more likely to adapt to smaller entrance angles. Therefore the following investigations refer to the ANN trained with entrance angles 40° - 90° and 60° - 90°.

Table 2. Variation of network size and entrance angle in training data.

Pattern	Network size s (busbar frequency f_0)	Entrance angle in degrees
CI	100km → 750Hz 150km → 650Hz 200km → 550Hz 300km → 450Hz 600km → 350Hz	40 - 90
CII	One ANN is trained with one frequency 1th ANN 100km → 750Hz 2nd ANN 150km → 650Hz 3th ANN 200km → 550Hz etc.	40 - 90
CIII	150km → 650Hz 300km → 450Hz	40 - 90 0 - 30 30 - 60 60 - 90

To assess the performance of the trained ANN, the absolute mean error E_{mae} for a simulated test data with an amount of 25 % of the number of training data was used. These test data included load cases and faulty phases different from the training data. Regarding network size, entrance angle and fault resistance, the test data covered the same range as the data used for the ANN training.

The optimal number of hidden neurons for different training patterns was studied, too. As an example Fig. 2. shows the E_{mae} over the number of hidden neurons n_j for training pattern CIII belonging to ANN with the voltage and current input and the fault distance output. With training pattern CI the necessary estimation performance was not achieved. Training with the patterns CII and CIII leads to test errors below 2.5%, when ANN structures CII (n_j = [18, 20]) and CIII (n_j = [17, 26]) were used. The first figure in the brackets means the number of hidden neurons for voltage input and the second figure means the corresponding one for voltage and current input.

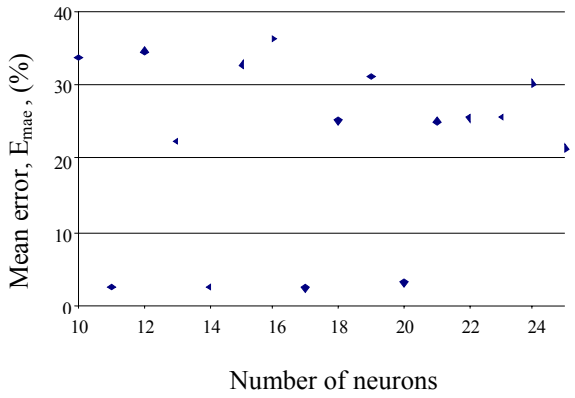

Fig.2. Mean average error $E_{mae} = f(n_j)$ over different number of neurons in the case of the training pattern CIII.

B. Input and Output Relations

Conventional distance algorithms evaluate charge transients of the phase voltage and current. Regarding the network model especially the fault distance (inductance and resistance of the faulty line segment) affects the transient phase to earth voltage. As output parameters the fault distance d (1 output neuron), the fault distance combined with the fault resistance R_U (2 output neurons), and the fault resistance combined with the fault inductance L_F (2 output neurons) were investigated.

The results showed that estimating the pure fault distance is the most promising way to design the ANN output, because only one single output neuron is needed. It was also clearly to be seen that the training pattern CIII provided higher fault distance estimation performance than CII. The reason might be that the ANN trained with CII are specialised for a too small range of frequency. Because different load cases lead to changes in frequency behaviour, these ANN can hardly cope with changes in both load and network size. The input vector including both voltage and current gave for both training pattern better results.

C. Input Data Scaling

The network size affects both the charge frequency and the amplitude of the transients. Besides this fact the frequency varies with the fault distance. For an ANN trained with in an appropriate range of the network size (charge frequency F_0) and the entrance angle ν_0, - so that a good generalisation performance is provided - there will be a small span in frequency and entrance angles where the ANN processes very exact results. The main idea of the scaling is to adapt the actual voltage and current sample to the ANN-specific range F_0 and ν_0. This can be done by

0-7803-5938-0/00/$10.00 (c) 2000 IEEE

changing these data due to the network size (time scaling) and to the entrance angle (amplitude scaling). Both parameters can be determined by measuring or processing.

The purpose of the time scaling is to move the actual frequency into the range of the trained frequency band. The scaling of the frequency is done by stretching or shortening the cycle period, see Fig. 3. At first, the reference frequency Fo must be determined for which the ANN was trained. Further on the frequency f_0 that corresponds to the actual distribution network must be determined. The scaling factor is SC=fo/Fo. For this kind of curve fitting a Pascal program that utilises the Newton Method was developed. The program uses the scaling factor SC and the voltage and current transients as input values and gives out the voltage and current input vectors with modified frequency. The amplitudes of the transients are not affected by the time scaling method.

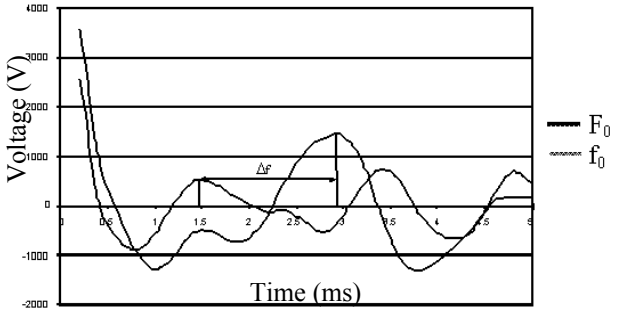

Fig. 3. Time scaling

Regarding the moment of fault entrance, the amplitude of the transients increases with the entrance angle υ [0° ≤ υ ≤ 90°]. The transient current amplitude increases with the enlargement of the power distribution network, but the amplitude of the transient voltage remains almost constant. The amplitude scaling factors SU for voltage and SI for current were determined by testing a number of simulated and measured data, see Fig. 4. By varying the amplitude scaling factors the mean estimation error E_{mae} for a certain entrance angle and network size was processed as a function of SU and SI. The value giving the minimum error E_{mae} was considered as the optimal scaling factor for the regarded entrance angle and charge frequency. To simplify the problem only the current samples were scaled in case of ANN with voltage and current input.

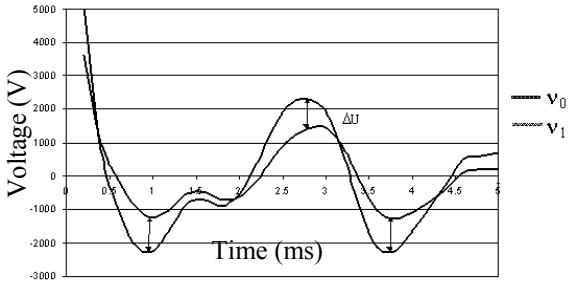

Fig. 4. Amplitude scaling

VI. CONVENTIONAL ALGORITHMS

A. Wavelet Algorithm

The discrete wavelet transform was used to find the complex wavelet coefficients W_s. Let us call T the sampling period, k and n are integers, and f_c is the estimated charge transient frequency. For a chosen frequency f and for a "location" of wavelet kT [4]:

$$W_s(kT,f) = \sum_n s(nT)\cdot\sqrt{f/f_c}\cdot\overline{\Psi}\left[(f/f_c)\cdot(nT-kT)\right]\cdot T \cdot \qquad (1)$$

The complex "mother wavelet" Ψ(t) introduced in [8] was chosen. The earth fault distance can be estimated by first calculating the inductance as follows:

$$L_f = \frac{1}{\omega}\,\mathrm{Im}\left[\frac{U_w(kT,f)}{I_w(kT,f)}\right] = \frac{1}{3}\left(L'_1 + L'_2 + L'_0\right)\cdot l\,, \qquad (2)$$

where l is the fault distance, L'_1, L'_2, L'_0 are the inductances per unit length of the positive-, negative- and zero-sequence systems, L_f is the equivalent fault inductance, U_w and I_w are the complex wavelet coefficients of the voltage and current transients and $\omega = 2\pi f$.

The algorithm first determines the maximum wavelet coefficient of the current including the amplitude, frequency and location of the wavelet. Using this frequency with different time translations, the equivalent fault inductances are calculated with (2). The 2 ms inductance interval, corresponding to 10 subestimates, is then determined with the smallest standard deviation. The mean value of the inductance, calculated in this interval, is finally used to determine the fault distance.

B. Differential Equation Algorithm

Differential-equation algorithms solve the line inductance directly in time domain, if three equally spaced pairs of phase current and voltage samples are available as follows

$$L = \frac{\Delta t}{2}\left[\frac{(i_{k+1}+i_k)(u_{k+2}+u_{k+1}) - (i_{k+2}+i_{k+1})(u_{k+1}+u_k)}{(i_{k+1}+i_k)(i_{k+2}-i_{k+1}) - (i_{k+2}+i_{k+1})(i_{k+1}-i_k)}\right]. \qquad (3)$$

The above equation yields the total inductance of the faulty line length, which in the case of a single phase to earth fault is composed of a series connection of zero-, positive- and negative-sequence inductances (compare (2)).

In this study, the differential equation algorithm is used in its basic form as described in (3). The computation is made for a window of 12 subsequent samples. Equation (3) is applied for ten times, and the average value and statistical deviation is computed for the inductance estimates. Starting from the first sample of the transient, this procedure is repeated for 20 times, shifting the starting

0-7803-5938-0/00/$10.00 (c) 2000 IEEE

point gradually forward. The final estimate of the inductance is the one having the smallest deviation.

VII. COMPARISON OF THE DISTANCE ESTIMATION TECHNIQUES

The performance of the introduced ANN method were compared with the differential equation algorithm and the wavelet algorithm, see Tables 3-5. The test data consist of field tests with staged faults from distribution networks with partially compensated, compensated and unearthed neutral. The different ANNs were trained for compensated and unearthead networks using the fault resistances from 0 Ω to 15 Ω. The ANN using scaling method with voltage and current inputs was a bit better than the conventional algoritms when the fault resistance was zero. In this case, the mean error was about 1 km for ANN systems and about 2 km for other algorithms. The ANN with single voltage input reached an absolute mean error of 3.4 km. With higher fault resistances the conventional algorithms worked better and the mean error was about 2 km. Considering different earthing systems, the differential equation algorithm was more accurate in the partially compensated and unearthed networks, whereas the ANN and wavelet methods were better in the compensated case.

Table 3. Calculated fault distances and absolute errors in the partially compensated network.

Exact fault distance (km)	Fault resistance (Ω)	Artificial neural network				Differential equation algorithm		Wavelet algorithm	
		voltage		voltage/current					
		distance (km)	error (km)	distance (km)	error (km)	distance (km)	error (km)	distance (km)	error (km)
25.4	0	26.1	0.7	25.3	0.1	27.2	1.8	31.9	6.5
25.4	0	25.6	0.2	26.2	0.8	32.0	6.6	29.8	4.4
25.4	0	25.6	0.2	27.6	2.2	22.7	2.7	30.1	4.7
25.4	0	22.4	3.0	28.4	3.0	24.0	1.4	27.8	2.4
25.4	0	22.8	2.6	25.2	0.2	25.2	0.2	27.0	1.6
36.0	0	35.5	0.5	36.3	0.3	34.5	1.5	33.7	2.3
36.0	0	35.4	0.6	37.3	1.3	34.2	1.8	32.2	3.8
36.0	0	37.5	1.5	34.6	1.4	32.3	3.7	29.7	6.3

Table 4. Calculated fault distances and absolute errors in the compensated network.

Exact fault distance (km)	Fault resistance (Ω)	Artificial neural network				Differential equation algorithm		Wavelet algorithm	
		voltage		voltage/current					
		distance (km)	error (km)	distance (km)	error (km)	distance (km)	error (km)	distance (km)	error (km)
0.76	0	0.67	0.08	0.02	0.74	0.46	0.3	0.36	0.4
0.76	0	5.6	4.8	0.02	0.74	0.42	0.34	0.36	0.4
10.4	0	24.2	13.8	11.0	0.6	12.9	2.5	10.2	0.2
10.4	0	24.1	13.7	9.7	0.7	12.6	2.2	10.1	0.3
14.2	0	16.3	2.1	13.0	1.16	17.4	3.2	14.6	0.4
14.2	0	17.5	3.3	15.7	1.5	15.8	1.6	14.4	0.2
10.4	50	0.99	9.4	12.0	1.6	15.8	5.4	11.2	0.8
10.4	50	0.99	9.4	2.5	7.9	11.6	1.2	17.1	6.8
14.2	50	24.8	10.6	15.6	1.4	17.5	3.3	13.2	1.0
14.2	50	22.8	8.6	23.5	9.3	9.7	4.5	13.2	1.0

Table 5. Calculated fault distances and absolute errors in the unearthed network.

Exact fault distance (km)	Fault resistance (Ω)	Artificial neural network				Differential equation algorithm		Wavelet algorithm	
		voltage		voltage/current					
		distance (km)	error (km)	distance (km)	error (km)	distance (km)	error (km)	distance (km)	error (km)
13.3	47	5.5	7.8	5.6	7.7	13.2	0.1	12.0	1.3
13.3	47	5.4	7.9	9.3	4.0	10.9	2.4	11.3	2.0
20.0	47	6.9	13.1	4.8	15.2	19.0	1.0	19.9	0.1
20.0	47	5.6	14.4	4.8	15.2	19.0	1.0	18.3	1.7

VIII. CONCLUSIONS

In networks with an isolated or compensated neutral, fault distance estimation is not possible using the fundamental frequency signals. That is why transient based techniques have been studied. In high impedance earthed networks, the charge transient, which is due to the voltage rise of the two sound phases, is the most useful component for fault location purposes. Neural network approach is an alternative to the more conventional solutions for ground fault distance estimation, since it does not require the explicit formulation of the solution algorithm. It is able to implicitly utilise various dependencies in the training data.

This paper compares the ANN method to the differential equation algorithm and to the wavelet algorithm. Special focus was given to the scaling and adaptation of the input data enabling one single ANN to estimate the fault distance in power distribution networks of different sizes. The ANN-type Multilayer Perceptron with one hidden layer and trained with Backpropagation method was used. The performance of the ANN was comparable to that of the conventional algorithms. Regarding only the earth faults with very low fault resistance the ANN with voltage and current input vector gave even better results. The mean error in absolute terms was about 1.0 km for ANN method and about 2.0 km for the conventional algorithms in the field tests. The ANN with single voltage input reached an absolute mean error of 3.7 km. Conventional algorithms worked better with higher fault resistances. The performance of earth fault location is restricted by the attenuation of the transients. The highest fault resistance, that allowed for fault location, was 50 Ω.

IX. REFERENCES

[1] P. Schegner, Digitaler Erdschlußuniversalschutz. Konzept und erste Realisierung, Dissertation, Universität des Saarlandes, Saarbrücken, 1989, p. 186.

[2] M. Igel, Neuartige Verfahren für den Erdschluß-distanzschutz in isoliert und kompensiert betriebenen Netzen. Signale und Algoritmen im Frequenzbereich, Dissertation, Universität des Saarlandes, Saarbrücken, 1990, p. 181.

[3] M. Lehtonen, Transient analysis for ground fault distance estimation in electrical distribution networks, Dissertation, Technical Research Centre of Finland, Publications No 115. Espoo 1992, p. 181 + app.

[4] S. Hänninen, M. Lehtonen, T. Hakola and R. Rantanen, "Comparison of Wavelet and Differential Equation Algorithms in Earth Fault Distance Computation," Proceedings of the PSCC'99, 13th Power Systems Computation Conference. Trondheim, Norway, June 28- July 2, 1999. Volume 2. pp. 801-807.

[5] D. Eickmeyer, Einsatz künstlicher neuronaler Netze bei der Ortung von Erdschlüssen", Dissertation, TU Berlin, 1997, p. 136.

[6] S. Haykin, Neural Networks - A comprehensive foundation Prentice Hall International Editions, 1994, p. 696.

[7] A. Zell, Simulation neuronaler Netze, Addison-Wesley, 1994, p. 624.

[8] O. Chaari, M. Meunier, and F. Brouaye, "Wavelets: A new tool for the resonant grounded power distribution systems relaying," IEEE Transactions on Power Delivery, vol. 11, no. 3, July 1996. pp 1301-1308.

X. BIOGRAPHIES

Gerit Eberl was born in Karl-Marx-Stadt (Chemnitz), Germany, on September 23, 1974. She graduated from the Real-Gymnasium Chemnitz, and studied at the Technical University of Dresden electrical engineering with specialty in electrical power systems. In 1999 she was employed at the Helsinki University of Technology where she concentrated on the earth fault distance estimation by means of artificial neural networks. Her special fields of interest include the earth fault problem and artificial intelligence. (Technische Universität Dresden, Institut für Elektroenergieversorgung, D-01062 Dresden, Fax: +49 351/463-7036, Email: Eberl@eev.et.tu-dresden.de)

Seppo Hänninen (1956) has been with VTT Energy, Espoo, Finland since 1987. His current position is research scientist in the research group, Electricity Distribution. He received his Master's degree in Electrical Power Engineering from Tampere University of Technology in 1980 and Licenciate degree in Electromechanics from Helsinki University of Technology in 1991. His main fields of interest are earth fault problems, distribution automation in medium voltage networks and reliability engineering. (VTT Energy, P.O.Box 1606, FIN-02044 VTT, Finland, Tel. +358 9 4566759, Fax +358 9 4566538, E-mail: Seppo.Hanninen@vtt.fi)

Matti Lehtonen (1959) has been with VTT Energy, Espoo, Finland since 1987 and since 1999 with Helsinki University of Technology, where he is a Professor of IT applications in power systems. Matti Lehtonen received his Master's and Licenciate degrees in Electrical Engineering, both from Helsinki University of Technology, in 1984 and 1989 respectively, and the Doctor of Technology degree from Tampere University of Technology in 1992. The main activities of Dr. Lehtonen include earth fault problems, harmonic related issues and applications of information technology in distribution automation and distribution energy management. (Helsinki University of Technology, Power Systems Laboratory, P.O.Box 3000, FIN-02015 HUT, Finland, Tel. +358 9 4515484, Fax +358 9 460224, E-mail: Matti.Lehtonen@hut.fi)

Prof. Dr.-Ing. Peter Schegner (1955), VDE, is head of the Institut of Electrical Power Engineering of the Dresden University of Technology (Germany). He studied Electrical Power Engineering at the Darmstadt University of Technology (Germany) and worked as system engineer in the field of power system control. He became a member of the scientific staff at the Saarland University, receiving his degree with a thesis on the earth-fault distance protection. From 1989 until 1995 he worked as head of the development department respectively product-management department of protection systems of AEG, Frankfurt a.M./Germany. (Technische Universität Dresden, Institut für Elektroenergieversorgung, D-01062, Dresden, Tel.: +49 351/463-4374, Fax: +49 351/463-7036, Schegner@eev.et.tu-dresden.de)

0-7803-5938-0/00/$10.00 (c) 2000 IEEE

Appendix G

G

Reprinted with permission from the publisher.
In: Proc. of the IEEE PES SM2001, Vancouver, Canada, July 15–19, 2001,
CD-ROM 01CH37262C. 6 p.

Earth Fault Distance Computation with Artificial Neural Network Trained by Neutral Voltage Transients

S. Hänninen
VTT Energy, Energy Systems
Espoo, Finland

M. Lehtonen
Helsinki University of Technology
Power Systems Laboratory
Espoo, Finland

Abstract: A novel application of the neural network approach for transient based earth fault location in 20 kV radial power distribution networks is presented. The items discussed are earth fault transients, signal pre-processing, ANN training and the performance of the proposed distance estimation method. The distribution networks considered are either unearthed or resonant earthed. Neural networks trained by the harmonic content of neutral voltage transients were found to be applicable to fault distance computation in the case of very low fault resistance. The mean error in fault location was about 1 km in the field tests using staged faults, which were recorded in real power systems.
Keywords: Neural networks, ground faults, relay algorithms

I. INTRODUCTION

In power systems with high impedance grounding, i.e. with an ungrounded or compensated neutral, the currents of single-phase faults are usually too small for reliable fault distance estimation. To mitigate this problem, methods that exploit the earth fault charge transients have been studied. The solutions proposed include the differential equation algorithm [1], Fourier analysis [2] and curve fitting methods [3]. More recently the use of wavelet transform has also been proposed [4].

The methods mentioned above require simultaneous measurements of the phase currents and voltages in the faulty feeder. This paper presents a novel application of the Artificial Neural Network (ANN), which uses the harmonic components of the neutral voltage transients for earth fault distance computation. The benefit of this method is that only one measurement per primary transformer is needed. The results are compared to other ANNs trained by phase current and voltage samples [5]. To make the different solutions comparable, a similar signal preprocessing was applied to all the cases considered. The signal pre-processing, which covers the extraction of the dominating transient component from the other signal parts, is discussed first. The different alternatives for the ANN selection are then discussed. Special focus is also given to the scaling and adaptation of the input data, aiming for high correlation in the training information and enabling one single ANN to estimate fault distances in power distribution networks of different sizes. Finally the algorithm presented is tested using simulated data and staged faults recorded in real power systems.

II. SIGNAL PRE-PROCESSIG

The key issue in signal pre-processing is to extract the charge transient, used for earth fault distance computation, from the other parts of the measured signals. The signal pre-processing is made in the following steps:

1. Removal of the fundamental frequency component.
2. Spectrum analysis for estimating the charge transient frequency.
3. Low-pass filtering in order to remove the higher frequency components.

For the fundamental frequency removal a straightforward technique is used: $g(t)=f(t)-f(t+T)$, where $g(t)$ is the output of the filter, $f(t)$ is the original signal and T is the period of the fundamental frequency. The filter removes, in addition to the fundamental frequency, also its steady state harmonic components. Theoretically the transients are affected as well, but since in real power system circumstances there always is some attenuation present, this effect is very small and can be ignored [3]. The spectrum analysis is performed by a Fourier algorithm, which covers only a 20 ms window, starting from the beginning of the transient. The frequency band used is from 100 Hz to 833 Hz, corresponding to a 5 kHz sampling frequency. The highest amplitude spectrum component is assumed to be the one corresponding to the charge transient frequency.

The cut-off frequency of the low-pass filter is set 400 Hz higher than the estimated charge transient frequency. A second order Bessel filter is applied. The attractive feature of this filter is that it has a flat transition band. However, because of the recursive nature, the transient effects of the filter itself are difficult to control. To mitigate this problem, the measured signals are processed in a reversed order. In the harmonic based approach the neutral voltage components of 125 to 833 Hz are used.

III. ARTIFICIAL NEURAL NETWORK FOR EARTH FAULT DISTANCE ESTIMATION

A. ANN-Structure

The Artificial Neural Network (ANN) seems to be a very attractive tool for the ground fault distance estimation problem, since it does not require the explicit formulation of the solution algorithm, but is able to implicitly utilise various dependencies in the training data [6]. Analysing the charge transient can be regarded as the evaluation of special characteristics (frequency, amplitude and damping) with respect to the information content of the fault distance. It is therefore a task of pattern recognition, which corresponds to the abilities of the ANN. In this work an ANN structure known as the Multilayer Perceptron was used. It consists of the input vector, one hidden layer and the output layer, see Fig. 1.

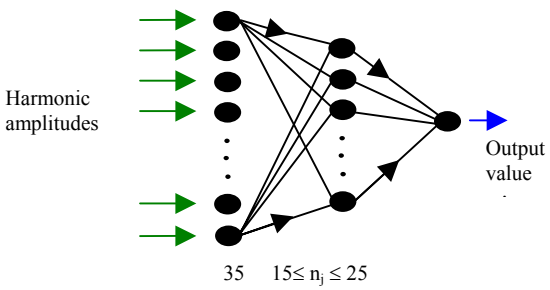

Fig. 1. Scructure of the Multilayer Perceptron

B. Input and Output Vectors

A data window of 20 ms starting from the beginning of the transient determined the input data. The resulting number of harmonic components used as input values was 35. The harmonic amplitudes were scaled to the range of -1 to 1 due to their maximum. It has been proved that, in general, one hidden layer is sufficient for representing any given input-output transformation [7]. Using more than one hidden layer is necessary if the pattern recognition task seems to be quite sophisticated and if there is a large number of input neurons. In this work the ANN consisted of only one hidden layer. The number of the hidden neurons n_j was varied in the range $[15 \le n_j \le 25]$. The fault distance was given by the activation of one single output neuron. Because the maximum activation of a neuron is 1, the output parameters were scaled to the maximum values that occurred.

IV. TRAINING OF ANN

A. Implementation

The Backpropagation method with the Levenberg-Marquart training algorithm provides a fast and stable training process and a sufficient error decrease for the ANN. The training process was done several (50) times each with different initial values. This is because the error minimum depends on the random initial values of the weights and biases. The lowest training error that could be achieved was used for assessing the performance of the ANN. Training was done in the so-called "batch" or "offline training" mode. This means all training patterns must be put through the ANN before the network parameters – the weights – are changed in one single step. Doing so, the order of the training patterns has no importance to the weight changes and to the learning success [8]. For implementation, training and verification of the ANN, the software MATLAB version 5.3 and its ANN toolbox were applied [9].

B. Training Data

For training and testing of the ANN a large data set of neutral voltage samples is necessary. The affecting parameters must be varied within an appropriate range to provide the ANN with all the important features, see Table 1. Earth faults were simulated by the common simulation tool "Alternative Transients Program" (ATP/EMTP). The basic 20 kV overhead lines were modelled using the Line Constants ATP/EMTP Program taking into account the real geometrical and electrical values [10].

Table 1. Variation of the network and fault parameters

Parameter	**Varied range**	**Number of variations**
Fault distance d	1km …40km (Δd = 1km)	40
Network size s (busbar frequency f_0)	s → f_0 300km → 450Hz 420km → 390Hz	2
Load Load angle cosϕ	I_{Load} 0p.u. → 0A 0.2p.u. → 40A 0.5p.u. → 100A resistive; cosϕ = 1 resistive/inductive; cosϕ = 0.8	6
Grounding	Unearthed	1
Entrance angle	45°; 70°; 90°	3
Fault resistance	0.1Ω ;5Ω ;10Ω ;15Ω	4
Phase	R, S	2
Data sets		11520

V. TRAINING DATA PATTERNS

A. Network Size

The fault distance estimation system must be able to work properly in networks of different sizes, and under different load conditions and fault entrance angles; i.e. the phase to ground voltage angle that exists when the fault occurs. However, the earlier research [5] has shown that an ANN gives the best results if trained only for the one network size for which it was intended. This is due to the fact that the transient frequency is very dependent on the network size. Two different ANNs were trained for the network sizes of 300 km and 420 km respectively. Altogether 11520 data sets were used for training. The input data covered different ranges of the entrance angles. It was found that ANNs trained with high entrance angles (45° - 90°), are more powerful and more likely to adapt to smaller entrance angles. Therefore the following investigations refer to the ANNs trained with entrance angles of 45° - 90°. To assess the performance of the trained ANN, the absolute mean error E_{mae} for the data from the simulated tests with 20 % of the training data was used. This test data included network sizes, load cases and faulty phases that differed from the training data. Regarding the entrance angle and fault resistance, the test data covered the same range as the data used for the ANN training. The optimal number of hidden neurons was also studied. Fig. 2. shows the E_{mae} over the number of hidden neurons n_j for the network size of 300 km. The test errors varied between 1.0 % and 1.4%, and were the smallest when the numbers of hidden neurons were 18 and 22. The training time depends on, among other things, the structure of the ANN and the number of the hidden neurons. Therefore, in the subsequent analysis, the number of hidden neurons was chosen to be 18.

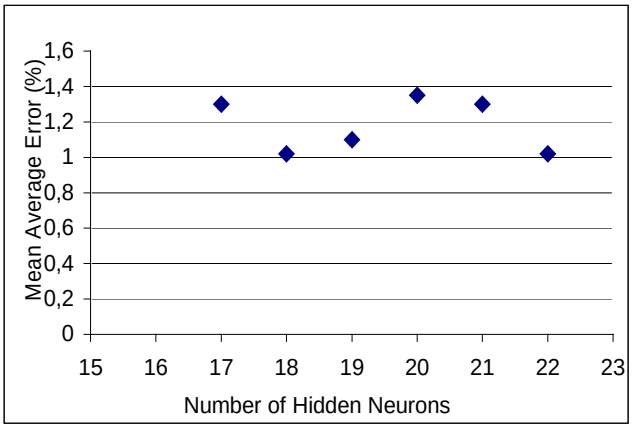

Fig. 2. Mean average error $E_{mae} = f(n_j)$ for different numbers of hidden neurons for the network size of 300 km

B. Input and Output Relations

Conventional distance algorithms evaluate the charge transients of the phase voltage and current. Regarding the network model especially, the fault distance (inductance and resistance of the faulty line segment) affects the transient phase to earth voltage. In this study the harmonic components from 125 Hz to 833 Hz of the neutral voltage were used as inputs. According to previous studies [5] the fault distance d (1 output neuron), the fault distance combined with the fault resistance (2 output neurons), and the fault resistance combined with the fault inductance (2 output neurons) were investigated as output parameters. The results showed that estimating the pure fault distance is the most promising way to design the ANN output, because only one single output neuron is needed.

VI. INPUT DATA SCALING

The network size affects both the charge frequency and the amplitude of the transients. Besides this fact, the frequency varies with the fault distance, see Fig. 3. For an ANN trained within an appropriate range of the network size, charge frequency f_0 and the entrance angle ν_0, there will be a small span in frequency and entrance angles where the ANN produces very exact results. The main idea of the scaling is to adapt the harmonic components to the ANN-specific range f_0 and ν_0. This can be done by changing the data due to the network size (frequency scaling) and to the entrance angle (amplitude scaling). Both parameters can be determined by measuring or processing. The purpose of the frequency scaling is to move the actual frequency into the range of the trained frequency band.

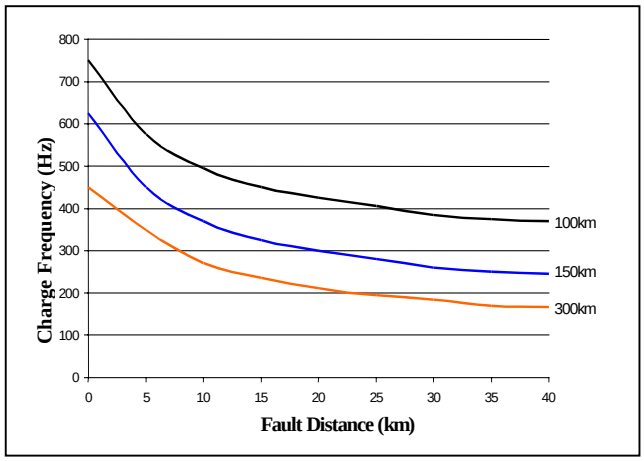

Fig. 3. Charge frequency f_A as a function of fault distance for different network sizes (20 kV overhead lines)

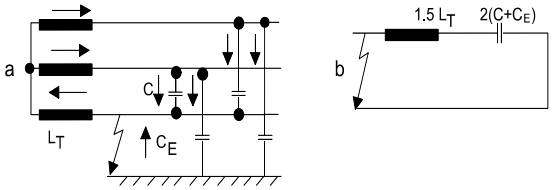

Fig. 4. The network model for the charge transient (a) and the corresponding equivalent circuit (b)

This is accomplished by stretching or shortening the spectrum of the harmonic components. The network size and the fault distance can be taken into account by a linear function, see Fig. 3. The scaling factor (SF) for the spectrum of the harmonic components can be obtained as follows:

$$SF = \frac{f_0 - f_{30}}{f'_0 - f'_{30}} \quad (1)$$

where f_0 and f_{30} are the frequencies of the charge transients for the distribution network used for the ANN training, when the fault point is at the busbar and at the distance of 30 km from the substation. f'_0 and f'_{30} are the corresponding frequencies for the actual distribution network.

For the undamped condition, frequencies f_0 and f'_0 can be determined as follows, see Fig. 4. [11]:

$$f_0 = \frac{1}{2\pi\sqrt{L_{eq}C_{eq}}} = \frac{1}{2\pi\sqrt{3L_T(C+C_E)}} \quad (2)$$

$$L_{eq} = 1.5L_T \quad ; \quad C_{eq} = 2(C + C_E) \quad (3)$$

The frequencies f_{30} and f'_{30} referred to above can be determined by writing the differential equation with the aid of voltage equations around the loops of the circuit in Fig. 5. The resistances are neglected. The natural frequencies of the circuit can be solved as the roots of the characteristic equation in the following way [3]:

$$f_{30} = \frac{1}{2\pi}\sqrt{\frac{L_1C_1 + L_2C_2 + L_1C_2}{2L_1L_2C_1C_2} - \sqrt{\left(\frac{L_1C_1 + L_2C_2 + L_1C_2}{2L_1L_2C_1C_2}\right)^2 - \frac{1}{L_1L_2C_1C_2}}} \quad (4)$$

$L_1 = 2L_T$
$L_2 = L_{l,p}+L_{l,n}+L_{l,0}=2L_{l,p}+L_{l,0}$
$C_1 = 0.5C_E+1{,}5C$
$C_2 = C_E$
L_T = substation transformer inductance
L_1 = inductance of the faulty line
$L_{1,p}$, $L_{1,n}$, $L_{1,0}$ = sequence inductances of the faulty line length
C_E = earth capacitance of the network
C = phase to phase capacitance of the network

The harmonic frequencies were multiplied by the scaling factor SF meaning that the spectrum was stretched or shrunk while the amplitudes remained unchanged. The scaled harmonic spectrum for the distance computation was finally determined by interpolation due to the fact that the harmonic frequencies must be the same as used for the ANN training. Fig. 6 shows an example of the scaling in the case where the earth fault was 20 km from the substation and SF= 0.873. Regarding the moment of fault entrance, the amplitude of the transients increases with the entrance angle υ [$0° \le \upsilon \le 90°$]. The transient current amplitude increases with the enlargement of the power distribution network, but the amplitude of the transient voltage remains almost constant.

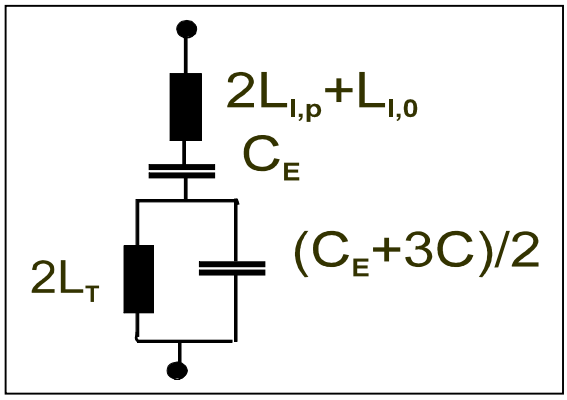

Fig. 5. The composite connection of the sequence networks for isolated networks

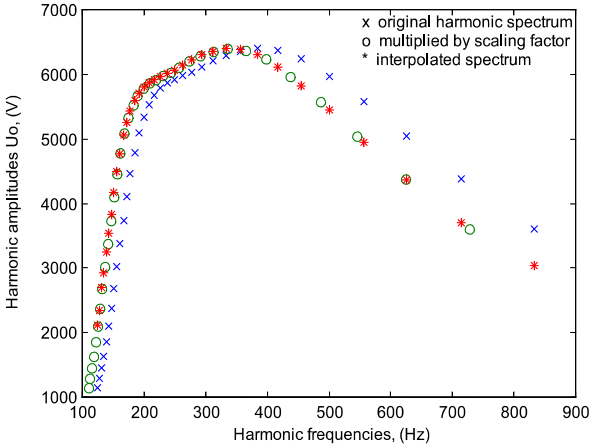

Fig. 6. Input data scaling

Table 2. Comparison of different ANN methods using simulated test data. Fault distances were from 1 km to 40 km in 1km steps, and the fault entrance angles were 40°, 60° and 90° for each network size. The errors are absolute mean values

Network size (km)	Fault resistance (Ω)	Artificial neural network input		
		Voltage	Voltage/current	Uo spectrum
		error (km)	error (km)	error (km)
200	0	3.64	1.09	2.92
275	0	2.00	0.80	1.04
360	0	2.48	1.28	3.79
450	0	2.49	1.62	1.15
200	15	2.49	1.67	3.11
275	15	3.04	1.02	1.03
360	15	3.86	1.35	1.83
450	15	5.46	1.57	1.97

Table 3. Comparison of different ANN methods using field test data. The errors are absolute mean values computed from the repeated earth fault tests

Network earthing	Exact fault distance (km)	Fault resistance (Ω)	Artificial neural network input		
			Voltage	Voltage/current	Uo spectrum
			error (km)	error (km)	error (km)
Compensated	0.76	0	2.4	0.7	1.7
Compensated	10.4	0	13.8	0.7	0.9
Compensated	14.2	0	2.7	1.3	0.2
Partially compensated	25.4	0	1.3	1.3	0.2
Partially compensated	36.0	0	0.9	1.0	2.5
Unearthed	13.3	47	7.9	5.9	5.0
Unearthed	20.0	47	13.8	15.2	5.8

VII. COMPARISON OF THE DISTANCE STIMATION TECHNIQUES

The performance of ANNs trained by the harmonic spectra of neutral voltage transients was compared to the previous transient based ANN methods [5]. In the last mentioned cases the ANNs were trained either by phase voltage or phase voltage and current samples of transients, and the network sizes were 150 and 300 km. The different ANNs were trained for compensated and unearthed networks using the fault resistances from 0 Ω to 15 Ω. The scaling methods used for those ANNs were explained in [5]. The ANNs using neutral voltage harmonic inputs (Uo) were trained only for unearthed networks.

The comparison was done using simulated data and field data. The test data consisted of field tests with staged faults from distribution networks with partially compensated, compensated, and unearthed neutral. Together 18 earth faults were carried out with fault resistances of 0 Ω to 50 Ω at different line locations. Simulated data (Table 2) shows that a harmonic trained ANN is on a par with current/voltage trained ANNs and clearly works better than ANNs trained with voltage samples. In the case of field test data, if the fault resistance was zero, the mean error was a bit higher than 1 km, see Table 3. The drawback is that with higher fault resistances (50 Ω) the transients are attenuated and errors are increased drastically. The accuracy was also very sensitive to the frequency scaling due to the different network sizes. The best results were achieved when the scaling factor for input data adaptation was in the range of 0.85 to 1.15.

VIII. CONCLUSIONS

In networks with an isolated or compensated neutral, earth fault distance estimation is not possible using the fundamental frequency signals. That is why transient based techniques have been studied. In high impedance earthed networks, the charge transient, which is due to the voltage rise of the two sound phases, is the most useful component for fault location purposes. The neural network approach is an alternative to the more conventional solutions for ground fault distance estimation, since it does not require the explicit formulation of the solution algorithm. It is able to implicitly utilise various dependencies in the training data.

This paper presents a novel earth fault distance computation application based on an ANN. Special focus was given to the scaling and adaptation of the input data enabling one single ANN to estimate fault distances in power distribution networks of different sizes. The ANN-type Multilayer Perceptron, with one hidden layer and trained with the Backpropagation algorithm, was used in each case. The performance of the ANN trained by harmonic spectra of the neutral voltage transients was comparable to previous ANN developments with voltage and current input. Considering only the earth faults with very low fault resistance, the mean error in absolute terms was about 1 km in the field tests. The performance of earth fault location is restricted by the attenuation of the transients. The highest fault resistance that made possible fault location was about 50 Ω. The method is also sensitive to the frequency scaling in cases where input data adaptation is needed due to different network sizes. The best results were achieved when the

input data adaptation was small, i.e. when the scaling factor was in the range of 0.85 to 1.15.

IX. REFERENCES

[1] P. Schegner, "Digitaler Erdschlußuniversalschutz. Konzept und erste Realisierung," Dissertation, Universität des Saarlandes, Saarbrücken, 1989, p. 186.

[2] M. Igel, "Neuartige Verfahren für den Erdschluß-distanzschutz in isoliert und kompensiert betriebenen Netzen. Signale und Algoritmen im Frequenzbereich," Dissertation, Universität des Saarlandes, Saarbrücken, 1990, p. 181.

[3] M. Lehtonen, "Transient analysis for ground fault distance estimation in electrical distribution networks," Dissertation, Technical Research Centre of Finland, Publications no. 115. Espoo 1992, p. 181 + app.

[4] S. Hänninen, M. Lehtonen, T. Hakola and R. Rantanen, "Comparison of Wavelet and Differential Equation Algorithms in Earth Fault Distance Computation," Proceedings of the PSCC'99, 13th Power Systems Computation Conference. Trondheim, Norway, June 28- July 2, 1999. Volume 2. pp. 801-807.

[5] G. Eberl, S. Hänninen, M. Lehtonen and P. Schegner, "Comparison of artificial neural networks and conventional algorithms in ground fault distance computation," 2000 IEEE Power Engineering Society Winter Meeting, 23 - 27 January 2000, Singapore. Proceedings IEEE PES [CD-ROM] 00CH37077C, p. 6.

[6] D. Eickmeyer, "Einsatz künstlicher neuronaler Netze bei der Ortung von Erdschlüssen," Dissertation, TU Berlin, 1997, p. 136.

[7] S. Haykin, "Neural Networks - A comprehensive foundation," Macmillan, NY, Prentice Hall International Editions, 1994, p. 696.

[8] A. Zell, "Simulation neuronaler Netze," Addison-Wesley, 1994, p. 624.

[9] H. Demuth, M. Beale, "Neural Network Toolbox for Use with Matlab. User's Guide Version 3," The Math Works Inc., 1998, pp. 5-58.

[10] EEUG, European EMTP-ATP Users Group e.V., "Alternative Transients Program, ATP," Reference Manual.

[11] H. Pundt, "Untersuchungen der Ausgleichsvorgänge bei Erdschluß in Hochspannungsnetzen mit isoliertem Sternpunkt und induktiver Sternpunkterdung als Grundlage zur selektiven Erdschlußerfassung," Dissertation, TU Dresden, 1963, p.167 + app.

X BIOGRAPHIES

Seppo Hänninen (1956) has been with VTT Energy, Espoo, Finland since 1987. His current position is special research scientist in the research group, Electric Energy and IT. He received his Master's degree in Electrical Power Engineering from Tampere University of Technology in 1980 and Licenciate degree in Electromechanics from Helsinki University of Technology in 1991. His main fields of interest are earth fault problems, distribution automation in medium voltage networks and reliability engineering. (VTT Energy, P.O.Box 1606, FIN-02044 VTT, Finland, Tel. +358 9 4566759, Fax +358 9 4566538, E-mail: Seppo.Hanninen@vtt.fi)

Matti Lehtonen (1959) has been with VTT Energy, Espoo, Finland since 1987 and since 1999 with Helsinki University of Technology, where he is a Professor of IT applications in power systems. Matti Lehtonen received his Master's and Licenciate degrees in Electrical Engineering, both from Helsinki University of Technology, in 1984 and 1989 respectively, and the Doctor of Technology degree from Tampere University of Technology in 1992. The main activities of Dr. Lehtonen include earth fault problems, harmonic related issues and applications of information technology in distribution automation and distribution energy management. (Helsinki University of Technology, Power Systems Laboratory, P.O.Box 3000, FIN-02015 HUT, Finland, Tel. +358 9 4515484, Fax +358 9 460224, E-mail: Matti.Lehtonen@hut.fi)

Published by

Vuorimiehentie 5, P.O.Box 2000, FIN–02044 VTT, Finland
Phone internat. +358 9 4561
Fax +358 9 456 4374

Series title, number and report code of publication

VTT Publications 453
VTT–PUBS–453

Author(s)
Hänninen, Seppo

Title

Single phase earth faults in high impedance grounded netwotrks

Characteristics, indication and location

Abstract

The subject of this thesis is the single phase earth fault in medium voltage distribution networks that are high impedance grounded. Networks are normally radially operated but partially meshed. First, the basic properties of high impedance grounded networks are discussed. Following this, the characteristics of earth faults in distribution networks are determined based on real case recordings. Exploiting these characteristics, new applications for earth fault indication and location are then developed.

The characteristics discussed are the clearing of earth faults, arc extinction, arcing faults, fault resistances and transients. Arcing faults made up at least half of all the disturbances, and they were especially predominant in the unearthed network. In the case of arcing faults, typical fault durations are outlined, and the overvoltages measured in different systems are analysed. In the unearthed systems, the maximum currents that allowed for autoextinction were small. Transients appeared in nearly all fault occurrences that caused the action of the circuit breaker. Fault resistances fell into two major categories, one where the fault resistances were below a few hundred ohms and the other where they were of the order of thousands of ohms.

Some faults can evolve gradually, for example faults caused by broken pin insulators, snow burden, downed conductor or tree contact. Using a novel application based on the neutral voltage and residual current analysis with the probabilistic method, it is possible to detect and locate resistive earth faults up to a resistance of 220 kΩ.

The main results were also to develop new applications of the transient based differential equation, wavelet and neural network methods for fault distance estimation. The performance of the artificial neural network methods was comparable to that of the conventional algorithms. It was also shown that the neural network, trained by the harmonic components of the neutral voltage transients, is applicable for earth fault distance computation. The benefit of this method is that only one measurement per primary transformer is needed. Regarding only the earth faults with very low fault resistance, the mean error in absolute terms was about 1.0 km for neural network methods and about 2.0 km for the conventional algorithms in staged field tests. The restriction of neural network methods is the huge training process needed because so many different parameters affect the amplitude and frequency of the transient signal. For practical use the conventional methods based on the faulty line impedance calculation proved to be more promising.

Keywords

power distribution, distribution networks, earth faults, detection, positioning, fault resistance, arching, neutral voltage, residual current, transients

Activity unit

VTT Energy, Energy Systems, Tekniikantie 4 C, P.O.Box 1606, FIN–02044 VTT, Finland

ISBN	Project number
951–38–5960–6 (soft back ed.) 951–38–5961–4 (URL: http://www.inf.vtt.fi/pdf/)	

Date	Language	Pages	Price
November 2001	English	78 p. + app. 61 p.	C

Name of project	Commissioned by

Series title and ISSN	Sold by
VTT Publications 1235–0621 (soft back ed.) 1455–0849 (URL: http://www.inf.vtt.fi/pdf/)	VTT Information Service P.O.Box 2000, FIN–02044 VTT, Finland Phone internat. +358 9 456 4404 Fax +358 9 456 4374